NASA/TM–2010-216725

HyBoLT Flight Experiment

Fang-Jenq (Frank) Chen and Scott A. Berry
Langley Research Center, Hampton, Virginia

July 2010

NASA STI Program . . . in Profile

Since its founding, NASA has been dedicated to the advancement of aeronautics and space science. The NASA scientific and technical information (STI) program plays a key part in helping NASA maintain this important role.

The NASA STI program operates under the auspices of the Agency Chief Information Officer. It collects, organizes, provides for archiving, and disseminates NASA's STI. The NASA STI program provides access to the NASA Aeronautics and Space Database and its public interface, the NASA Technical Report Server, thus providing one of the largest collections of aeronautical and space science STI in the world. Results are published in both non-NASA channels and by NASA in the NASA STI Report Series, which includes the following report types:

- TECHNICAL PUBLICATION. Reports of completed research or a major significant phase of research that present the results of NASA programs and include extensive data or theoretical analysis. Includes compilations of significant scientific and technical data and information deemed to be of continuing reference value. NASA counterpart of peer-reviewed formal professional papers, but having less stringent limitations on manuscript length and extent of graphic presentations.

- TECHNICAL MEMORANDUM. Scientific and technical findings that are preliminary or of specialized interest, e.g., quick release reports, working papers, and bibliographies that contain minimal annotation. Does not contain extensive analysis.

- CONTRACTOR REPORT. Scientific and technical findings by NASA-sponsored contractors and grantees.

- CONFERENCE PUBLICATION. Collected papers from scientific and technical conferences, symposia, seminars, or other meetings sponsored or co-sponsored by NASA.

- SPECIAL PUBLICATION. Scientific, technical, or historical information from NASA programs, projects, and missions, often concerned with subjects having substantial public interest.

- TECHNICAL TRANSLATION. English-language translations of foreign scientific and technical material pertinent to NASA's mission.

Specialized services also include creating custom thesauri, building customized databases, and organizing and publishing research results.

For more information about the NASA STI program, see the following:

- Access the NASA STI program home page at *http://www.sti.nasa.gov*

- E-mail your question via the Internet to help@sti.nasa.gov

- Fax your question to the NASA STI Help Desk at 443-757-5803

- Phone the NASA STI Help Desk at 443-757-5802

- Write to:
  NASA STI Help Desk
  NASA Center for AeroSpace Information
  7115 Standard Drive
  Hanover, MD 21076-1320

NASA/TM–2010-216725

HyBoLT Flight Experiment

Fang-Jenq (Frank) Chen and Scott A. Berry
Langley Research Center, Hampton, Virginia

National Aeronautics and
Space Administration

Langley Research Center
Hampton, Virginia 23681-2199

July 2010

Available from:

NASA Center for AeroSpace Information
7115 Standard Drive
Hanover, MD 21076-1320
443-757-5802

Contents

Abstract 1

Nomenclature 2

List of Tables 3

List of Figures 4

1. Introduction 6

2. Mission Objectives 7

3. Vehicle Constraints and Geometry 7

4. Science Objectives and Experimental Design 8

4.1 Side A Nature Transition 8
4.1.1 Transition Prediction 8
4.1.2 Instrumentation 9
4.1.2.a Low-frequency instrumentation 9
4.1.2.b High-frequency instrumentation 9
4.2 Side B Roughness Transition 10
4.2.1 Trip Sizing 10
4.2.2 Instrumentation 11

5. Verification of Instruments and Sensor Functions by Flight Data 11

5.1 Thermocouple Data 11
5.2 Surface Static Pressure Data 12
5.3 Differential Pressure Data for Angle of Attack and Angle of Yaw 12
5.4 Boundary-Layer Pressure Rake Data 12
5.5 Differential Pressure Data for Flow Angle at Boundary-Layer Pressure Rakes 13
5.6 Acceleration Data 13
5.7 Surface Hot-Film Data 13
5.8 Dynamic Pressure Data from Three-Dynamic-Pressure Gages 13
5.9 Dynamic Data from Other Dynamic Pressure Gages, Freestream Probe and Vibrometer 13

6. Concluding Remarks 14

7. Acknowledgements 14

References 15

Abstract

HyBoLT was a Hypersonic Boundary Layer Transition flight experiment funded by the Hypersonics Project of the Fundamental Aeronautics Program in NASA's Aeronautics Research Mission Directorate. The HyBoLT test article mounted on the top of the ALV X-1 rocket was launched from Virginia's Wallops Island on August 22, 2008. Unfortunately a problem in the rocket's flight control system caused the vehicle to veer off the designed flight course. Launch officials activated a self-destruct mechanism in the rocket's nose cone after 20 seconds into flight. This report is a closeout document about the HyBoLT flight experiment. Details are provided of the objectives and approach associated with this experimental program as well as the 20 seconds flight data acquired before the vehicle was destroyed.

Nomenclature

k = protuberance height above the surface (in)

L, D, W = cavity length, depth, and width (in)

M_e = Mach number at the boundary layer edge

P = surface static pressure (psia)

ΔP = differential pressure (psid)

Re_k = Reynolds number based on properties at trip height

Re_θ = momentum thickness Reynolds number

$T0$ = ALV X-1 rocket liftoff time

T_e = temperature at the boundary layer edge

T_w = temperature at the wall

V_{cavity} = cavity volume

X, Y, Z = location on vehicle referenced from virtual origin

α = angle of attack (deg)

α_{Tot} = total angle of attack (deg) = $\sqrt{\alpha^2 + \beta^2}$ with respect to vehicle body centerline

β = angle of yaw (deg)

δ = boundary layer thickness (in)

δ^* = displacement thickness

θ = momentum thickness

ϕ_A = flow angle at Side A boundary-layer pressure rake

ϕ_B = flow angle at Side B boundary-layer pressure rake

List of Tables

1 Key nominal trajectory points prior to Stage 1 burn-out ……...…… 16

2 Local edge properties at key trajectory points for outboard trip station (X=20 Y=0) …… 16

3 Local edge properties at key trajectory points for centerline trip station (X=20 Y=±5) ……...… 16

4 Trip dimensions at key trajectory points for centerline trip station (X=20 Y=0) ……...…… 17

5 Trip dimensions at key trajectory points for outboard trip station (X=20 Y=±5) ……..... 17

6 Side A detailed instrument list ……...…… 18

7 Side B detailed instrument list …… 22

8 Miscellaneous instrument list …… 24

9 Thermocouple reference temperature blocks …… 25

10 Relationships between measured and computed differential pressures, and measured static pressures for angle of attack and angle of yaw ……..……..…… 25

11 Relationships between measured and computed differential pressures, and measured static pressures for flow angles at boundary-layer pressure rakes ……..…… 25

List of Figures

1 Liftoff of HyBoLT mounted on the ALV X-1 rocket from WFF Launch Pad 0B 26
2 Artistic rendering of HyBoLT during launch from Wallops Flight Facility 26
3 Planned ALV X-1 flight profile 27
4 HyBoLT trajectory points and data criticality window 27
5 Trajectory outlook of vehicle orientation 28
6 Instrumentation coordinate system (Forward looking Aft) 28
7 Side A transition prediction results 29
8 Side A instrumentation layout 29
9 Side A boundary layer pressure rake 30
10 Side A freestream dynamic pressure probe 30
11 Side A three dynamic pressure probe 31
12 Side A surface hot-film plug 31
13 Side B roughness elements 31
14 Side B instrumentation layout 32
15 Side B instrumentation layout w.r.t. expected turbulent wedges downstream of boundary trips 32
16 Flight Mach number and Reynolds number from ALV data 33
17 Flight alpha, beta and total alpha from ALV data 33
18a Side A thermocouple data, TA001-TA009 34
18b Side A thermocouple data, TA010-TA018 34
18c Side A thermocouple data, TA019-TA027 35
18d Side A thermocouple data, TA028-TA036 35
18e Side A thermocouple data, TA037-TA045 36
18f Side A thermocouple data, TA046-TA054 36
18g Side A thermocouple data, TA055-TA063 37
18h Side A thermocouple data, TA064-TA072 37
18i Side A thermocouple data, TA073-TA077 38
19a Side B thermocouple data, TB001-TB009 38
19b Side B thermocouple data, TB010-TB018 39
19c Side B thermocouple data, TB019-TB027 39
19d Side B thermocouple data, TB028-TB036 40
19e Side B thermocouple data, TB037-TB045 40
19f Side B thermocouple data, TB046-TB054 41
19g Side B thermocouple data, TB055-TB063 41
19h Side B thermocouple data, TB064-TB072 42
19i Side B thermocouple data, TB073-TB081 42
19j Side B thermocouple data, TB082-TB090 43
19k Side B thermocouple data, TB091-TB099 43
20a Thermocouple reference temperature data, TRTC01-TRTC08 44
20b Thermocouple reference temperature data, TRTC09-TRTC16 44
21a Side A surface static pressure data, starboard side (+*Y*) 45
21b Side A surface static pressure data, port side (-*Y*) 45
22a Differential pressure data for angle of attack and angle of yaw 46
22b Static pressure data for angle of attack and angle of yaw 46
23a Side A boundary-layer pressure rake data 47
23b Side B boundary-layer pressure rake data 47
24a Boundary-layer pressure profile data at *T0*+5.00s 48
24b Boundary-layer pressure profile data at *T0*+10.00s 48

24c Boundary-layer pressure profile data at *T0*+15.00s 49
24d Boundary-layer pressure profile data at *T0*+18.20s 49
24e Boundary-layer pressure profile data at *T0*+20.15s 50
25 Pressure data of flow angles at boundary-layer pressure rakes 50
26 Acceleration data from 3-axis accelerometers 51
27 Surface hot-film DC voltage data 51
28a Surface hot-film HF3A11 time series data 52
28b Surface hot-film HF3A12 time series data 52
29a Surface hot-film HF3A51 time series data 53
29b Surface hot-film HF3A52 time series data 53
30a Standard deviations of surface hot-film HF3A1# time series data 54
30b Standard deviations of surface hot-film HF3A5# time series data 54
31a Amplitude spectra of surface hot-film HF3A11 data 55
31b Amplitude spectra of surface hot-film HF3A12 data 55
31c Amplitude spectra of surface hot-film HF3A13 data 56
32a Amplitude spectra of surface hot-film HF3A51 data 56
32b Amplitude spectra of surface hot-film HF3A52 data 57
32c Amplitude spectra of surface hot-film HF3A53 data 57
33a Three-dynamic-pressure gage P3DA11 time series data 58
33b Three-dynamic-pressure gage P3DA12 time series data 58
34a Three-dynamic-pressure gage P3DA21 time series data 59
34b Three-dynamic-pressure gage P3DA22 time series data 59
35a Maximum pressure fluctuations of three-dynamic-pressure gage P3DA1# time series data 60
35b Maximum pressure fluctuations of three-dynamic-pressure gage P3DA2# time series data 60
36a Amplitude spectra of three-dynamic-pressure gage P3DA11 time series data of Figure 33a 61
36b Amplitude spectra of three-dynamic-pressure gage P3DA12 time series data of Figure 33b 61
37a Amplitude spectra of three-dynamic-pressure gage P3DA21 time series data of Figure 34a 62
37b Amplitude spectra of three-dynamic-pressure gage P3DA22 time series data of Figure 34b 62
38a Amplitude spectra of three-dynamic-pressure gage P3DA11 data 63
38b Amplitude spectra of three-dynamic-pressure gage P3DA12 data 63
38c Amplitude spectra of three-dynamic-pressure gage P3DA13 data 64
39a Amplitude spectra of three-dynamic-pressure gage P3DA21 data 64
39b Amplitude spectra of three-dynamic-pressure gage P3DA22 data 65
39c Amplitude spectra of three-dynamic-pressure gage P3DA23 data 65
40a Amplitude spectra of surface dynamic pressure gage PDA01 data 66
40b Amplitude spectra of surface dynamic pressure gage PDA02 data 66
40c Amplitude spectra of surface dynamic pressure gage PDA03 data 67
40d Amplitude spectra of surface dynamic pressure gage PDA04 data 67
40e Amplitude spectra of surface dynamic pressure gage PDA05 data 68
40f Amplitude spectra of surface dynamic pressure gage PDA06 data 68
41a Amplitude spectra of surface dynamic pressure gage PDA13 data 69
41b Amplitude spectra of surface dynamic pressure gage PDA14 data 69
41c Amplitude spectra of surface dynamic pressure gage PDA15 data 70
41d Amplitude spectra of surface dynamic pressure gage PDA16 data 70
42 Amplitude spectra of freestream dynamic pressure probe PFSD01 data 71
43 Amplitude spectra of embedded vibrometer VIB1Z data 71

1. Introduction

Hypersonic boundary layer transition is a critically important discipline with potential impact on all future designs for high-speed applications. For instance, a spacecraft entering Earth's atmosphere initially experiences a heating environment associated with a laminar boundary layer. Eventually, as the atmosphere becomes denser and/or the vehicle surface becomes rougher, the boundary layer becomes turbulent and the heating rate at the surface can increase by a factor four or more. Our ability to understand and predict when this transition to turbulence and higher heating will occur has design implications for the thermal protection system (TPS) needed to protect the vehicle and crew during entry. Typically TPS designers try to use a conservative approach such as using an all-turbulent heating profile to select material and size thickness, as was adopted for some of the recent X-vehicle designs (for instance X-34[1]) and more recently for the Crew Exploration Vehicle (CEV). One advantage of an all-turbulent design approach is that it avoids the issues associated with having to define boundary layer transition criteria. For the CEV the all-turbulent approach provides the means to assess initial TPS concepts. However, as vehicle designs mature, quantification of when (during flight) the boundary layer will transition to the higher heating rates will typically allow for reduced TPS weight and thus have a direct impact on the final design.

For smooth bodies, the transition process can generally be computationally modeled for simple shapes thanks to progress made on understanding the physical instability mechanisms within laminar boundary layers.[2] Boundary layer disturbances, either excited by the outside environment (receptivity of pressure, velocity, or temperature fluctuations) or the surface (roughness), can exponentially grow (as wave-like structures) causing the eventual breakdown to turbulence. Computational tools are now available[3] to determine if and when these instability waves (primarily Tollmien-Schlichting, crossflow, or Görtler type disturbances) will evolve to secondary and/or non-linear instabilities and then breakdown to turbulence. These computational tools simulate the physical processes within the laminar boundary layer, but still must be calibrated against actual data. In the absence of large boundary layer modifiers (extreme roughness or noise) that encourage bypass mechanisms, stability calculations have been shown (by comparison to both ground-based and flight data) to accurately predict transition onset.[4] Furthermore, recent advances[5] have tried to account for small (or subcritical) distributed roughness as inputs to the transition prediction model, although the transient growth theory has not yet had the opportunity to be compared against flight results.

Most flight programs account for the vehicle surface roughness, as dictated by the state of the TPS, in development and application of a boundary layer transition criteria. The TPS roughness plays an integral role in determining the probable transition onset time during reentry. Most spacecraft designed for reentry have some form of inherent surface roughness, whether in the form of misaligned TPS tiles on the Shuttle Orbiters or, in the case of TPS designed for planetary entry or lunar return, irregularities on the surface formed during entry by ablation and/or spallation due to extremely high surface temperatures. Traditional ceramic-based TPS tiles such as those used on the Orbiters are susceptible to inadvertent roughness such as damage from launch in the form of cavities and/or gap filler protrusions. The inherent roughness is usually of a distributed nature, characteristically small and abundant. The inadvertent roughness is usually of a discrete nature, typically much larger in scale than distributed and isolated (or infrequent). For the Space Shuttle Orbiters, the slight misalignments (steps and gaps) between windward acreage TPS tiles represent the background distributed-roughness that in the absence of any large discrete trips will induce boundary layer transition at a Mach number on the order of 8. On two occasions (STS-28 and 73) the Orbiters have experienced early boundary layer transition at Mach numbers nearer to 18 as a result of large protruding gap fillers.

As a result of the Columbia accident investigation, a concerted effort was expended, in support of the Shuttle Orbiter Return-to-Flight (RTF) program, on a boundary layer transition (BLT) prediction tool[6] that is now part of a suite of engineering tools for assessing damage to the TPS. The group of analytic tools was developed for real-time mission support in the event of observed TPS damage, in order to determine if the vehicle is safe to fly as is, or if repair is required.[7] The BLT Tool calculates the expected time of boundary layer transition during entry based on observed damage and/or repair locations and geometries. The program includes a database of computed boundary layer parameters that cover a range of nominal trajectories for entry and utilizes an interpolation tool to extract specific local properties for determining the boundary layer state during the mission trajectory.[8] The BLT Tool is provided as a first step with which to establish the proper heating environment to baseline for the Cavity and Protuberance Heating tools. Calibration of the BLT Tool has been carried out by comparison of predicted transition results to several of the historical high Mach number flight cases.[9]

Prior to STS-114, the issue of protruding gap fillers (discrete roughness) was viewed within the Shuttle community to be mainly of engineering interest as opposed to a safety of flight issue. Two large protrusions were identified during the mission[10] that were significantly larger than those previously found on post-flight ground inspections. The resulting BLT Tool prediction times were thus much earlier than any historical precedent that represents the basis for the assessing the aeroheating environments for the flight. Recognizing that a large uncertainty was associated with BLT predictions outside of prior experience, the Shuttle program decided it was safer to perform a risky in-space repair (to send an astronaut out to remove the gap fillers) instead of reentering with the gap fillers left in place. A post-flight close call investigation report, dated Nov. 28, 2005, states: "reducing BLT prediction uncertainty only marginally through targeted tests and/or analysis, if technically feasible and programmatically affordable (in both time and money), might provide the data necessary to allow an otherwise inconclusive assessment to be shown as acceptable for entry as-is. Such additional test and analyses seem prudent to provide helpful data in making a risk-risk trade when the choice is not as simple as that which was presented by the [protruding gap fillers] on STS-114." The present fundamental hypersonics experimental effort was established with this last statement in mind, with the hope of providing critical boundary layer transition data for validating and/or calibrating existing simulation and engineering tools.

2. Mission Objectives

A flight of opportunity was provided through the termination of a scramjet-powered test vehicle that was to be the primary payload with the initial launch by ATK of a multi-stage rocket, the ALV X-1. The original offer was a ride of the Scramjet Flight Experiment (SFX) in exchange for NASA providing range support and launch-indemnification. NASA terminated the SFX program in March 2006 due to cost and schedule concerns, which left the ALV X-1 without a primary payload for the front of the rocket. The HyBoLT flight experiment developed as a replacement for SFX with the goal of having minimal impact to the ALV X-1 launch schedule. The ALV X-1 was originally scheduled to launch from NASA Wallops Flight Facility (WFF) on the northeastern shore of Virginia in fall of 2006. However, the launch date was postponed several times due to many unforeseeable technical issues. ALV X-1 was finally launched on August 22, 2008. Figure 1 shows a photograph of HyBoLT mounted on the top of the ALV X-1 rocket as it lifted off at the WFF Launch Pad 0B. The flight experiment had two separate sides with independent objectives, with one side being dedicated to investigating smooth wall transition (referred to as Side A) and the other discrete roughness transition (Side B).

3. Vehicle Constraints and Geometry

To minimize launch schedule impacts (and at the same time maximize the return on investment with the cancelled program), the decision was made to utilize the SFX nose cone design. This mature design had already gone through several detailed reviews. Any deviation from the SFX nose shape would have meant a new design and qualification effort and thus an immediate delay to the launch schedule. The nose geometry that was adopted by HyBoLT is shown in Figure 2, a conceptual image during launch. The forebody was a 6º half-angle wedge shape with semi-conical contour on both shoulders. The leading edge had a radius of 0.15 inches. The experimental surfaces of interest, shown in copper color, were ½-inch thick flat copper plates that extended downstream from the leading edge a total of 90 inches. The white color regions in the sketch were aluminum structure protected by cork ablative insulation. The two flat wedge surfaces, each bounded between the conical shoulders, provided the two independent sides that constitute the HyBoLT flight experiment. HyBoLT was attached to the ATK launch vehicle (ALV X-1) with an aft module and booster adapter.

The flight profile for the multi-stage ALV X-1 rocket is shown in Figure 3. The rocket was designed to have a gross weight of 43,000 lbs., a length of 54 ft., a diameter of 50 in., and was expected to achieve a maximum Mach number of 11.4 and altitude of 275 nautical miles. The HyBoLT nose cone stayed attached to the ALV X-1 through second-stage burn out with separation at 158 seconds after lift-off. HyBoLT was not designed to be recoverable and splashdown was planned for the Atlantic ocean, northeast of Antigua. The critical data collection window for HyBoLT was the first 65 seconds, as shown in Figure 4 along with key trajectory analysis points, which are also

listed in Table 1. The nominal angle of attack planned was nearly zero throughout the flight profile so that both sides would experience similar environments. Figure 5 shows a trajectory outlook of the vehicle orientation. Side A is on the skyward side (compression side) and Side B on the groundward side (expansion side) of the vehicle.

HyBoLT had a dedicated data acquisition and telemetry system that included on-board processing to provide compression of high-frequency content to allow all data to fit within telemetry reception limits. Details of the instrumentation will be discussed in greater detail in the sections to follow. Additional important measurements for the flight (for instance, Mach number, Reynolds number, and angle of attack) were to be obtained from post-flight "best-estimated trajectory" reconstruction of the entire integrated rocket data obtained from (1) the ALV-X1 telemetry which includes an inertial navigation system; and/or (2) ground-based radar tracking facilities.

4. Science Objectives and Experimental Design

4.1 Side A Natural Transition

The objective for Side A was to obtain hypersonic boundary layer transition data to be used to understand natural transition flow physics and for code validation. To support this activity, in-flight measurement of smooth wall transition characteristics (transition front movement, disturbance frequencies and movement, and boundary layer profiles) and freestream disturbance levels were planned. To insure that the measured transition onset results would be in close agreement with the predictions based on stability theory[4], strict smoothness requirements were specified for Side A: surface finish of 16 μ-in RMS over the first 40-in and 32 μ-in RMS thereafter; no forward facing steps, only aft facing steps of 0.01-in or less; no gaps over the first 60-in and the maximum allowable gap thereafter (to allow for thermal growth) was restricted to 0.10-in; and for waviness, only 0.00025-in over 0.5-in for short waves and 0.005-in over 6-in for long waves were allowed.

4.1.1 Transition Prediction

Transition predictions based on boundary layer stability computations (unpublished work by Dr. Balakumar using the $e^{Malik3d}$ code[11]) indicated that, due to pressure gradients produced by the leading edge corner and conical shoulder, transition on HyBoLT Side A would be dominated by crossflow instabilities occurring off-centerline in the Mach number range of 2.5 to 4.5 with the unit Reynolds number changing from 7.8×10^6/ft to 2.5×10^6/ft. The transition stability analysis also indicated that, due to the combined effects of cold wall and leading edge bluntness, the growth of 1st or 2nd mode Tollmien-Schlichting waves were not expected to be significant enough to cause boundary layer transition anywhere on Side A up to Mach 8 during the flight. Therefore, the experimental plan for Side A is mainly concentrated to characterize crossflow instabilities.

Figure 6 shows the HyBoLT coordinate system in a viewpoint of forward looking aft with *Y* and *Z* depicted but *X* is referenced from the virtual leading edge – positive in the aft direction. The HyBoLT coordinates use a left handed coordinate system in order to match the *Y* and *Z* coordinates of ALV. Because of symmetry, transition prediction results are plotted on the upper half (positive *Y*) only in Figure 7, which shows the top view of Side A. Note that the coordinate is stretched in the *Y*-direction in this plot. The virtual leading edge (if sharp) is located at *X*=0 inch while the actual blunt leading edge is at *X*=1.285 inches. The trapezoidal region bounded between two inclined red lines from the leading edge to 90.0 inches is the flat plate portion of the copper experimental plate. This plot shows for Side A the predicted transition front movement as a function of Mach number. The solid green lines represent the local streamlines in this outboard region, while the dashed red lines represent constant values of disturbance growth (*N*-factors between 6 and 11). Since most of the predicted transition front locations for Mach 3.0 and 4.2 take place on the outboard portion of the flat section, the critical transition detection sensors were concentrated in this region for the Side A experiment. Note that for Mach 5.5, transition was predicted to occur on the conical shoulders, which were covered by surface thermal insulation (outboard of the blue lines in Figure 7) that prevented our acquiring any meaningful transition data at this location.

4.1.2 Instrumentation

The goals for the Side A experiment were to measure boundary layer transition locations, fluctuation intensities, disturbance frequencies and propagation speeds and directions, plus boundary conditions that consist of surface temperature distributions, surface pressure distributions, boundary layer profiles, and flow directions. An array of surface flush mounted thermocouples were installed to provide transition front movement data. Specially designed surface hot-film sensors were included to detect stationary and/or traveling waves. In addition, dynamic pressure sensor arrays were included to provide phase angle and phase velocity information of any traveling waves.

The instrumentation layout for HyBoLT Side A is shown in Figure 8. Side A instrumentation includes both low- and high-frequency sensors. The low-frequency sensors were sampled at 300 samples per second (sps) or slower and provide time-averaged observations of transition location, surface pressure distribution, boundary layer profile, and flow direction. High-frequency sensors were sampled at either 20 kHz or 100 kHz and were intended to identify frequencies, wave propagation speeds, direction and types of crossflow instabilities in order to determine the reasons for changes in the time-averaged observations.

4.1.2.a Low-frequency instrumentation

An array of 77 thermocouples was included to perform transition front mapping. All thermocouples were surface flush-mounted except one located just under the surface on the HyBoLT leading edge. A total of 22 surface static pressure ports were distributed on the shoulder sides and downstream of the sensor layout region to avoid any possibility of contamination of disturbances from these pressure ports. Two pairs of pressure ports along the centerline on Side A and Side B were used to collect differential pressures for independent verification of the ALV X-1 angle of attack, α, during the flight test. Another two pairs of pressure ports on the opposite shoulder edges were used to measure the angle of yaw, β. A 'probeless' pressure rake, as shown in Figure 9, approximately 2-in high by 0.5-in wide by 2-in long was used to measure the boundary layer profile. A pair of pressure ports on the rake's opposite wedge side surfaces was used to determine the mean flow direction towards the top of the boundary layer. A second version of this boundary layer rake was located on centerline of Side B.

4.1.2.b High-frequency instrumentation

A dynamic pressure probe stand equipped with a high frequency dynamic pressure transducer (2.5-in high by 0.75-in wide by 1.625-in long), as shown in Figure 10, was used to monitor the freestream disturbance levels outside the boundary layer. The tip of the transducer was recessed 0.175 inches from the front surface and protected by a ceramic sleeve to alleviate heat load damage to the sensing element.

Six dynamic pressure transducers aligned in a row and flush mounted on the port side (negative Y) at $X \approx 20$ inches, as shown in Figure 8, were used to monitor any possible disturbances coming from the leading edge corner. Another four dynamic pressure transducers were distributed near the edge of the experimental plate to monitor surface pressure fluctuations. Two three-dynamic-pressure gages were located in the crossflow region. Each gage had three dynamic pressure transducers, as shown in Figure 11, that were arranged in a triangular formation at a spacing of less than one wavelength of a crossflow vortex. The top surface was flush mounted at locations on the starboard and port sides of the experimental plate and were designed to measure the wave velocity and direction (phase velocity) of crossflow instabilities.

Surface hot-film gages that have three active filaments located inside one wavelength (predicted for crossflow disturbance) along the sensor centerline and three passive filaments distributed on the top surface of a quartz plug are shown in Figure 12 with an accompanying photograph. Two of these hot-film sensors were located in the predicted crossflow region and were designed to determine the crossflow instability (stationary or traveling) characteristics. The function of the passive filaments was to measure local surface temperatures for adjustment of proper compensation of the active filaments. The hot-film gages were also planned to be used to detect the occurrence of boundary layer transition by the change of RMS levels of their AC output.

The final high frequency measurement was a one-axis vibrometer (*Z*-axis, 100 kHz) that was used to monitor the vibration of the experimental plate. All high-frequency content was processed onboard to compress the data to the 5Mbits/sec telemetry bandwidth limit. The processed data included spectral averaging of amplitude spectra, correlations in space, and statistics, to be used to document the physics of the transition process as completely as possible. Since transition physics changes appreciably as the Mach number increases, any real-time analysis had to be accomplished within the timestep equivalent of a change in Mach number of 0.02; that is, within 104 milliseconds (ms). One selected 5kHz channel was downlinked in total to the ground station for post-flight post-processing to verify onboard data processing.

4.2 Side B Roughness Transition

HyBoLT Side B was proposed to provide flight data comparing the relative effectiveness of various boundary layer (BL) trips relevant to the Shuttle Return to Flight (RTF) program. The Side B science objective was to obtain hypersonic boundary layer data from a known fixed transition position using boundary layer trips representative of damage (protrusions or cavities) to Shuttle Thermal Protection System (TPS). These data were intended to support engineering code validation for the RTF BLT tool. [6]

The Side B roughness experiment had three separate discrete BL trips selected for side-by-side comparison. Two trips were used to compare protuberances of the same height (a gap filler type representing flight versus a ground-based "pizza box") and the third trip was a cavity designed (based on ground data) to trip at nearly the same point in the trajectory as the protuberances. The gap filler and cavity represent realistic damage scenarios for the Shuttle program and the new in-flight assessment capability developed as a result of the Columbia accident investigation. The cavity was located on centerline, while the protuberances were placed 5-in on either side of centerline, all at the trip station 20 inches back from the leading edge, as shown in Figure 13. These three BL trips were all designed and machined as an integral part of the flat copper plate used for the Side B assembly.

4.2.1 Trip Sizing

The trips used for HyBoLT Side B were sized based on the approach and methodology of the RTF BLT Tool Version 1.[6] For protuberances, the trip height (k) is predicted, based on a two-sigma confidence level, to initiate the onset of transition based on 27 times the boundary layer thickness (δ) divided by the momentum thickness Reynolds number over the edge Mach number (Re_θ/M_e). A similar correlation for cavities was generated from the ground-based data[12] as part of an update to Version 2 the BLT Tool[13] using the cavity volume (V). The local parameters used to generate the RTF BLT correlations were based on the engineering code, LATCH[14], while the present HyBoLT parameters used to size the trips are based on viscous CFD solutions. The inconsistency between correlation development and application was initially acceptable due to the relative nature of the resulting data. Based on the ground-based data and correlations, the transition front movement behind all three trips was expected to begin at about the same time during flight and the absolute time in comparison to expectations was less important. The impact of using viscous CFD solutions for extracting the local properties will be further investigated as the RTF BLT Tool is upgraded to Version 2, which is based solely on a CFD database.

Tables 2 and 3 provide the local boundary layer edge properties extracted from the CFD solutions for the nominal trajectory at the trip locations. The relevant parametric space for the Orbiter is values of Re_θ/M_e between 50 and 200 (with M_e on the order of 2.8) and values of k/δ between 0.2 and 1.2. A quick scan of the trajectory points shown in Tables 2 and 3 reveal that Shuttle-like edge Mach numbers (roughly M_e=2.8) are obtained at the trip locations between Mach 6.5 and 7.5. The corresponding Re_θ/M_e for these trajectory points are between 80 and 130, which are in the range of interest for Shuttle. Tables 4 and 5 provide the calculated trip dimensions obtained using the RTF BLT Tool methodologies corresponding to local properties listed in Tables 2 and 3, respectively. Based on feedback from the manufacturer on the largest trip height that can be built integral to the copper surface, 0.0683-in protuberances at Y=±5-in were selected (see Table 5), which corresponds to the Mach 7 trajectory point and a k/δ of 0.2724. The matching cavity based on the RTF ground-based data for the centerline at X=20-in is length 2.749-in, depth 0.377-in, and width 0.916-in (see Table 4). These dimensions were selected based on feedback from the RTF

Cavity Heating Team who recommended a cavity with a length-to-depth ratio of L/D=7.3. Note, since Version 1 of the RTF BLT Tool, as mentioned earlier, is based on the LATCH engineering code and not the GASP code used here, these calculated dimensions cannot be considered exact and analysis continues to define the exact scaling between the two codes. For this reason, rounding off of the calculated dimensions to two significant digits seemed appropriate. The final height dimension for both protuberances was 0.07-in. The final cavity dimensions were 2.75-in length, 0.38-in depth, and 0.92-in width.

4.2.2 Instrumentation

The surface thermocouple layout, shown in Figures 14 and 15, was primarily dedicated to provide adequate coverage for identifying the movement of transition during the flight. Of the 99 surface thermocouples, 82 sensors were intended for identifying the transition onset on the face of the wedge, four sensors were on the shoulder regions, and the remaining 13 sensors were located in and around the BL trips (shown in the inset of Figure 14). The sensors in the vicinity of the trips were to obtain local heating information during the flight. For the protuberances, one thermocouple was placed on the top center of the "pizza box", while another was placed in front of the "gap filler", both with two additional sensors behind each element at X=21 and 22-in. On the cavity floor, a distribution of sensors is placed along the centerline at X = 20.5, 21, 21.5, 22, and 22.5-in, while two are placed at Y = ±0.35-in at X = 22.25-in. All Side B sensors are considered low-frequency instrumentation, sampled at 100 sps (all thermocouples, including those on Side A, are sampled at this lower rate).

5. Verification of Instruments and Sensor Functions by Flight Data

HyBoLT, mounted on the top of the ALV X-1 rocket, was launched from the Launch Pad 0B at Wallops Flight Facility of NASA Goddard Space flight Center, Wallops Island, Virginia at 5:10 am EDT on August 22, 2008. Unfortunately a problem in the flight control system caused the vehicle to veer off the designed flight course. Launch officials activated a self-destruct mechanism in the rocket's nose cone after 20 seconds into the flight. Figure 16 shows that the Mach number and the Reynolds number only reached approximately Mach 1 and $9x10^6$ per foot respectively, at the end of flight. These flight conditions were far below the designed test conditions and no boundary layer transition was observed in this flight range. Although the angle of attack, α, the angle of yaw, β, and the total angle of attack, α_{Tot}, approached the designed zero angle during the flight, they never stabilized, as shown in Figure 17. Therefore, the flight data from the HyBoLT instrumentation and sensors will not provide any useful information to serve the original designed scientific objectives. All data presented in this report only provide verification of the functioning of the onboard instruments and sensors.

Detailed instrument lists for Side A and Side B are summarized in Tables 6 and 7, respectively. Additional miscellaneous instruments, such as the vibrometer, accelerometers, differential pressure gauges, secondary pressure gauges, isothermal blocks for the thermocouple reference temperature, etc., are listed in Table 8. Cross-reference to instruments by the ID name used in these tables will facilitate the following discussions of HyBoLT data. Most of the HyBoLT data are presented in engineering units in terms of temperatures (ºF), pressures (psia), etc., except the hot-film data is in milli-volts (mV) or volts (V). Because of lack of scientific value, further data reduction to get physical quantities, such as flow velocities, flow angles, Mach numbers and Reynolds numbers, etc., has not been pursued. All data presented in the following sections are during (*T0*-10s) to (*T0*+20s), where *T0* is the ALV X-1 rocket liftoff time, i.e., flight time zero.

5.1 Thermocouple Data

All thermocouple data for Side A and Side B are presented in Figures 18a-18i and 19a-19k, respectively. During the pre-launch sensor verification check, five thermocouples had been noted as being suspect: TA045, TA056, TB006, TB052, and TB099, while four others were deemed questionable: TA035, TB039, TB065, and TB094. Of those only four were identified as bad thermocouples during flight, TA035 in Figure 18d, TA056 in Figure 18g, TB006 in Figure 19a and TB065 in Figure 19h. Generally all thermocouples indicate a steady and rapid temperature

rise approximately 12 seconds after liftoff. But, only the thermocouples on Side B show a jump up about 0.1 ºF around 1 second after liftoff. This small temperature jump is thought to be attributed to an electronic instrumentation glitch caused by improper grounding between the thermocouples and the isothermal reference blocks. During pre-launch checks, these grounding issues were noted during power switching activities. It is believed that an internal power switch occurred at around that time during launch. Table 9 shows the connection scheme of thermocouples to the reference temperature blocks. Totally sixteen reference temperature blocks were used with eleven thermocouples connected to each block separately. The reference temperature readings from each block are plotted in Figures 20a and 20b. For some unknown reasons, the reference temperature blocks, TRTC11, TRTC12, TRTC15 and TRTC16, show about 2 ºF higher readings than others as indicated in Figure 20b and noted in Table 9. Higher reference temperatures cause the thermocouples connected to these blocks to read about 8 ºF higher than normal. A spread of less than 2 °F is within the experimental uncertainty for these Type-T thermocouples, but the 8 °F spread is likely due to the anomalies with the suspect isothermal blocks. Such anomalies in the reference temperature blocks should be investigated for future tests.

5.2 Surface Static Pressure Data

There are 14 surface static pressure ports on Side A with 7 each on the starboard (positive *Y*) and port (negative *Y*) sides and none Side B. As shown in Figures 21a and 21b, all surface static pressures were decreasing smoothly after liftoff until about 3 seconds (*T0*+17s) before the vehicle destruction. Afterward, the extraneous pressure readings indicate that the vehicle underwent erratic motions just moment before the end of flight. Also, the surface static pressure pattern is not symmetric on the starboard and port sides. That is probably attributed to the nonzero angle of yaw, as shown in Figure 22a and further discussed in the next section.

5.3 Differential Pressure Data for Angle of Attack and Angle of Yaw

The directly measured differential pressure data PAOA01 and PAOA02 for the angle of attack, α, and PYAW01 and PYAW02 for the angle of yaw, β, are plotted in Figure 22a along with the computed differential pressures DpAOA1 and DpAOA2 for α and DpAOY1 and DpAOY2 for β computed from the surface static pressures. The individual static pressures are shown in Figure 22b, for the corresponding pairs of pressure ports. Their relationships are listed in Table 10. It is suspected that PSB02 and PSA17 had insufficient zero offsets as indicated by their relatively low readings before approximately (*T0*+5s), as shown in Figure 22b. That, in turn, causes relatively low computed DpAOA2 and DpAOY1 at the flight time less than (*T0*+5s), as shown in Figure 22a. Also, it is suspected that there might have been a leak in the tube connections for PAOA02, PSB02 and PSB02S. Note that these three pressure transducers were connected to the same surface pressure port by split junctions. A leak in the tube connection would cause higher correspondent readings than those of PAOA01 (or, DpAOA1) in Figure 22a and PSB01 in Figure 22b at the flight time greater than (*T0*+13s). The vehicle erratic motion before the end of flight discussed previously is also observed in these data.

5.4 Boundary-Layer Pressure Rake Data

There were two ‘probeless’ boundary-layer pressure rakes, with one on each side, installed on HyBoLT. The one on Side A is off centerline at $Y = +4.0$ inches and the other one on Side B is on the centerline. Both rakes were located at $X \approx 85.0$ inches from the virtual leading edge. Figures 23a and 23b show the time traces of total pressures measured by the rake on Side A and Side B, respectively. The total pressure data measured by the Side A rake appear to reveal the vehicle’s erratic motion before the end of flight but not by the Side B data.

The boundary-layer profiles in terms of total pressures measured by the pressures rakes are plotted in Figures 24a to 24e for flight times at (*T0*+5.00s), (*T0*+10.00s), (*T0*+15.00s), (*T0*+18.20s), and (*T0*+20.15s), respectively. It shows the boundary layer thickness increasing with the flight time becoming larger than the height of the pressure rake on Side A, i.e., under expansion with a positive angle of attack as shown in Figure 22a, approaching to the end of flight.

5.5 Differential Pressure Data for Flow Angle at Boundary-Layer Pressure Rakes

The flow angles, ϕ_A and ϕ_B at the boundary-layer pressure rakes on Side A and Side B, represented by the measured differential pressure data PRSA11 and PRSB01 are plotted in Figure 25 along with the differential pressures DPRSA and DPRSB. The individual pressures that are used to compute DPRSA and DPRSB are also shown in the figure. Their relationships are listed in Table 11. The measured and the computed differential pressures represented by lines and symbols, respectively, match to each other quiet well. Except for the time period approximately from (*T0*+16.2s) to (*T0*+18.8s), the differential pressure transducer for PRSA11 was over range (+/-5 psid). Also, the pressure readings of PRSA12 (25 psia gauge) and its spare PRSA1S (75 psia gauge) match to each other very well. All these data showing a negative flow angle indicate that the vehicle was turning to the right (starboard) during the flight.

5.6 Acceleration Data

Figure 26 presents the vehicle acceleration data measured by the 3-axis accelerometers installed under the surface. Before takeoff, the vehicle axial direction (*X*-axis) was normal to the ground surface and the *X*-axis accelerometer read 1 G. During the flight, the major acceleration was along the vehicle axial direction.

5.7 Surface Hot-Film Data

There were two surface hot-film gages, with one located in the Mach 3 zone and another one in the Mach 4.2 zone of the predicted crossflow transition regions. Figure 27 presents the DC voltage outputs from different sensing filaments on each gage. Before takeoff, the different levels of the DC voltage output were attributed to the different inherent resistance associated with each individual sensing filament. Generally, all sensing filaments showed increasing DC voltage outputs during the flight, except HF3P52. Also, the DC voltage outputs of HF3P51, HF3P52 and HF3P53 showed a flat drop from (*T0*+8.3s) to (*T0*+10.8s). These observations could be related to the measured hot-film AC signals. Figures 28a, 28b, 29a and 29b present the selected hot-film time series data and Figures 30a and 30b present the standard deviation data. It is indicated that HF3A52, as shown in Figures 29b and 30b, is not so sensitive in response to air flow fluctuations as compared to other sensing filaments. The flat drop of DC voltage outputs of HF3P51, HF3P52 and HF3P53 is correspondent to the relatively quiescent period observed by HF3A51, HF3A52 and HF3A53, as shown in Figures 30b and 29a. It is surmised that a pocket of cool air or a drop of water passed over that hot-film gage during that flight time. Or, it could be simply another electronic glitch.

Figures 31 and 32 present the amplitude spectra of hot-film data for the frequency band from 100 Hz up to 5 kHz or 25 kHz, depending on the preset filter band and the data sampling rates. These spectra generally represent the broadband turbulent signals with magnitudes increasing with the flight time.

5.8 Dynamic Pressure Data from Three-Dynamic-Pressure Gages

There were two three-dynamic-pressure gages with one each located on the starboard and port sides separately. Figures 33a, 33b, 34a and 34b present the selected time series of pressure fluctuation data and Figures 35a and 35b show the variations of their maxima during the flight. All data show peak fluctuations within 5 seconds right after launch. After that, the pressure fluctuations increase with time until the end of flight. Figures 36 and 37 show the typical turbulent amplitude spectra processed from the correspondent time series data of Figures 33 and 34. However, the onboard DSP processed amplitude spectra of these gages, as shown in Figures 38 and 39 only indicate signals within the frequency band of 100 Hz to 1.5 kHz near the beginning and/or the end of flight. It is suspected that the onboard DSP data processing had problems.

5.9 Dynamic Data from Other Dynamic Pressure Gages, Freestream Probe and Vibrometer

All onboard processed amplitude spectra of the surface dynamic pressure gages, the freestream dynamic pressure probe and the embedded vibrometer, as shown in Figures 40, 41, 42 and 43, show the similar questionable spectral distributions as the three-dynamic-pressure gages. The DSP team is investigating this problem.

6. Concluding Remarks

Details of the unsuccessful HyBoLT flight experiment are provided, including the objectives and approach associated with each experimental program, with limited data during the short-life flight. It verifies that most of the sensors were functioning normally and presented typical turbulent boundary-layer flow signals. Plausible explanations are provided to explain most of the observed flight data results and abnormalities except that the behavior of some dynamic data, discussed at the end of last section, is still under investigation. A valuable lesson learned in this flight experiment is that it is crucial to collect the critical data in various forms for cross-verification. Doing so provides multiple clues to investigate any abnormal results in post flight data analysis.

7. Acknowledgments

The following individuals have provided significant support of the HyBoLT flight experiment: Mary Wusk, Mark Croom, Steve Syrett, Mike Alexander, Manuel Salas, Sharon Graves, Rudy King, Kamran Daryabeigi, Scott Holland, Tom Jentink, Randy Voland, Mujeeb Malik, Ponnampalam Balakumar, George Beeler, Stephen Wilkinson, Mike Scott, Walter Bruce, Vincent Cruz, Carol Harrison and Philip Hamory from NASA; and Warren Frick, Alex Betti, Robert Foelsche, Mike Touma, Greg Wurst, and Dan Tilmont from ATK.

References

1. Wurster, K. E., Riley, C. J., and Zoby, E. V., "Engineering Aerothermal Analysis for X-34 Thermal Protection System Design," *Journal of Spacecraft and Rockets*, Vol.36, No.2, March-April 1999, pp. 216-228.

2. Reshotko, E., "Boundary Layer Stability and Transition," *Annual Review of Fluid Mechanics*, Vol. 8, pp. 311-349, 1976.

3. Malik, M. R., Li, F., Choudhari, M. M., and Chang, C. L., "Secondary instability of crossflow vortices and swept-wing boundary-layer transition", *J. Fluid Mechanics*, Vol. 399, pp. 85-115, 1999.

4. Malik, M. R., "Prediction and Control of Transition in Supersonic and Hypersonic Boundary Layers," *AIAA Journal*, Vol. 27, No. 11, pp. 1487-1493, 1989.

5. Reshotko, E., "Transition Issues for Atmospheric Entry," AIAA Paper 2007-0304, Jan. 2007.

6. Berry, S. A., Horvath, T. J., Greene, F. A., Kinder, G. R., and Wang, K. C., "Overview of Boundary Layer Transition Research in Support of Orbiter Return To Flight," AIAA-2006-2918, June 2006.

7. Campbell, C., Anderson, B., Bourland, G., Bouslog, S., Cassady, A., Horvath, T., Berry, S., Gnoffo, P., Wood, B., Reuther, J., Driver, D., Chao, D., and Picetti, D., "Orbiter Return To Flight Entry Aeroheating," AIAA-2006-2917, June 2006.

8. Greene, F. A., and Hamilton, H., "Development of a Boundary Layer Properties Interpolation Tool in Support of Orbiter Return-To-Flight," AIAA-2006-2920, June 2006.

9. McGinley, C., Berry, S. A., Kinder, G. R., Barnwell, M., Wang, K. C., and Kirk, B. S., "Review of Orbiter Flight Boundary Layer Transition Data," AIAA-2006-2921, June 2006.

10. Berry, S. A., Horvath, T. J., Cassady, A. M., Kirk, B. S., Wang, K.C., and Hyatt, A. J., "Boundary Layer Transition Results From STS-114," AIAA-2006-2922, June 2006.

11. Malik, M. R., "eMalik3d: An e^N Code for Three-Dimensional Flow over Finite-Swept Wings," High Technology report No. HTC-9502 (version 2), April 1995.

12. Horvath, T. J., Berry, S. A., Merski, N. R., Berger, K. T., Liechty, D. S., Buck, G. M., and Schneider, S. P., "Shuttle Damage/Repair From the Perspective of Hypersonic Boundary Layer Transition – Experimental Results," AIAA-2006-2918, June 2006.

13. King, R. A., Kegerise, M. A., and Berry, A. A., "Version 2 of the Protuberance Correlations for the Shuttle-Orbiter Boundary Layer Transition Tool," NASA TP-2009-215951, December 2009.

14. Hamilton, H. H., II, Greene, F. A., and DeJarnette, F. R., "Approximate Method for Calculating Heating Rates on Three-Dimensional Vehicles," *Journal of Spacecraft and Rockets*, Vol.31, No.3, 1994, pp. 345-354.

Table 1. Key nominal trajectory points prior to Stage 1 burn-out.

TIME (S)	MACH	ALTITUDE (FT)	RANGE (NMI)	VELOCITY (FT/SEC)	ANGLE OF ATTACK (DEG)	REYNOLDS NUMBER
35.5	3.0	34468	3.7	2961.3	0.03	7.42E+06
42.5	4.2	52993	6.3	4063.6	0.03	4.32E+06
49.2	5.5	76025	9.8	5362.2	0.04	1.85E+06
51.5	6.0	85599	11.3	5888.1	-0.13	1.27E+06
54.0	6.6	96438	13.1	6490.7	-0.17	8.28E+05
56.0	7.1	106032	14.6	7029.6	-0.20	5.66E+05
58.0	7.5	116359	16.3	7611.9	-0.23	3.63E+05
60.0	8.0	127482	18.2	8252.2	-0.27	2.29E+05
62.0	8.5	139489	20.2	8965.2	-0.30	1.42E+05

Table 2. Local edge properties at key trajectory points for outboard trip station (X=20 Y=0)

Mach	δ (in)	δ^* (in)	θ (in)	Re_θ/M_e	M_e	T_e/T_w
3.0	0.0358	0.0135	0.0043	779.89	1.947	1.039
4.2	0.0631	0.0208	0.0077	436.77	2.282	1.413
5.5	0.1249	0.0338	0.0153	220.66	2.548	1.982
6.0	0.1542	0.0439	0.0202	169.50	2.618	2.260
6.5	0.2019	0.0563	0.0263	132.30	2.718	2.526
7.0	0.2721	0.0750	0.0341	105.99	2.849	2.765
7.5	0.3475	0.1028	0.0450	80.16	2.996	3.059
8.0	0.4680	0.1514	0.0581	63.12	3.246	3.238
8.5	0.5847	0.2111	0.0714	49.52	3.526	3.362

Table 3. Local edge properties at key trajectory points for centerline trip station (X=20 Y=±5).

Mach	δ (in)	δ^* (in)	θ (in)	Re_θ/M_e	M_e	T_e/T_w
3.0	0.0338	0.0124	0.0039	678.31	1.996	1.017
4.2	0.0591	0.0190	0.0072	394.63	2.300	1.401
5.5	0.1216	0.0323	0.0146	208.73	2.560	1.972
6.0	0.1508	0.0424	0.0195	161.33	2.632	2.247
6.5	0.1973	0.0542	0.0253	125.84	2.733	2.512
7.0	0.2508	0.0699	0.0326	99.13	2.837	2.775
7.5	0.3559	0.1029	0.0438	77.65	3.036	3.013
8.0	0.4680	0.1495	0.0565	60.80	3.275	3.200
8.5	0.5767	0.2046	0.0697	47.32	3.535	3.350

Table 4. Trip dimensions at key trajectory points for centerline trip station (X=20 Y=0).

Mach	k_{inc} (in)	k_{inc}/δ	V_{cavity}	L (in)	D (in)	W (in)
3.0	0.0012	0.0346	0.0001	0.1094	0.0150	0.0365
4.2	0.0039	0.0618	0.0011	0.2927	0.0401	0.0976
5.5	0.0153	0.1224	0.0309	0.8784	0.1203	0.2928
6.0	0.0246	0.1593	0.0872	1.2407	0.1700	0.4136
6.5	0.0412	0.2041	0.2860	1.8434	0.2525	0.6145
7.0	0.0693	0.2547	0.9485	2.7489	0.3766	0.9163
7.5	0.1171	0.3368	2.9483	4.0118	0.5496	1.3373
8.0	0.2002	0.4278	10.0396	6.0356	0.8268	2.0119
8.5	0.3188	0.5452	30.4456	8.7362	1.1967	2.9121

Table 5. Trip dimensions at key trajectory points for outboard trip station (X=20 Y=±5).

Mach	k_{inc} (in)	k_{inc}/δ	V_{cavity}	L (in)	D (in)	W (in)
3.0	0.0013	0.0398	0.0001	0.1341	0.0184	0.0447
4.2	0.0040	0.0684	0.0016	0.3297	0.0452	0.1099
5.5	0.0157	0.1294	0.0387	0.9464	0.1296	0.3155
6.0	0.0252	0.1674	0.1071	1.3288	0.1820	0.4299
6.5	0.0423	0.2146	0.3518	1.9750	0.2705	0.6583
7.0	0.0683	0.2724	1.0376	2.8324	0.3880	0.9441
7.5	0.1238	0.3477	3.9071	4.4065	0.6036	1.4688
8.0	0.2078	0.4441	12.6137	6.5127	0.8922	2.1709
8.5	0.3291	0.5706	37.3981	9.3562	1.2817	3.1187

Table 6. Side A detailed instrument list.

Name	Description	Diff Ref / Cross-Corr	Station Location			Instrument				Output	Sample Rate
			X (in)	Y (in)	Z (in)	Range	Typ. Accuracy	Units	Make / Model / Module	Volts	SPS
PSA01	Static Pressure Port	PDA13	38.000	11.000	-3.271	0-15	+/-0.1% FSO	psia	KUL-ETM-15A	0-5 VDC	305.2
PSA02	Static Pressure Port	P3DA1/PDA14	59.500	7.000	-6.251	0-15	+/-0.1% FSO	psia	KUL-ETM-15A	0-5 VDC	305.2
PSA03	Static Pressure Port		68.500	7.000	-7.130	0-15	+/-0.1% FSO	psia	KUL-ETM-15A	0-5 VDC	305.2
PSA04	Static Pressure Port		77.500	7.000	-7.945	0-15	+/-0.1% FSO	psia	KUL-ETM-15A	0-5 VDC	305.2
PSA05	Static Pressure Port		85.000	7.000	-8.589	0-15	+/-0.1% FSO	psia	KUL-ETM-15A	0-5 VDC	305.2
PSA06	Static Pressure Port		85.000	5.000	-8.922	0-15	+/-0.1% FSO	psia	KUL-ETM-15A	0-5 VDC	305.2
PSA07	Static Pressure Port		85.000	3.000	-8.934	0-15	+/-0.1% FSO	psia	KUL-ETM-15A	0-5 VDC	305.2
PSA08	AOA Sensor 1 - Static Absolute - A Side	-PAOA01	81.000	0.000	-8.513	0-15	+/-0.1% FSO	psia	KUL-ETM-15A	0-5 VDC	610.0
PSA09	AOA Sensor 2 - Static Absolute - A Side	-PAOA02/PSA09S	84.000	0.000	-8.829	0-15	+/-0.1% FSO	psia	KUL-ETM-15A	0-5 VDC	610.0
PSA10	Static Pressure Port	PDA1,2,3,4,5,6,15	38.000	-11.000	-3.271	0-15	+/-0.1% FSO	psia	KUL-ETM-15A	0-5 VDC	305.2
PSA11	Static Pressure Port	P3DA2/PDA16	59.500	-7.000	-6.251	0-15	+/-0.1% FSO	psia	KUL-ETM-15A	0-5 VDC	305.2
PSA12	Static Pressure Port		68.500	-7.000	-7.130	0-15	+/-0.1% FSO	psia	KUL-ETM-15A	0-5 VDC	305.2
PSA13	Static Pressure Port		77.500	-7.000	-7.945	0-15	+/-0.1% FSO	psia	KUL-ETM-15A	0-5 VDC	305.2
PSA14	Static Pressure Port		85.000	-7.000	-8.589	0-15	+/-0.1% FSO	psia	KUL-ETM-15A	0-5 VDC	305.2
PSA15	Static Pressure Port		85.000	-5.000	-8.922	0-15	+/-0.1% FSO	psia	KUL-ETM-15A	0-5 VDC	305.2
PSA16	Static Pressure Port		85.000	-3.000	-8.934	0-15	+/-0.1% FSO	psia	KUL-ETM-15A	0-5 VDC	305.2
PSA17	Yaw Sensor 1 - Static Absolute - Left Side	+PYAW01	34.000	12.620	0.000	0-15	+/-0.1% FSO	psia	KUL-ETM-15A	0-5 VDC	610.0
PSA18	Yaw Sensor 2 - Static Absolute - Left Side	+PYAW02	39.000	12.719	0.000	0-15	+/-0.1% FSO	psia	KUL-ETM-15A	0-5 VDC	305.2
PSA19	Yaw Sensor 1 - Static Absolute - Right Side	-PYAW01	34.000	-12.620	0.000	0-15	+/-0.1% FSO	psia	KUL-ETM-15A	0-5 VDC	610.0
PSA20	Yaw Sensor 2 - Static Absolute - Right Side	-PYAW02	39.000	-12.719	0.000	0-15	+/-0.1% FSO	psia	KUL-ETM-15A	0-5 VDC	305.2
PDA01	Dynamic Pressure Port (Med Frequency)	PSA10	19.000	-7.700	-1.997	+/-5	0.25% FSO	psid	KUL-XCS-062-5D	0.5-4.5 VDC	20000
PDA02	Dynamic Pressure Port (Med Frequency)	PSA10	18.900	-7.200	-1.986	+/-5	0.25% FSO	psid	KUL-XCS-062-5D	0.5-4.5 VDC	20000
PDA03	Dynamic Pressure Port (Med Frequency)	PSA10	18.800	-6.700	-1.976	+/-5	0.25% FSO	psid	KUL-XCS-062-5D	0.5-4.5 VDC	20000
PDA04	Dynamic Pressure Port (Med Frequency)	PSA10	18.700	-6.200	-1.965	+/-5	0.25% FSO	psid	KUL-XCS-062-5D	0.5-4.5 VDC	20000
PDA05	Dynamic Pressure Port (Med Frequency)	PSA10	18.600	-5.700	-1.955	+/-5	0.25% FSO	psid	KUL-XCS-062-5D	0.5-4.5 VDC	20000
PDA06	Dynamic Pressure Port (Med Frequency)	PSA10	18.500	-5.200	-1.944	+/-5	0.25% FSO	psid	KUL-XCS-062-5D	0.5-4.5 VDC	20000
PDA13	Dynamic Pressure Port (High Frequency)	PSA01	38.000	10.000	-3.779	+/-5	0.25% FSO	psid	KUL-XCS-062-5D	0.5-4.5 VDC	100000
PDA14	Dynamic Pressure Port (High Frequency)	PSA02	50.500	7.000	-5.308	+/-5	0.25% FSO	psid	KUL-XCS-062-5D	0.5-4.5 VDC	100000
PDA15	Dynamic Pressure Port (High Frequency)	PSA10	38.000	-10.000	-3.779	+/-5	0.25% FSO	psid	KUL-XCS-062-5D	0.5-4.5 VDC	100000
PDA16	Dynamic Pressure Port (High Frequency)	PSA11	50.500	-7.000	-5.308	+/-5	0.25% FSO	psid	KUL-XCS-062-5D	0.5-4.5 VDC	100000
P3DA11	3-Dynamic Pressure Port (High Frequency) #1	PSA02	44.000	7.000	-4.625	+/-5	0.25% FSO	psid	KUL-XCS-062-5D	0.5-4.5 VDC	100000
P3DA12	3-Dynamic Pressure Port (High Frequency) #2	PSA02	44.000	7.000	-4.625	+/-5	0.25% FSO	psid	KUL-XCS-062-5D	0.5-4.5 VDC	100000
P3DA13	3-Dynamic Pressure Port (High Frequency) #3	PSA02	44.000	7.000	-4.625	+/-5	0.25% FSO	psid	KUL-XCS-062-5D	0.5-4.5 VDC	100000
P3DA21	3-Dynamic Pressure Port (Med Frequency) #1	PSA11	44.000	-7.000	-4.625	+/-5	0.25% FSO	psid	KUL-XCS-062-5D	0.5-4.5 VDC	20000
P3DA22	3-Dynamic Pressure Port (Med Frequency) #2	PSA11	44.000	-7.000	-4.625	+/-5	0.25% FSO	psid	KUL-XCS-062-5D	0.5-4.5 VDC	20000
P3DA23	3-Dynamic Pressure Port (Med Frequency) #3	PSA11	44.000	-7.000	-4.625	+/-5	0.25% FSO	psid	KUL-XCS-062-5D	0.5-4.5 VDC	20000
PFSD01	FreeStream Dynamic Pressure Probe	PRTA18	84.817	-4.000	-10.674	+/-5	0.25% FSO	psid	KUL-XCS-062-5D	0.5-4.5 VDC	100000

Table 6. Side A detailed instrument list (Continued).

Name	Description	Diff Ref / Cross-Corr	Station Location			Instrument				Output	Sample Rate
			X (in)	Y (in)	Z (in)	Range	Typ. Accuracy	Units	Make / Model / Module	Volts	SPS
PRTA11	Pressure Rake (Probless Pitot) #T1		84.993	4.000	-8.997	0-75	+/-0.1% FSO	psia	KUL-ETM-75A	0-5 VDC	305.2
PRTA12	Pressure Rake (Probless Pitot) #T2		84.987	4.000	-9.058	0-75	+/-0.1% FSO	psia	KUL-ETM-75A	0-5 VDC	305.2
PRTA13	Pressure Rake (Probless Pitot) #T3		84.980	4.000	-9.129	0-75	+/-0.1% FSO	psia	KUL-ETM-75A	0-5 VDC	305.2
PRTA14	Pressure Rake (Probless Pitot) #T4		84.969	4.000	-9.232	0-75	+/-0.1% FSO	psia	KUL-ETM-75A	0-5 VDC	305.2
PRTA15	Pressure Rake (Probless Pitot) #T5		84.953	4.000	-9.381	0-75	+/-0.1% FSO	psia	KUL-ETM-75A	0-5 VDC	305.2
PRTA16	Pressure Rake (Probless Pitot) #T6		84.928	4.000	-9.618	0-75	+/-0.1% FSO	psia	KUL-ETM-75A	0-5 VDC	305.2
PRTA17	Pressure Rake (Probless Pitot) #T7		84.883	4.000	-10.051	0-75	+/-0.1% FSO	psia	KUL-ETM-75A	0-5 VDC	305.2
PRTA18	Pressure Rake (Probless Pitot) #T8	PFSD01	84.817	4.000	-10.674	0-75	+/-0.1% FSO	psia	KUL-ETM-75A	0-5 VDC	305.2
PRSA11	Pressure Rake (Probless Pitot) #S1 - Differential	PRSA-12/+13	85.403	4.000	0.000	+/-5	+/-0.1% FSO	psid	KUL-XTL-3-375-5D	0-5 VDC	610
PRSA12	Pressure Rake (Probless Pitot) #S2 - Static Absolute	-PRSA11/PRSA1S	85.403	3.898	-10.485	0-25	+/-0.1% FSO	psia	KUL-ETM-25A	0-5 VDC	610
PRSA13	Pressure Rake (Probless Pitot) #S3 - Static Absolute	+PRSA11	85.403	4.102	-10.485	0-25	+/-0.1% FSO	psia	KUL-ETM-25A	0-5 VDC	610
TA001	Thermocouple (only this TC under skin)		3.300	0.000	0.000	-328-750	1.8 or 0.75%	deg F	TC-T-L	-6→+21mV	152.5
TA002	Thermocouple		11.000	0.000	-1.156	-328-750	1.8 or 0.75%	deg F	TC-T-90-11521	-6→+21mV	152.5
TA003	Thermocouple		20.000	0.000	-2.102	-328-750	1.8 or 0.75%	deg F	TC-T-90-11521	-6→+21mV	152.5
TA004	Thermocouple		29.000	0.000	-3.048	-328-750	1.8 or 0.75%	deg F	TC-T-90-11521	-6→+21mV	152.5
TA005	Thermocouple		38.000	0.000	-3.994	-328-750	1.8 or 0.75%	deg F	TC-T-0-11522	-6→+21mV	152.5
TA006	Thermocouple		46.000	0.000	-4.835	-328-750	1.8 or 0.75%	deg F	TC-T-90-11521	-6→+21mV	152.5
TA007	Thermocouple		55.000	0.000	-5.781	-328-750	1.8 or 0.75%	deg F	TC-T-90-11521	-6→+21mV	152.5
TA008	Thermocouple		64.000	0.000	-6.727	-328-750	1.8 or 0.75%	deg F	TC-T-90-11517	-6→+21mV	152.5
TA009	Thermocouple		73.000	0.000	-7.673	-328-750	1.8 or 0.75%	deg F	TC-T-90-11517	-6→+21mV	152.5
TA010	Thermocouple		16.750	7.750	-1.761	-328-750	1.8 or 0.75%	deg F	TC-T-0-11522	-6→+21mV	152.5
TA011	Thermocouple		16.750	6.000	-1.761	-328-750	1.8 or 0.75%	deg F	TC-T-90-11521	-6→+21mV	152.5
TA012	Thermocouple		13.500	7.000	-1.419	-328-750	1.8 or 0.75%	deg F	TC-T-0-11522	-6→+21mV	152.5
TA013	Thermocouple		11.000	5.000	-1.156	-328-750	1.8 or 0.75%	deg F	TC-T-90-11521	-6→+21mV	152.5
TA014	Thermocouple		11.000	3.000	-1.156	-328-750	1.8 or 0.75%	deg F	TC-T-90-11521	-6→+21mV	152.5
TA015	Thermocouple		24.500	7.750	-2.575	-328-750	1.8 or 0.75%	deg F	TC-T-0-11522	-6→+21mV	152.5
TA016	Thermocouple		24.500	4.000	-2.575	-328-750	1.8 or 0.75%	deg F	TC-T-90-11521	-6→+21mV	152.5
TA017	Thermocouple		20.000	7.000	-2.102	-328-750	1.8 or 0.75%	deg F	TC-T-0-11522	-6→+21mV	152.5
TA018	Thermocouple		20.000	5.000	-2.102	-328-750	1.8 or 0.75%	deg F	TC-T-90-11521	-6→+21mV	152.5
TA019	Thermocouple		20.000	3.000	-2.102	-328-750	1.8 or 0.75%	deg F	TC-T-90-11521	-6→+21mV	152.5
TA020	Thermocouple		33.500	6.000	-3.521	-328-750	1.8 or 0.75%	deg F	TC-T-90-11521	-6→+21mV	152.5
TA021	Thermocouple		33.500	4.000	-3.521	-328-750	1.8 or 0.75%	deg F	TC-T-90-11521	-6→+21mV	152.5
TA022	Thermocouple		29.000	7.000	-3.048	-328-750	1.8 or 0.75%	deg F	TC-T-0-11522	-6→+21mV	152.5
TA023	Thermocouple		29.000	5.000	-3.048	-328-750	1.8 or 0.75%	deg F	TC-T-90-11521	-6→+21mV	152.5
TA024	Thermocouple		29.000	3.000	-3.048	-328-750	1.8 or 0.75%	deg F	TC-T-90-11521	-6→+21mV	152.5
TA025	Thermocouple		37.000	10.000	-3.968	-328-750	1.8 or 0.75%	deg F	TC-T-0-11522	-6→+21mV	152.5
TA026	Thermocouple		38.000	7.000	-3.994	-328-750	1.8 or 0.75%	deg F	TC-T-0-11522	-6→+21mV	152.5
TA027	Thermocouple		38.000	5.000	-3.994	-328-750	1.8 or 0.75%	deg F	TC-T-0-11522	-6→+21mV	152.5
TA028	Thermocouple		38.000	3.000	-3.994	-328-750	1.8 or 0.75%	deg F	TC-T-0-11522	-6→+21mV	152.5
TA029	Thermocouple		46.000	7.000	-4.835	-328-750	1.8 or 0.75%	deg F	TC-T-90-11521	-6→+21mV	152.5
TA030	Thermocouple		46.000	5.000	-4.835	-328-750	1.8 or 0.75%	deg F	TC-T-90-11521	-6→+21mV	152.5
TA031	Thermocouple		46.000	3.000	-4.835	-328-750	1.8 or 0.75%	deg F	TC-T-90-11521	-6→+21mV	152.5
TA032	Thermocouple		55.000	7.000	-5.781	-328-750	1.8 or 0.75%	deg F	TC-T-90-11521	-6→+21mV	152.5
TA033	Thermocouple		55.000	5.000	-5.781	-328-750	1.8 or 0.75%	deg F	TC-T-90-11521	-6→+21mV	152.5
TA034	Thermocouple		55.000	3.000	-5.781	-328-750	1.8 or 0.75%	deg F	TC-T-90-11521	-6→+21mV	152.5
TA035	Thermocouple		64.000	7.000	-6.700	-328-750	1.8 or 0.75%	deg F	TC-T-90-11517	-6→+21mV	152.5

Table 6. Side A detailed instrument list (Continued).

Name	Description	Diff Ref / Cross-Corr	Station Location			Instrument				Output	Sample Rate
			X (in)	Y (in)	Z (in)	Range	Typ. Accuracy	Units	Make / Model / Module	Volts	SPS
TA036	Thermocouple		64.000	5.000	-6.727	-328-750	1.8 or 0.75%	deg F	TC-T-90-11517	-6→+21mV	152.5
TA037	Thermocouple		64.000	3.000	-6.727	-328-750	1.8 or 0.75%	deg F	TC-T-90-11517	-6→+21mV	152.5
TA038	Thermocouple		73.000	7.000	-7.545	-328-750	1.8 or 0.75%	deg F	TC-T-90-11517	-6→+21mV	152.5
TA039	Thermocouple		73.000	5.000	-7.673	-328-750	1.8 or 0.75%	deg F	TC-T-90-11517	-6→+21mV	152.5
TA040	Thermocouple		73.000	3.000	-7.673	-328-750	1.8 or 0.75%	deg F	TC-T-90-11517	-6→+21mV	152.5
TA041	Thermocouple		82.000	7.000	-8.335	-328-750	1.8 or 0.75%	deg F	TC-T-90-11517	-6→+21mV	152.5
TA042	Thermocouple		82.000	5.000	-8.619	-328-750	1.8 or 0.75%	deg F	TC-T-90-11517	-6→+21mV	152.5
TA043	Thermocouple		82.000	3.000	-8.619	-328-750	1.8 or 0.75%	deg F	TC-T-90-11517	-6→+21mV	152.5
TA044	Thermocouple		16.750	-7.750	-1.761	-328-750	1.8 or 0.75%	deg F	TC-T-0-11522	-6→+21mV	152.5
TA045	Thermocouple		16.750	-6.000	-1.761	-328-750	1.8 or 0.75%	deg F	TC-T-90-11521	-6→+21mV	152.5
TA046	Thermocouple		13.500	-7.000	-1.419	-328-750	1.8 or 0.75%	deg F	TC-T-0-11522	-6→+21mV	152.5
TA047	Thermocouple		11.000	-5.000	-1.156	-328-750	1.8 or 0.75%	deg F	TC-T-90-11521	-6→+21mV	152.5
TA048	Thermocouple		11.000	-3.000	-1.156	-328-750	1.8 or 0.75%	deg F	TC-T-90-11521	-6→+21mV	152.5
TA049	Thermocouple		24.500	-7.750	-2.575	-328-750	1.8 or 0.75%	deg F	TC-T-0-11522	-6→+21mV	152.5
TA050	Thermocouple		24.500	-4.000	-2.575	-328-750	1.8 or 0.75%	deg F	TC-T-90-11521	-6→+21mV	152.5
TA051	Thermocouple		20.000	-7.000	-2.102	-328-750	1.8 or 0.75%	deg F	TC-T-0-11522	-6→+21mV	152.5
TA052	Thermocouple		20.000	-5.000	-2.102	-328-750	1.8 or 0.75%	deg F	TC-T-90-11521	-6→+21mV	152.5
TA053	Thermocouple		20.000	-3.000	-2.102	-328-750	1.8 or 0.75%	deg F	TC-T-90-11521	-6→+21mV	152.5
TA054	Thermocouple		33.500	-6.000	-3.521	-328-750	1.8 or 0.75%	deg F	TC-T-90-11521	-6→+21mV	152.5
TA055	Thermocouple		33.500	-4.000	-3.521	-328-750	1.8 or 0.75%	deg F	TC-T-90-11521	-6→+21mV	152.5
TA056	Thermocouple		29.000	-7.000	-3.048	-328-750	1.8 or 0.75%	deg F	TC-T-0-11522	-6→+21mV	152.5
TA057	Thermocouple		29.000	-5.000	-3.048	-328-750	1.8 or 0.75%	deg F	TC-T-90-11521	-6→+21mV	152.5
TA058	Thermocouple		29.000	-3.000	-3.048	-328-750	1.8 or 0.75%	deg F	TC-T-90-11521	-6→+21mV	152.5
TA059	Thermocouple		37.000	-10.000	-3.968	-328-750	1.8 or 0.75%	deg F	TC-T-0-11522	-6→+21mV	152.5
TA060	Thermocouple		38.000	-7.000	-3.994	-328-750	1.8 or 0.75%	deg F	TC-T-0-11522	-6→+21mV	152.5
TA061	Thermocouple		38.000	-5.000	-3.994	-328-750	1.8 or 0.75%	deg F	TC-T-0-11522	-6→+21mV	152.5
TA062	Thermocouple		38.000	-3.000	-3.994	-328-750	1.8 or 0.75%	deg F	TC-T-0-11522	-6→+21mV	152.5
TA063	Thermocouple		46.000	-7.000	-4.835	-328-750	1.8 or 0.75%	deg F	TC-T-90-11521	-6→+21mV	152.5
TA064	Thermocouple		46.000	-5.000	-4.835	-328-750	1.8 or 0.75%	deg F	TC-T-90-11521	-6→+21mV	152.5
TA065	Thermocouple		46.000	-3.000	-4.835	-328-750	1.8 or 0.75%	deg F	TC-T-90-11521	-6→+21mV	152.5
TA066	Thermocouple		55.000	-7.000	-5.781	-328-750	1.8 or 0.75%	deg F	TC-T-90-11521	-6→+21mV	152.5
TA067	Thermocouple		55.000	-5.000	-5.781	-328-750	1.8 or 0.75%	deg F	TC-T-90-11521	-6→+21mV	152.5
TA068	Thermocouple		55.000	-3.000	-5.781	-328-750	1.8 or 0.75%	deg F	TC-T-90-11521	-6→+21mV	152.5
TA069	Thermocouple		64.000	-7.000	-6.700	-328-750	1.8 or 0.75%	deg F	TC-T-90-11517	-6→+21mV	152.5
TA070	Thermocouple		64.000	-5.000	-6.727	-328-750	1.8 or 0.75%	deg F	TC-T-90-11517	-6→+21mV	152.5
TA071	Thermocouple		64.000	-3.000	-6.727	-328-750	1.8 or 0.75%	deg F	TC-T-90-11517	-6→+21mV	152.5
TA072	Thermocouple		73.000	-7.000	-7.545	-328-750	1.8 or 0.75%	deg F	TC-T-90-11517	-6→+21mV	152.5
TA073	Thermocouple		73.000	-5.000	-7.673	-328-750	1.8 or 0.75%	deg F	TC-T-90-11517	-6→+21mV	152.5
TA074	Thermocouple		73.000	-3.000	-7.673	-328-750	1.8 or 0.75%	deg F	TC-T-90-11517	-6→+21mV	152.5
TA075	Thermocouple		82.000	-7.000	-8.335	-328-750	1.8 or 0.75%	deg F	TC-T-90-11517	-6→+21mV	152.5
TA076	Thermocouple		82.000	-5.000	-8.619	-328-750	1.8 or 0.75%	deg F	TC-T-90-11517	-6→+21mV	152.5
TA077	Thermocouple		82.000	-3.000	-8.619	-328-750	1.8 or 0.75%	deg F	TC-T-90-11517	-6→+21mV	152.5

Table 6. Side A instrument list (End).

Name	Description	Diff Ref / Cross-Corr	Station Location			Instrument				Output	Sample Rate
			X (in)	Y (in)	Z (in)	Range	Typ. Accuracy	Units	Make / Model / Module	Volts	SPS
HF3A11	Three Hot Film Active - Element #1		36.000	7.500	-3.784	400	TBD	deg F	HOTFILM-AC-H	+/- 1 VAC	20000
HF3A12	Three Hot Film Active - Element #2		36.000	7.500	-3.784	400	TBD	deg F	HOTFILM-AC-H	+/- 1 VAC	20000
HF3A13	Three Hot Film Active - Element #3		36.000	7.500	-3.784	400	TBD	deg F	HOTFILM-AC-H	+/- 1 VAC	20000
HF3A51	Three Hot Film Active - Element #1		25.000	6.000	-2.628	400	TBD	deg F	HOTFILM-AC-U	+/- 1 VAC	100000
HF3A52	Three Hot Film Active - Element #2		25.000	6.000	-2.628	400	TBD	deg F	HOTFILM-AC-U	+/- 1 VAC	100000
HF3A53	Three Hot Film Active - Element #3		25.000	6.000	-2.628	400	TBD	deg F	HOTFILM-AC-U	+/- 1 VAC	100000
HF3P11	Three Hot Film Passive - Element #1		36.000	7.500	-3.784	400	TBD	deg F	HOTFILM-DC-L	0-10 VDC	305.2
HF3P12	Three Hot Film Passive - Element #2		36.000	7.500	-3.784	400	TBD	deg F	HOTFILM-DC-L	0-10 VDC	305.2
HF3P13	Three Hot Film Passive - Element #3		36.000	7.500	-3.784	400	TBD	deg F	HOTFILM-DC-L	0-10 VDC	305.2
HF3P51	Three Hot Film Passive - Element #1		25.000	6.000	-2.628	400	TBD	deg F	HOTFILM-DC-L	0-10 VDC	305.2
HF3P52	Three Hot Film Passive - Element #2		25.000	6.000	-2.628	400	TBD	deg F	HOTFILM-DC-L	0-10 VDC	305.2
HF3P53	Three Hot Film Passive - Element #3		25.000	6.000	-2.628	400	TBD	deg F	HOTFILM-DC-L	0-10 VDC	305.2
DSP1E1	Cross-Corr Phase P3DA11, P3DA12	P3DA11/12	N/A	N/A	N/A	N/A	N/A	N/A	ELECTRIC	N/A	N/A
DSP1E2	Cross-Corr Phase P3DA11, P3DA13	P3DA11/13	N/A	N/A	N/A	N/A	N/A	N/A	ELECTRIC	N/A	N/A
DSP1E3	Cross-Corr Phase HF3A51, HF3A52	HF3A51/52	N/A	N/A	N/A	N/A	N/A	N/A	ELECTRIC	N/A	N/A
DSP1E4	Cross-Corr Phase HF3A51, HF3A53	HF3A51/53	N/A	N/A	N/A	N/A	N/A	N/A	ELECTRIC	N/A	N/A
DSP2E1	Cross-Corr Phase P3DA21, P3DA22	P3DA21/22	N/A	N/A	N/A	N/A	N/A	N/A	ELECTRIC	N/A	N/A
DSP2E2	Cross-Corr Phase P3DA21, P3DA23	P3DA21/23	N/A	N/A	N/A	N/A	N/A	N/A	ELECTRIC	N/A	N/A
DSP2E3	Cross-Corr Phase HF3A11, HF3A12	HF3A11/12	N/A	N/A	N/A	N/A	N/A	N/A	ELECTRIC	N/A	N/A
DSP2E4	Cross-Corr Phase HF3A11, HF3A13	HF3A11/13	N/A	N/A	N/A	N/A	N/A	N/A	ELECTRIC	N/A	N/A

Table 7. Side B detailed instrument list.

Name	Description	Diff Ref / Cross-Corr	Station Location			Instrument				Output	Sample Rate
			X (in)	Y (in)	Z (in)	Range	Typ. Accuracy	Units	Make / Model / Module	Volts	SPS
PSB01	AOA Sensor 1 - Static Absolute - B Side	+PAOA01	81.000	0.000	8.513	0-15	+/-0.1% FSO	psia	KUL-ETM-15A	0-5 VDC	610
PSB02	AOA Sensor 2 - Static Absolute - B Side	+PAOA02/PSB02S	84.000	0.000	8.829	0-15	+/-0.1% FSO	psia	KUL-ETM-15A	0-5 VDC	610
PRTB01	Pressure Rake (Probless Pitot) #T1		84.993	0.000	8.997	0-75	+/-0.1% FSO	psia	KUL-ETM-75A	0-5 VDC	305.2
PRTB02	Pressure Rake (Probless Pitot) #T2		84.987	0.000	9.058	0-75	+/-0.1% FSO	psia	KUL-ETM-75A	0-5 VDC	305.2
PRTB03	Pressure Rake (Probless Pitot) #T3		84.980	0.000	9.129	0-75	+/-0.1% FSO	psia	KUL-ETM-75A	0-5 VDC	305.2
PRTB04	Pressure Rake (Probless Pitot) #T4		84.969	0.000	9.232	0-75	+/-0.1% FSO	psia	KUL-ETM-75A	0-5 VDC	305.2
PRTB05	Pressure Rake (Probless Pitot) #T5		84.953	0.000	9.381	0-75	+/-0.1% FSO	psia	KUL-ETM-75A	0-5 VDC	305.2
PRTB06	Pressure Rake (Probless Pitot) #T6		84.928	0.000	9.618	0-75	+/-0.1% FSO	psia	KUL-ETM-75A	0-5 VDC	305.2
PRTB07	Pressure Rake (Probless Pitot) #T7		84.883	0.000	10.051	0-75	+/-0.1% FSO	psia	KUL-ETM-75A	0-5 VDC	305.2
PRTB08	Pressure Rake (Probless Pitot) #T8		84.817	0.000	10.674	0-75	+/-0.1% FSO	psia	KUL-ETM-75A	0-5 VDC	305.2
PRSB01	Pressure Rake (Probless Pitot) #S1 - Differential	PRSB+02/-03	85.403	0.000	0.000	+/-5	+/-0.1% FSO	psid	KUL-XTL-3-375-5D	0-5 VDC	610
PRSB02	Pressure Rake (Probless Pitot) #S2 - Static Absolute	+PRSB01	85.403	0.102	10.485	0-25	+/-0.1% FSO	psia	KUL-ETM-25A	0-5 VDC	610
PRSB03	Pressure Rake (Probless Pitot) #S3 - Static Absolute	-PRSB01	85.403	-0.102	10.485	0-25	+/-0.1% FSO	psia	KUL-ETM-25A	0-5 VDC	610
TB001	Thermocouple		10.500	0.000	1.104	-328-750	1.8 or 0.75%	deg F	TC-T-90-11521	-6→+21mV	152.5
TB002	Thermocouple		14.000	0.000	1.471	-328-750	1.8 or 0.75%	deg F	TC-T-90-11521	-6→+21mV	152.5
TB003	Thermocouple		18.000	0.000	1.892	-328-750	1.8 or 0.75%	deg F	TC-T-90-11521	-6→+21mV	152.5
TB004	Thermocouple		23.000	0.000	2.417	-328-750	1.8 or 0.75%	deg F	TC-T-0-11522	-6→+21mV	152.5
TB005	Thermocouple		28.000	0.000	2.943	-328-750	1.8 or 0.75%	deg F	TC-T-90-11521	-6→+21mV	152.5
TB006	Thermocouple		33.000	0.000	3.468	-328-750	1.8 or 0.75%	deg F	TC-T-90-11521	-6→+21mV	152.5
TB007	Thermocouple		38.000	0.000	3.994	-328-750	1.8 or 0.75%	deg F	TC-T-0-11522	-6→+21mV	152.5
TB008	Thermocouple		44.000	0.000	4.625	-328-750	1.8 or 0.75%	deg F	TC-T-90-11521	-6→+21mV	152.5
TB009	Thermocouple		48.000	0.000	5.045	-328-750	1.8 or 0.75%	deg F	TC-T-90-11521	-6→+21mV	152.5
TB010	Thermocouple		53.000	0.000	5.571	-328-750	1.8 or 0.75%	deg F	TC-T-90-11521	-6→+21mV	152.5
TB011	Thermocouple		58.000	0.000	6.096	-328-750	1.8 or 0.75%	deg F	TC-T-0-11522	-6→+21mV	152.5
TB012	Thermocouple		63.000	0.000	6.622	-328-750	1.8 or 0.75%	deg F	TC-T-0-11518	-6→+21mV	152.5
TB013	Thermocouple		68.000	0.000	7.147	-328-750	1.8 or 0.75%	deg F	TC-T-90-11517	-6→+21mV	152.5
TB014	Thermocouple		73.000	0.000	7.673	-328-750	1.8 or 0.75%	deg F	TC-T-90-11517	-6→+21mV	152.5
TB015	Thermocouple		78.000	0.000	8.198	-328-750	1.8 or 0.75%	deg F	TC-T-90-11517	-6→+21mV	152.5
TB016	Thermocouple		83.000	0.000	8.724	-328-750	1.8 or 0.75%	deg F	TC-T-90-11517	-6→+21mV	152.5
TB017	Thermocouple		10.500	2.500	1.104	-328-750	1.8 or 0.75%	deg F	TC-T-90-11521	-6→+21mV	152.5
TB018	Thermocouple		28.000	2.500	2.943	-328-750	1.8 or 0.75%	deg F	TC-T-90-11521	-6→+21mV	152.5
TB019	Thermocouple		38.000	2.500	3.994	-328-750	1.8 or 0.75%	deg F	TC-T-0-11522	-6→+21mV	152.5
TB020	Thermocouple		48.000	2.500	5.045	-328-750	1.8 or 0.75%	deg F	TC-T-90-11521	-6→+21mV	152.5
TB021	Thermocouple		58.000	2.500	6.096	-328-750	1.8 or 0.75%	deg F	TC-T-0-11522	-6→+21mV	152.5
TB022	Thermocouple		68.000	2.500	7.147	-328-750	1.8 or 0.75%	deg F	TC-T-90-11517	-6→+21mV	152.5
TB023	Thermocouple		78.000	2.500	8.198	-328-750	1.8 or 0.75%	deg F	TC-T-90-11517	-6→+21mV	152.5
TB024	Thermocouple		88.000	2.500	9.249	-328-750	1.8 or 0.75%	deg F	TC-T-0-11518	-6→+21mV	152.5
TB025	Thermocouple		10.500	-2.500	1.104	-328-750	1.8 or 0.75%	deg F	TC-T-90-11521	-6→+21mV	152.5
TB026	Thermocouple		28.000	-2.500	2.943	-328-750	1.8 or 0.75%	deg F	TC-T-90-11521	-6→+21mV	152.5
TB027	Thermocouple		38.000	-2.500	3.994	-328-750	1.8 or 0.75%	deg F	TC-T-0-11522	-6→+21mV	152.5
TB028	Thermocouple		48.000	-2.500	5.045	-328-750	1.8 or 0.75%	deg F	TC-T-90-11521	-6→+21mV	152.5
TB029	Thermocouple		58.000	-2.500	6.096	-328-750	1.8 or 0.75%	deg F	TC-T-0-11522	-6→+21mV	152.5
TB030	Thermocouple		68.000	-2.500	7.147	-328-750	1.8 or 0.75%	deg F	TC-T-90-11517	-6→+21mV	152.5
TB031	Thermocouple		78.000	-2.500	8.198	-328-750	1.8 or 0.75%	deg F	TC-T-90-11517	-6→+21mV	152.5
TB032	Thermocouple		88.000	-2.500	9.249	-328-750	1.8 or 0.75%	deg F	TC-T-0-11518	-6→+21mV	152.5
TB033	Thermocouple		10.500	5.000	1.104	-328-750	1.8 or 0.75%	deg F	TC-T-90-11521	-6→+21mV	152.5
TB034	Thermocouple		14.000	5.000	1.471	-328-750	1.8 or 0.75%	deg F	TC-T-90-11521	-6→+21mV	152.5
TB035	Thermocouple		18.000	5.000	1.892	-328-750	1.8 or 0.75%	deg F	TC-T-90-11521	-6→+21mV	152.5
TB036	Thermocouple		23.000	5.000	2.417	-328-750	1.8 or 0.75%	deg F	TC-T-0-11522	-6→+21mV	152.5
TB037	Thermocouple		28.000	5.000	2.943	-328-750	1.8 or 0.75%	deg F	TC-T-90-11521	-6→+21mV	152.5
TB038	Thermocouple		33.000	5.000	3.468	-328-750	1.8 or 0.75%	deg F	TC-T-90-11521	-6→+21mV	152.5
TB039	Thermocouple		38.000	5.000	3.994	-328-750	1.8 or 0.75%	deg F	TC-T-0-11522	-6→+21mV	152.5
TB040	Thermocouple		44.000	5.000	4.625	-328-750	1.8 or 0.75%	deg F	TC-T-90-11521	-6→+21mV	152.5
TB041	Thermocouple		48.000	5.000	5.045	-328-750	1.8 or 0.75%	deg F	TC-T-90-11521	-6→+21mV	152.5
TB042	Thermocouple		53.000	5.000	5.571	-328-750	1.8 or 0.75%	deg F	TC-T-90-11521	-6→+21mV	152.5

Table 7. Side B detailed instrument list (End).

Name	Description	Diff Ref / Cross-Corr	Station Location			Instrument				Output	Sample Rate
			X (in)	Y (in)	Z (in)	Range	Typ. Accuracy	Units	Make / Model / Module	Volts	SPS
TB043	Thermocouple		58.000	5.000	6.096	-328-750	1.8 or 0.75%	deg F	TC-T-0-11522	-6→+21mV	152.5
TB044	Thermocouple		63.000	5.000	6.622	-328-750	1.8 or 0.75%	deg F	TC-T-0-11518	-6→+21mV	152.5
TB045	Thermocouple		68.000	5.000	7.147	-328-750	1.8 or 0.75%	deg F	TC-T-90-11517	-6→+21mV	152.5
TB046	Thermocouple		73.000	5.000	7.673	-328-750	1.8 or 0.75%	deg F	TC-T-90-11517	-6→+21mV	152.5
TB047	Thermocouple		78.000	5.000	8.198	-328-750	1.8 or 0.75%	deg F	TC-T-90-11517	-6→+21mV	152.5
TB048	Thermocouple		83.000	5.000	8.719	-328-750	1.8 or 0.75%	deg F	TC-T-90-11517	-6→+21mV	152.5
TB049	Thermocouple		88.000	5.000	9.221	-328-750	1.8 or 0.75%	deg F	TC-T-0-11518	-6→+21mV	152.5
TB050	Thermocouple		10.500	-5.000	1.104	-328-750	1.8 or 0.75%	deg F	TC-T-90-11521	-6→+21mV	152.5
TB051	Thermocouple		14.000	-5.000	1.471	-328-750	1.8 or 0.75%	deg F	TC-T-90-11521	-6→+21mV	152.5
TB052	Thermocouple		18.000	-5.000	1.892	-328-750	1.8 or 0.75%	deg F	TC-T-90-11521	-6→+21mV	152.5
TB053	Thermocouple		23.000	-5.000	2.417	-328-750	1.8 or 0.75%	deg F	TC-T-0-11522	-6→+21mV	152.5
TB054	Thermocouple		28.000	-5.000	2.943	-328-750	1.8 or 0.75%	deg F	TC-T-90-11521	-6→+21mV	152.5
TB055	Thermocouple		33.000	-5.000	3.468	-328-750	1.8 or 0.75%	deg F	TC-T-90-11521	-6→+21mV	152.5
TB056	Thermocouple		38.000	-5.000	3.994	-328-750	1.8 or 0.75%	deg F	TC-T-0-11522	-6→+21mV	152.5
TB057	Thermocouple		44.000	-5.000	4.625	-328-750	1.8 or 0.75%	deg F	TC-T-90-11521	-6→+21mV	152.5
TB058	Thermocouple		48.000	-5.000	5.045	-328-750	1.8 or 0.75%	deg F	TC-T-90-11521	-6→+21mV	152.5
TB059	Thermocouple		53.000	-5.000	5.571	-328-750	1.8 or 0.75%	deg F	TC-T-90-11521	-6→+21mV	152.5
TB060	Thermocouple		58.000	-5.000	6.096	-328-750	1.8 or 0.75%	deg F	TC-T-0-11522	-6→+21mV	152.5
TB061	Thermocouple		63.000	-5.000	6.622	-328-750	1.8 or 0.75%	deg F	TC-T-0-11518	-6→+21mV	152.5
TB062	Thermocouple		68.000	-5.000	7.147	-328-750	1.8 or 0.75%	deg F	TC-T-90-11517	-6→+21mV	152.5
TB063	Thermocouple		73.000	-5.000	7.673	-328-750	1.8 or 0.75%	deg F	TC-T-90-11517	-6→+21mV	152.5
TB064	Thermocouple		78.000	-5.000	8.198	-328-750	1.8 or 0.75%	deg F	TC-T-90-11517	-6→+21mV	152.5
TB065	Thermocouple		83.000	-5.000	8.719	-328-750	1.8 or 0.75%	deg F	TC-T-90-11517	-6→+21mV	152.5
TB066	Thermocouple		88.000	-5.000	9.221	-328-750	1.8 or 0.75%	deg F	TC-T-0-11518	-6→+21mV	152.5
TB067	Thermocouple		18.000	7.500	1.892	-328-750	1.8 or 0.75%	deg F	TC-T-0-11522	-6→+21mV	152.5
TB068	Thermocouple		28.000	7.500	2.943	-328-750	1.8 or 0.75%	deg F	TC-T-0-11522	-6→+21mV	152.5
TB069	Thermocouple		38.000	7.500	3.994	-328-750	1.8 or 0.75%	deg F	TC-T-0-11522	-6→+21mV	152.5
TB070	Thermocouple		48.000	7.500	5.045	-328-750	1.8 or 0.75%	deg F	TC-T-90-11521	-6→+21mV	152.5
TB071	Thermocouple		58.000	7.500	6.070	-328-750	1.8 or 0.75%	deg F	TC-T-90-11521	-6→+21mV	152.5
TB072	Thermocouple		68.000	7.500	6.998	-328-750	1.8 or 0.75%	deg F	TC-T-90-11517	-6→+21mV	152.5
TB073	Thermocouple		78.000	7.500	7.858	-328-750	1.8 or 0.75%	deg F	TC-T-90-11517	-6→+21mV	152.5
TB074	Thermocouple		88.000	7.500	8.669	-328-750	1.8 or 0.75%	deg F	TC-T-90-11517	-6→+21mV	152.5
TB075	Thermocouple		18.000	-7.500	1.892	-328-750	1.8 or 0.75%	deg F	TC-T-0-11522	-6→+21mV	152.5
TB076	Thermocouple		28.000	-7.500	2.943	-328-750	1.8 or 0.75%	deg F	TC-T-0-11522	-6→+21mV	152.5
TB077	Thermocouple		38.000	-7.500	3.994	-328-750	1.8 or 0.75%	deg F	TC-T-0-11522	-6→+21mV	152.5
TB078	Thermocouple		48.000	-7.500	5.045	-328-750	1.8 or 0.75%	deg F	TC-T-90-11521	-6→+21mV	152.5
TB079	Thermocouple		58.000	-7.500	6.070	-328-750	1.8 or 0.75%	deg F	TC-T-90-11521	-6→+21mV	152.5
TB080	Thermocouple		68.000	-7.500	6.998	-328-750	1.8 or 0.75%	deg F	TC-T-90-11517	-6→+21mV	152.5
TB081	Thermocouple		78.000	-7.500	7.858	-328-750	1.8 or 0.75%	deg F	TC-T-90-11517	-6→+21mV	152.5
TB082	Thermocouple		88.000	-7.500	8.669	-328-750	1.8 or 0.75%	deg F	TC-T-90-11517	-6→+21mV	152.5
TB083	Thermocouple		18.000	12.373	0.000	-328-750	1.8 or 0.75%	deg F	TC-T-0-11522	-6→+21mV	152.5
TB084	Thermocouple		38.000	12.702	0.000	-328-750	1.8 or 0.75%	deg F	TC-T-0-11522	-6→+21mV	152.5
TB085	Thermocouple		18.000	-12.373	0.000	-328-750	1.8 or 0.75%	deg F	TC-T-0-11522	-6→+21mV	152.5
TB086	Thermocouple		38.000	-12.702	0.000	-328-750	1.8 or 0.75%	deg F	TC-T-0-11522	-6→+21mV	152.5
TB087	Thermocouple		20.500	0.000	1.773	-328-750	1.8 or 0.75%	deg F	TC-T-0-11522	-6→+21mV	152.5
TB088	Thermocouple		21.000	0.000	1.825	-328-750	1.8 or 0.75%	deg F	TC-T-0-11522	-6→+21mV	152.5
TB089	Thermocouple		21.500	0.000	1.878	-328-750	1.8 or 0.75%	deg F	TC-T-0-11522	-6→+21mV	152.5
TB090	Thermocouple		22.000	0.000	1.930	-328-750	1.8 or 0.75%	deg F	TC-T-0-11522	-6→+21mV	152.5
TB091	Thermocouple		22.500	0.000	1.983	-328-750	1.8 or 0.75%	deg F	TC-T-0-11522	-6→+21mV	152.5
TB092	Thermocouple		22.250	0.350	1.956	-328-750	1.8 or 0.75%	deg F	TC-T-0-11522	-6→+21mV	152.5
TB093	Thermocouple		22.250	-0.350	1.956	-328-750	1.8 or 0.75%	deg F	TC-T-0-11522	-6→+21mV	152.5
TB094	Thermocouple		20.000	5.000	2.102	-328-750	1.8 or 0.75%	deg F	TC-T-0-11522	-6→+21mV	152.5
TB095	Thermocouple		21.000	5.000	2.207	-328-750	1.8 or 0.75%	deg F	TC-T-0-11522	-6→+21mV	152.5
TB096	Thermocouple		22.000	5.000	2.312	-328-750	1.8 or 0.75%	deg F	TC-T-0-11522	-6→+21mV	152.5
TB097	Thermocouple		20.350	-5.000	2.209	-328-750	1.8 or 0.75%	deg F	TC-T-0-11522	-6→+21mV	152.5
TB098	Thermocouple		21.000	-5.000	2.207	-328-750	1.8 or 0.75%	deg F	TC-T-0-11522	-6→+21mV	152.5
TB099	Thermocouple		22.000	-5.000	2.312	-328-750	1.8 or 0.75%	deg F	TC-T-0-11522	-6→+21mV	152.5

Table 8. Miscellaneous instrument list.

Name	Description	Diff Ref / Cross-Corr	Station Location			Instrument				Output	Sample Rate
			X (in)	Y (in)	Z (in)	Range	Typ. Accuracy	Units	Make / Model / Module	Volts	SPS
ACL1Z	Accelerometer #1 - Z-axis (Positive in +Z Rocket Coord Sys)		50.000	0.000	0.907	+/-5	+/-1.0% FS	G's	ACCEL-L	0-5 VDC	1221
ACL1Y	Accelerometer #1 - Y-axis (Positive in +Y Rocket Coord Sys)		50.000	0.000	0.811	+/-5	+/-1.0% FS	G's	ACCEL-L	0-5 VDC	1221
ACL1X	Accelerometer #1 - X-axis (Positive in +X Rocket Coord Sys)		50.000	0.000	0.806	-5-20	+/-1.0% FS	G's	ACCEL-L	0-5 VDC	1221
VIB1Z	Vibrometer #1 - Z-axis		50.000	1.250	-4.752	+/-100	1%	Grms	VIBE-H	0-5 VDC	100000
PAOA01	Differential Pressure - Angle of Attack Sensor #1	-PSA08/+PSB01	81.000	0.000	0.000	+/-5	+/-0.1% FSO	psid	KUL-XTL-3-375-5D	0-5 VDC	610
PAOA02	Differential Pressure - Angle of Attack Sensor #2	-PSA09/+PSB02	84.000	0.000	0.000	+/-5	+/-0.1% FSO	psid	KUL-XTL-3-375-5D	0-5 VDC	610
PYAW01	Differential Pressure - Yaw Angle Sensor #1	PSA+17/-19	34.000	0.000	0.000	+/-5	+/-0.1% FSO	psid	KUL-XTL-3-375-5D	0-5 VDC	610
PYAW02	Differential Pressure - Yaw Angle Sensor #2	PSA+18/-20	39.000	0.000	0.000	+/-5	+/-0.1% FSO	psid	KUL-XTL-3-375-5D	0-5 VDC	305.2
TRTC01	Thermocouple Reference (TC Slice Temp) #1		76.854	-6.125	3.748	-67-302	+/-1.5 deg C FS	deg F	PSL-TB06	-550→+1500mV	152.5
TRTC02	Thermocouple Reference (TC Slice Temp) #2		76.930	-6.125	3.027	-67-302	+/-1.5 deg C FS	deg F	PSL-TB06	-550→+1500mV	152.5
TRTC03	Thermocouple Reference (TC Slice Temp) #3		77.006	-6.125	2.306	-67-302	+/-1.5 deg C FS	deg F	PSL-TB06	-550→+1500mV	152.5
TRTC04	Thermocouple Reference (TC Slice Temp) #4		77.082	-6.125	1.585	-67-302	+/-1.5 deg C FS	deg F	PSL-TB06	-550→+1500mV	152.5
TRTC05	Thermocouple Reference (TC Slice Temp) #5		76.854	-2.125	3.748	-67-302	+/-1.5 deg C FS	deg F	PSL-TB06	-550→+1500mV	152.5
TRTC06	Thermocouple Reference (TC Slice Temp) #6		76.930	-2.125	3.027	-67-302	+/-1.5 deg C FS	deg F	PSL-TB06	-550→+1500mV	152.5
TRTC07	Thermocouple Reference (TC Slice Temp) #7		77.006	-2.125	2.306	-67-302	+/-1.5 deg C FS	deg F	PSL-TB06	-550→+1500mV	152.5
TRTC08	Thermocouple Reference (TC Slice Temp) #8		77.082	-2.125	1.585	-67-302	+/-1.5 deg C FS	deg F	PSL-TB06	-550→+1500mV	152.5
TRTC09	Thermocouple Reference (TC Slice Temp) #9		76.854	2.125	3.748	-67-302	+/-1.5 deg C FS	deg F	PSL-TB06	-550→+1500mV	152.5
TRTC10	Thermocouple Reference (TC Slice Temp) #10		76.930	2.125	3.027	-67-302	+/-1.5 deg C FS	deg F	PSL-TB06	-550→+1500mV	152.5
TRTC11	Thermocouple Reference (TC Slice Temp) #11		77.006	2.125	2.306	-67-302	+/-1.5 deg C FS	deg F	PSL-TB06	-550→+1500mV	152.5
TRTC12	Thermocouple Reference (TC Slice Temp) #12		77.082	2.125	1.585	-67-302	+/-1.5 deg C FS	deg F	PSL-TB06	-550→+1500mV	152.5
TRTC13	Thermocouple Reference (TC Slice Temp) #13		76.854	6.125	3.748	-67-302	+/-1.5 deg C FS	deg F	PSL-TB06	-550→+1500mV	152.5
TRTC14	Thermocouple Reference (TC Slice Temp) #14		76.930	6.125	3.027	-67-302	+/-1.5 deg C FS	deg F	PSL-TB06	-550→+1500mV	152.5
TRTC15	Thermocouple Reference (TC Slice Temp) #15		77.006	6.125	2.306	-67-302	+/-1.5 deg C FS	deg F	PSL-TB06	-550→+1500mV	152.5
TRTC16	Thermocouple Reference (TC Slice Temp) #16		77.082	6.125	1.585	-67-302	+/-1.5 deg C FS	deg F	PSL-TB06	-550→+1500mV	152.5
PSA09S	Secondary Measurement of PSA09		84.000	0.000	-8.829	0-25	+/-0.1% FSO	psia	KUL-ETM-25A	0-5 VDC	305.2
PSB02S	Secondary Measurement of PSB02		84.000	0.000	8.829	0-25	+/-0.1% FSO	psia	KUL-ETM-25A	0-5 VDC	305.2
PRSA1S	Secondary Measurement of PRSA12		85.403	3.898	-10.485	0-75	+/-0.1% FSO	psia	KUL-ETM-75A	0-5 VDC	305.2

Table 9. Thermocouple reference temperature blocks.

Refeerence Block	Connected TC	Notes
TRTC01	TA001 ~ TA011	
TRTC02	TA012 ~ TA022	
TRTC03	TA023 ~ TA033	
TRTC04	TA034 ~ TA044	
TRTC05	TA045 ~ TA055	
TRTC06	TA056 ~ TA066	
TRTC07	TA067 ~ TA077	
TRTC08	TB001 ~ TB011	
TRTC09	TB012 ~ TB022	
TRTC10	TB023 ~ TB033	
TRTC11	TB034 ~ TB044	High Ref. Temperature
TRTC12	TB045 ~ TB055	High Ref. Temperature
TRTC13	TB056 ~ TB066	
TRTC14	TB067 ~ TB077	
TRTC15	TB078 ~ TB088	High Ref. Temperature
TRTC16	TB089 ~ TB099	High Ref. Temperature

Table 10. Relationships between measured and computed differential pressures, and measured static pressures for angle of attack and angle of yaw.

Angle	Measured ΔP	Computed ΔP
$\alpha 1$	PAOA01	DpAOA1 = PSB01 – PSA08
$\alpha 2$	PAOA02	DpAOA2 = PSB02 – PSA09
$\beta 1$	PYAW01	DpAOY1 = PSA17 – PSA19
$\beta 2$	PYAW02	DpAOY2 = PSA18 – PSA20

Table 11. Relationships between measured and computed differential pressures, and measured static pressures for flow angles at boundary-layer pressure rakes.

Angle	Measured ΔP	Computed ΔP
ϕ_A	PRSA11	DPRSA = PRSA13 – PRSA12
ϕ_B	PRSB01	DPRSB = PRSB02 – PRSB03

Figure 1. Liftoff of HyBoLT mounted on the ALV X-1 rocket from WFF Launch Pad 0B.

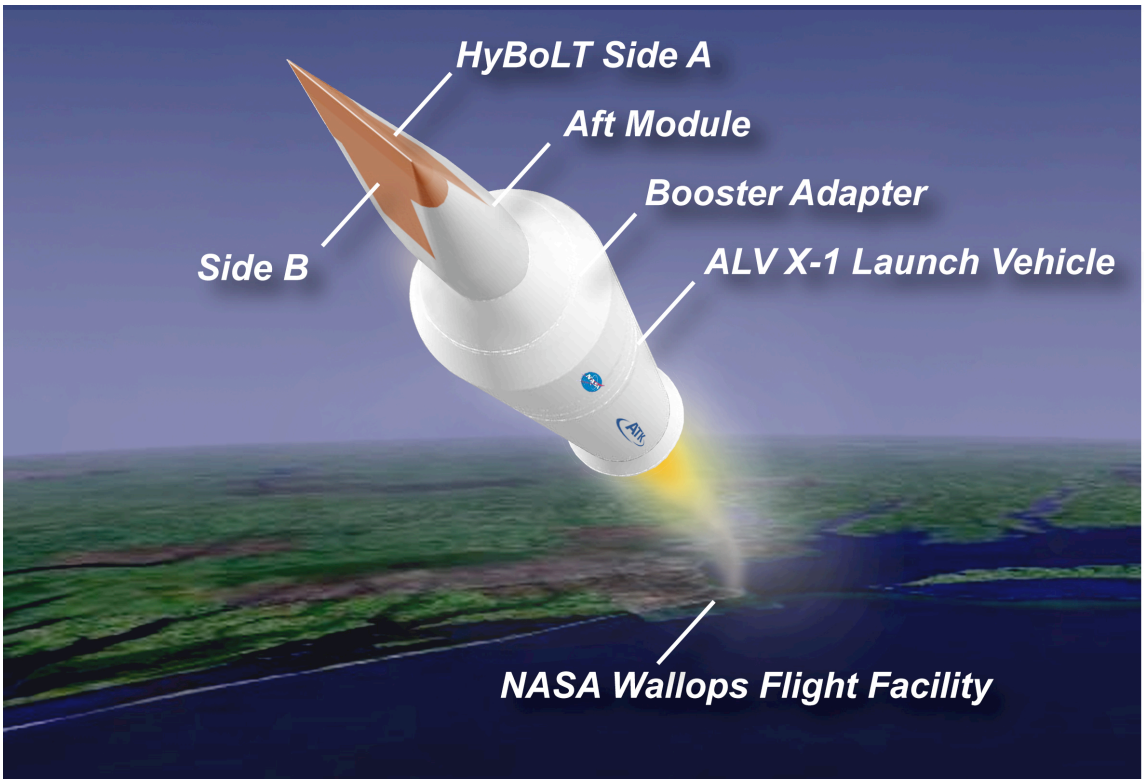

Figure 2. Artistic rendering of HyBoLT during launch from Wallops Flight Facility.

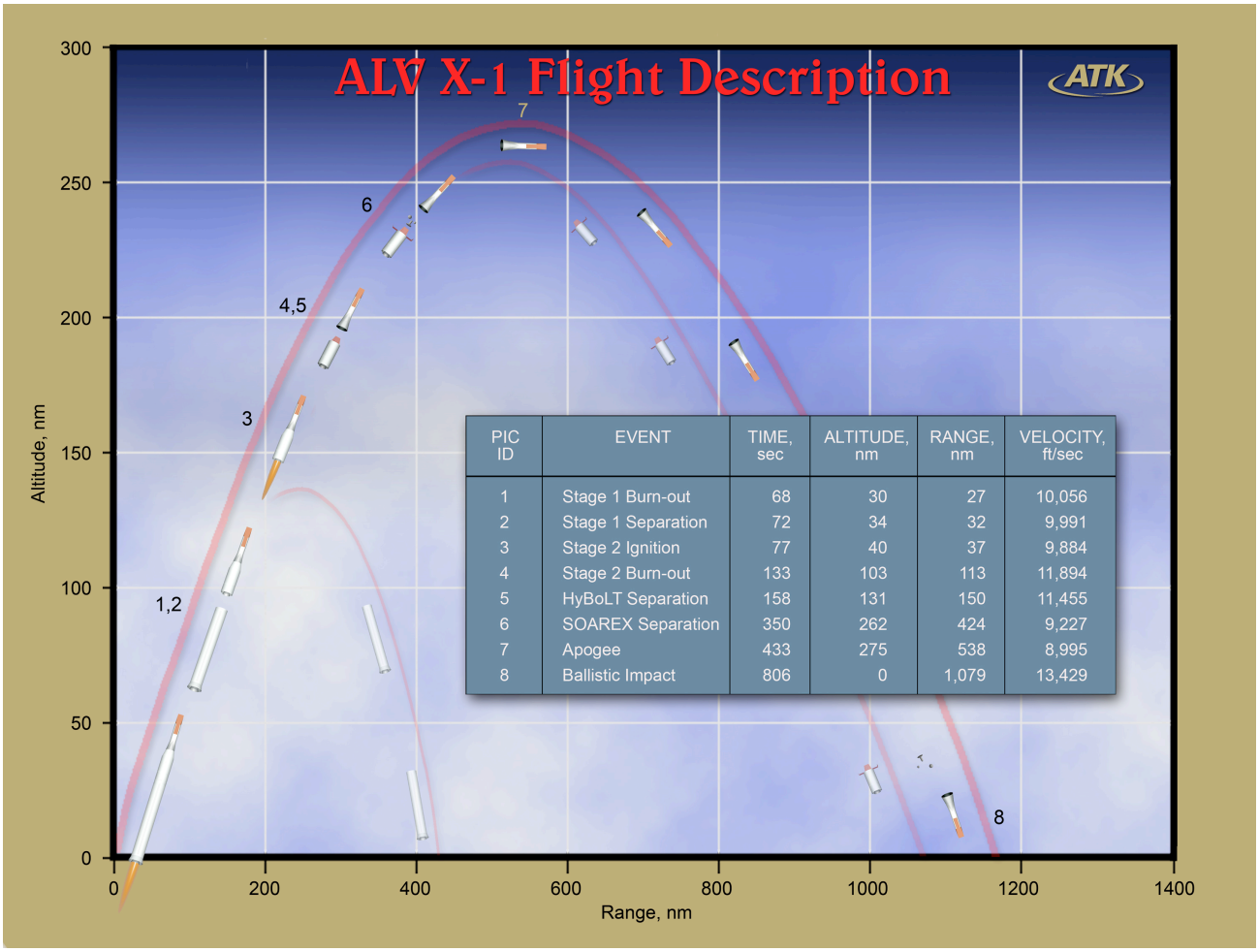

PIC ID	EVENT	TIME, sec	ALTITUDE, nm	RANGE, nm	VELOCITY, ft/sec
1	Stage 1 Burn-out	68	30	27	10,056
2	Stage 1 Separation	72	34	32	9,991
3	Stage 2 Ignition	77	40	37	9,884
4	Stage 2 Burn-out	133	103	113	11,894
5	HyBoLT Separation	158	131	150	11,455
6	SOAREX Separation	350	262	424	9,227
7	Apogee	433	275	538	8,995
8	Ballistic Impact	806	0	1,079	13,429

Figure 3. Planned ALV X-1 flight profile.

	Mach No.	Re/ft
Side A	3.0	7.42E+06
	4.2	4.32E+06
Side B	5.5	1.85E+06
	8.0	2.29E+05

Angle of attack = 0°

Angle of yaw = 0°

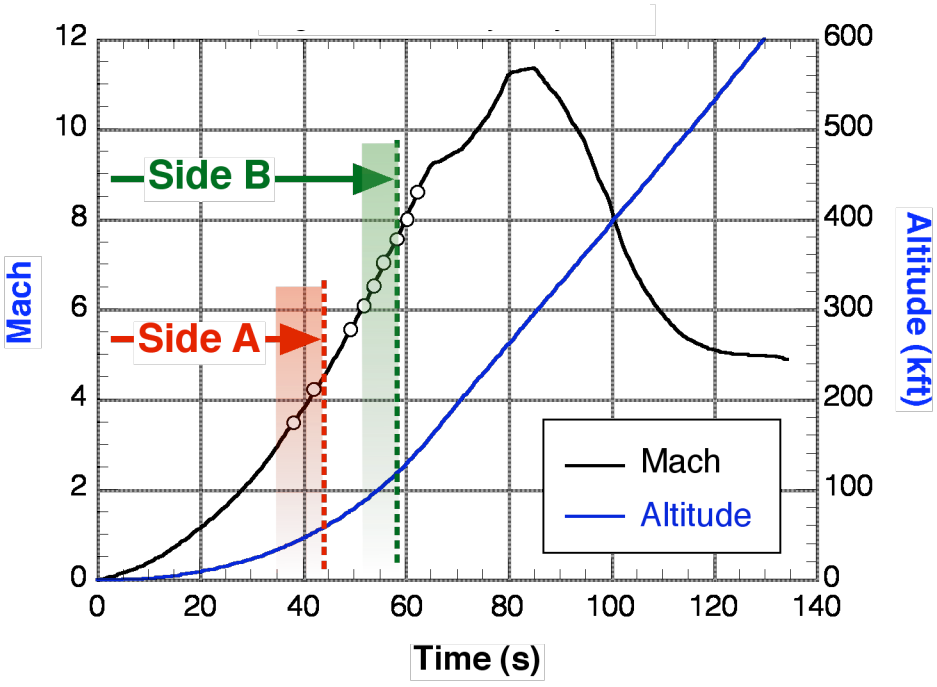

Figure 4. HyBoLT trajectory points and data criticality window.

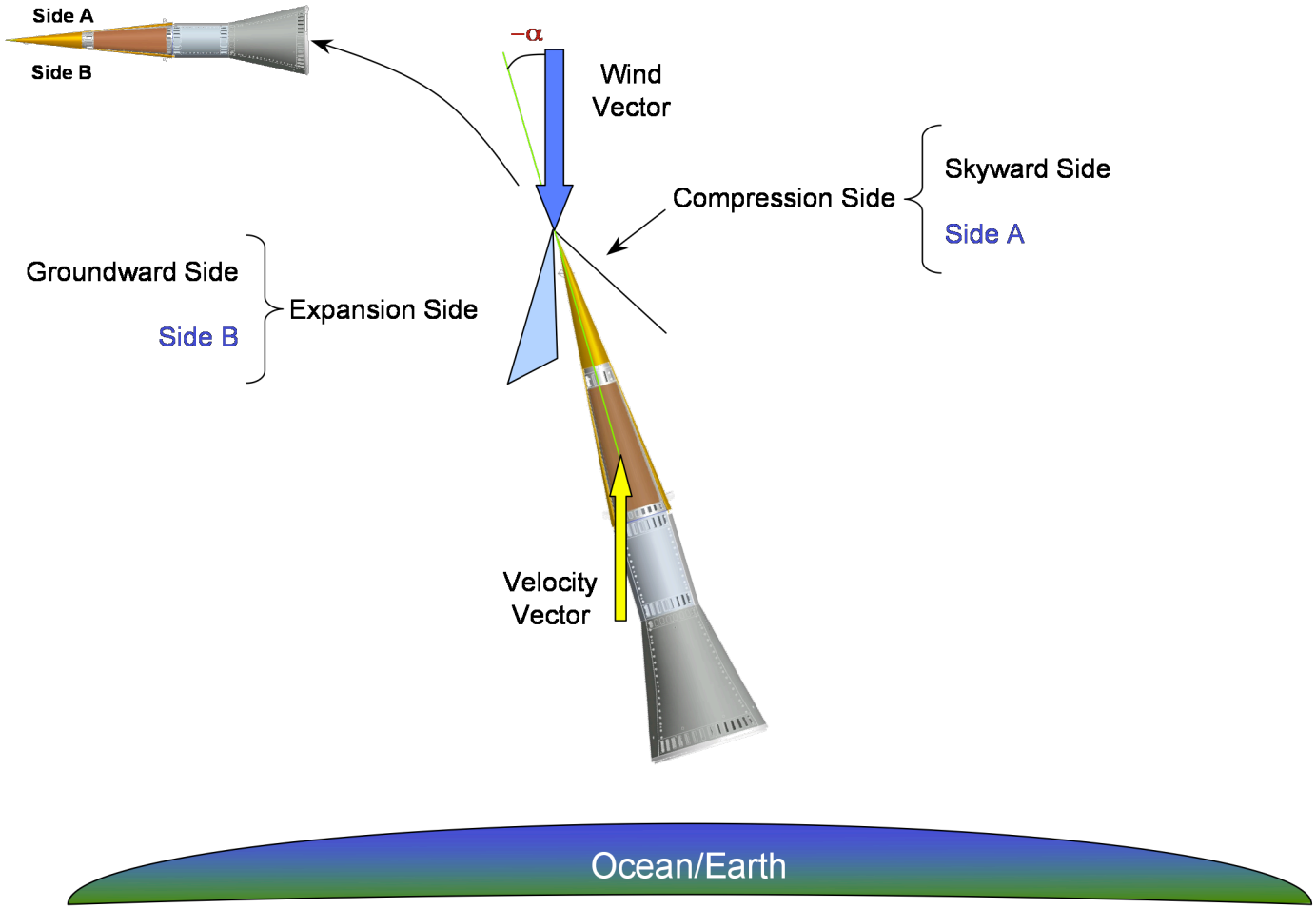

Figure 5. Trajectory outlook of vehicle orientation.

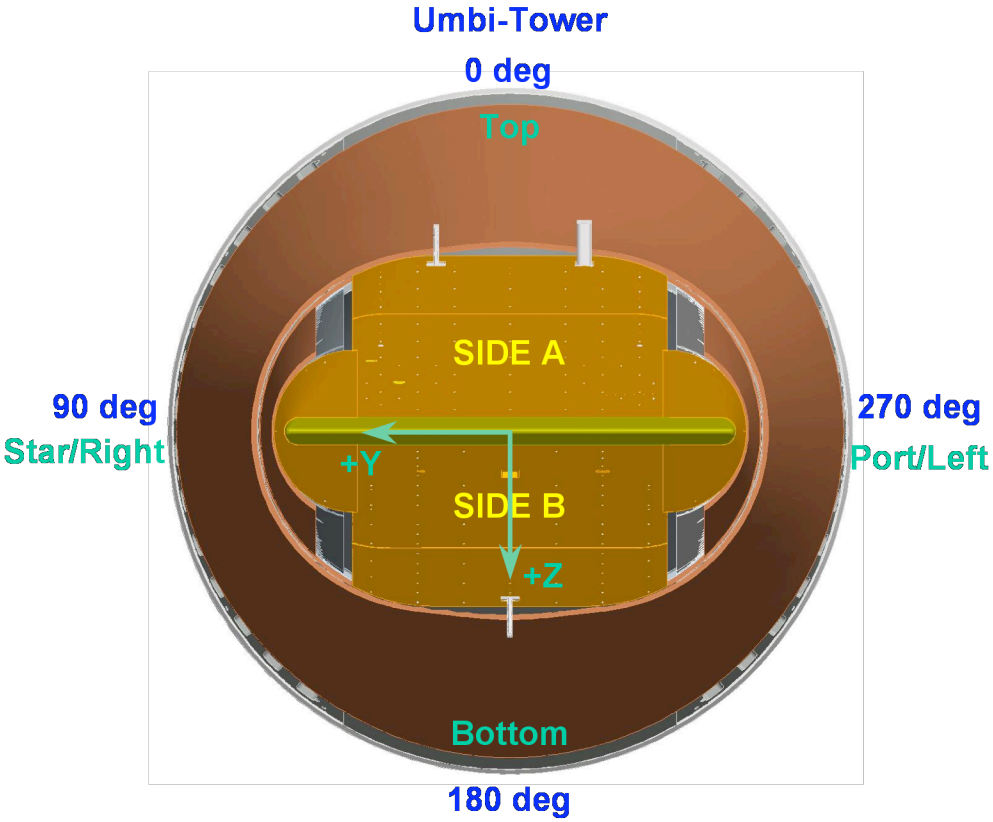

Figure 6. Instrumentation coordinate system (Forward looking Aft).

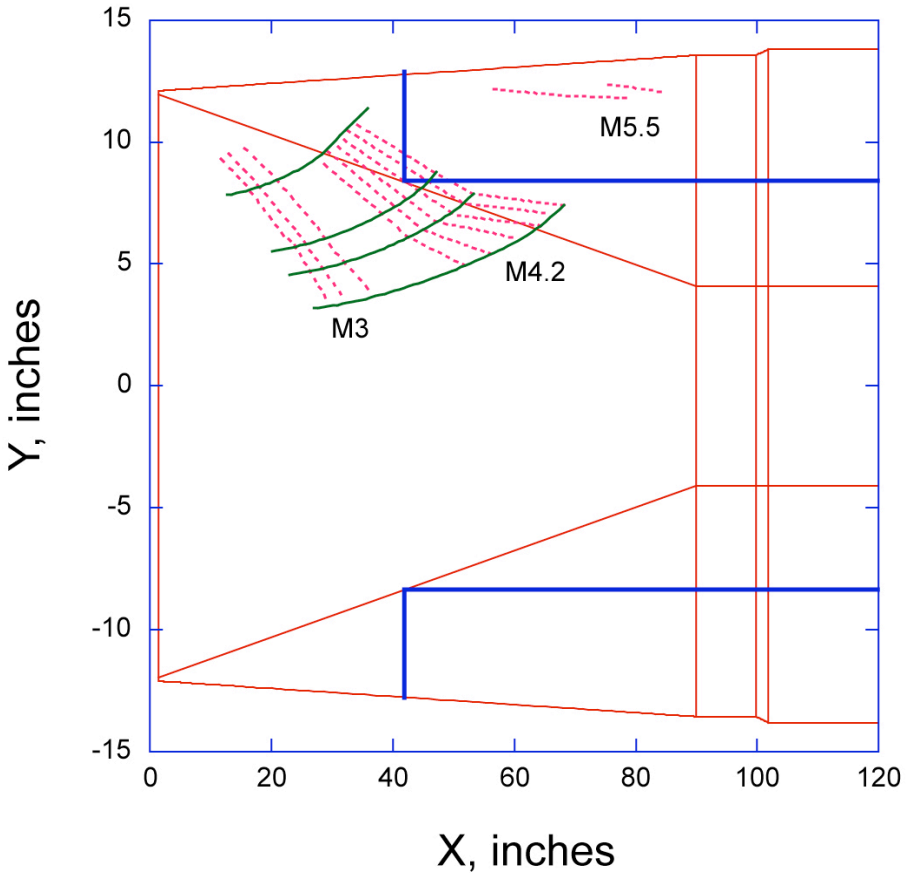

Figure 7. Side A transition prediction results.

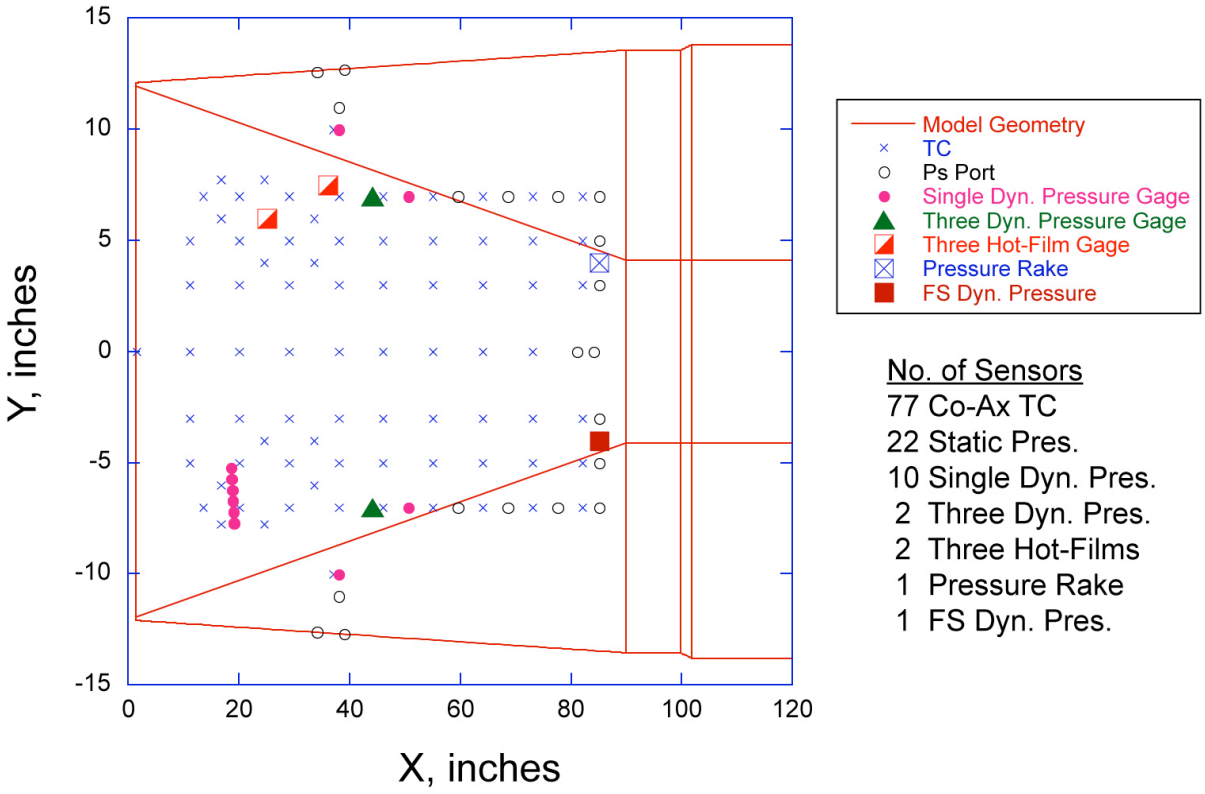

Figure 8. Side A instrumentation layout.

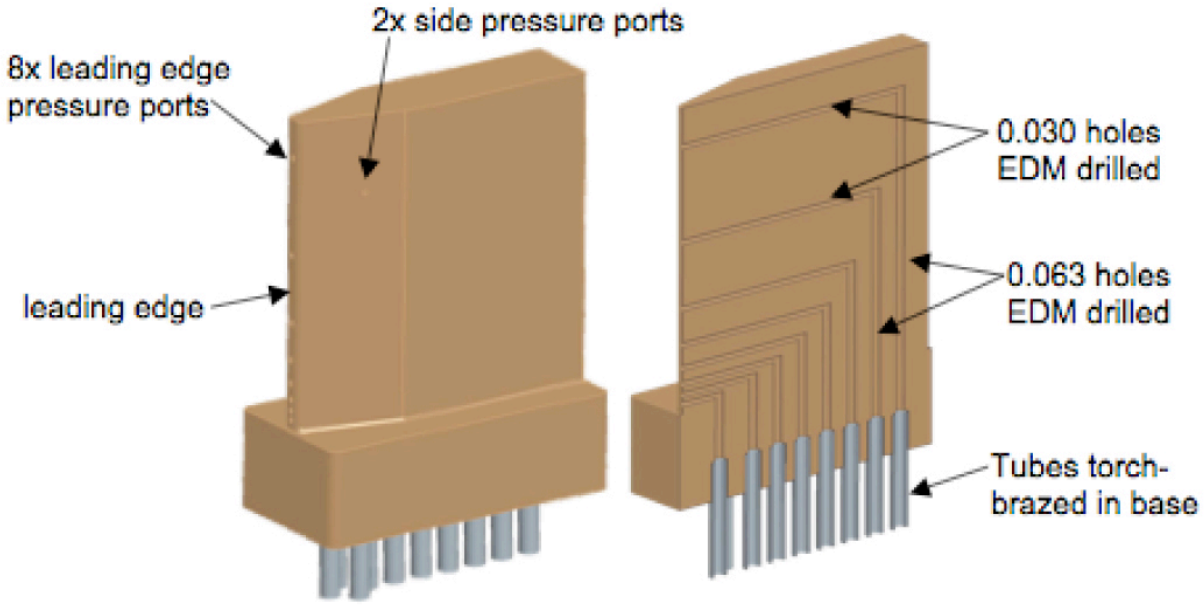

Figure 9. Side A boundary layer pressure rake.

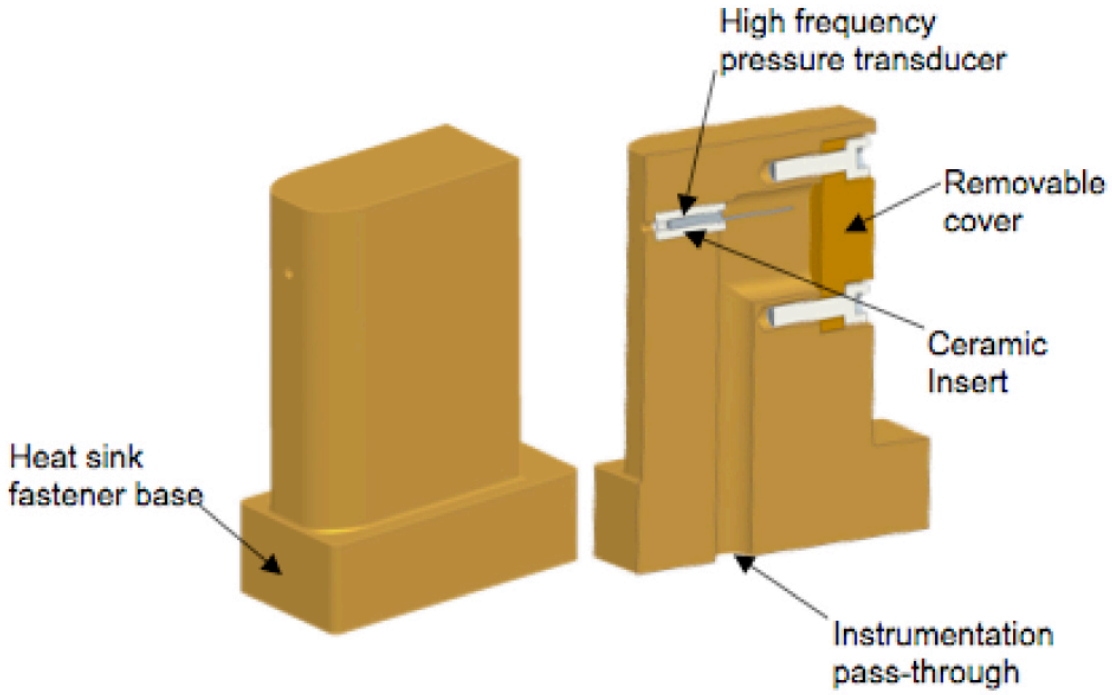

Figure 10. Side A freestream dynamic pressure probe.

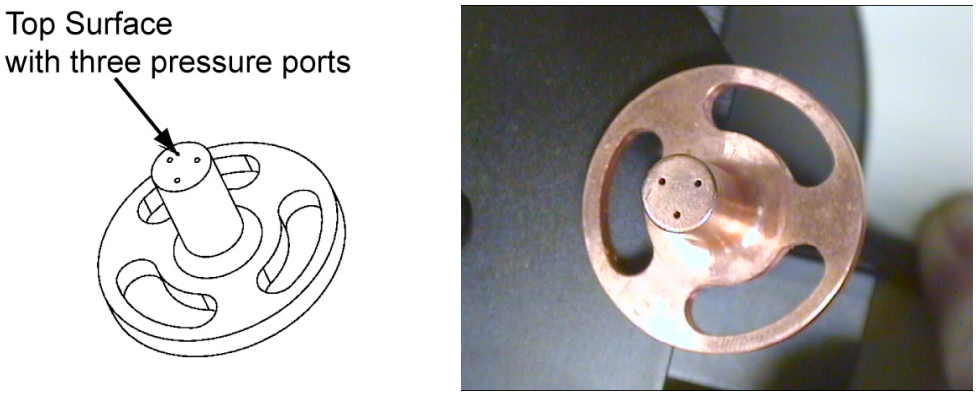

Figure 11. Side A three dynamic pressure probe.

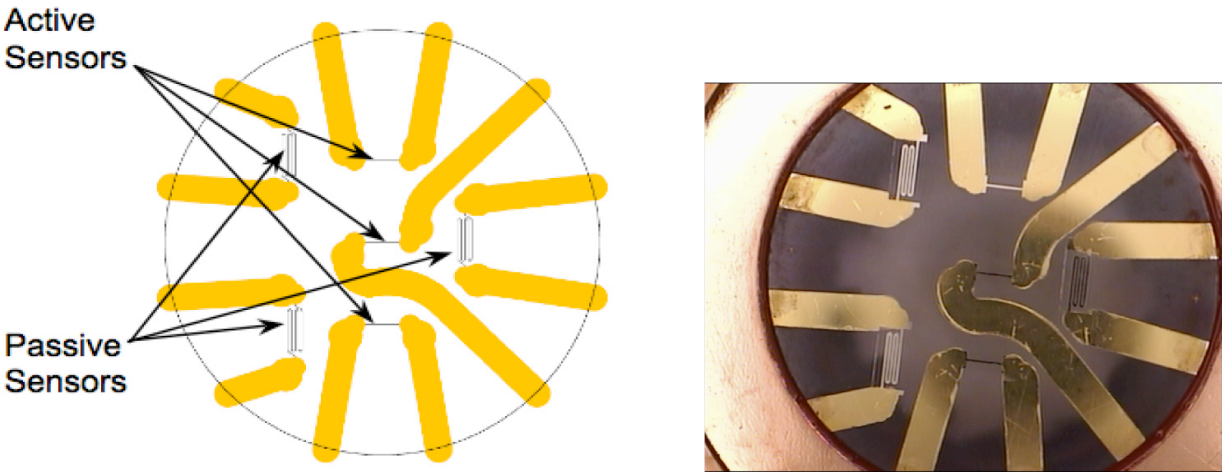

Figure 12. Side A surface hot-film plug.

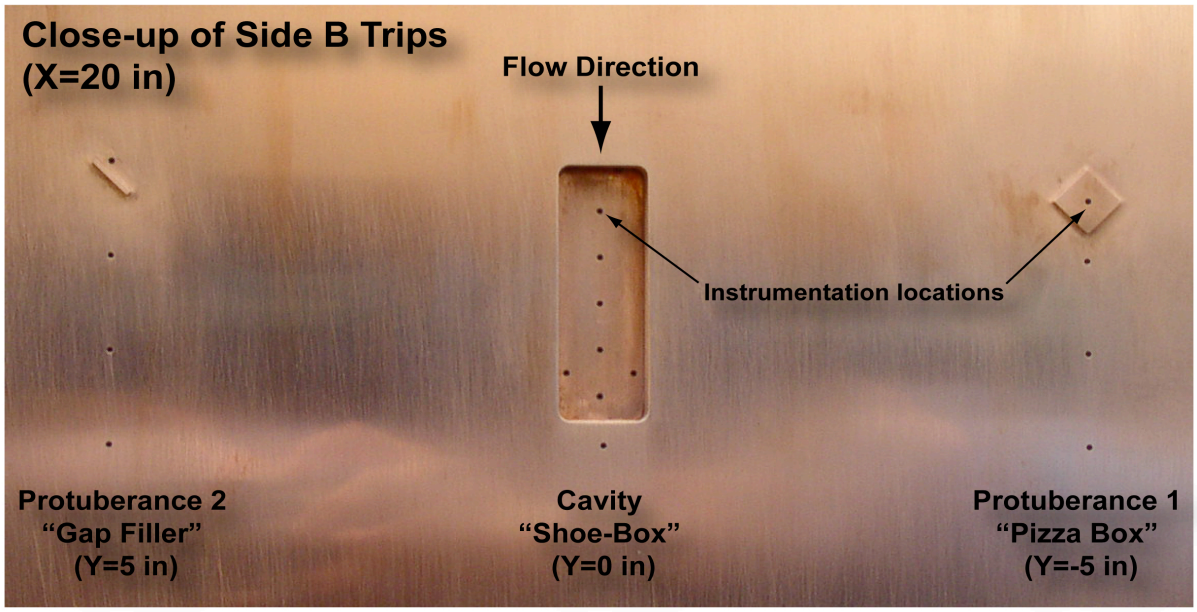

Figure 13. Side B roughness elements.

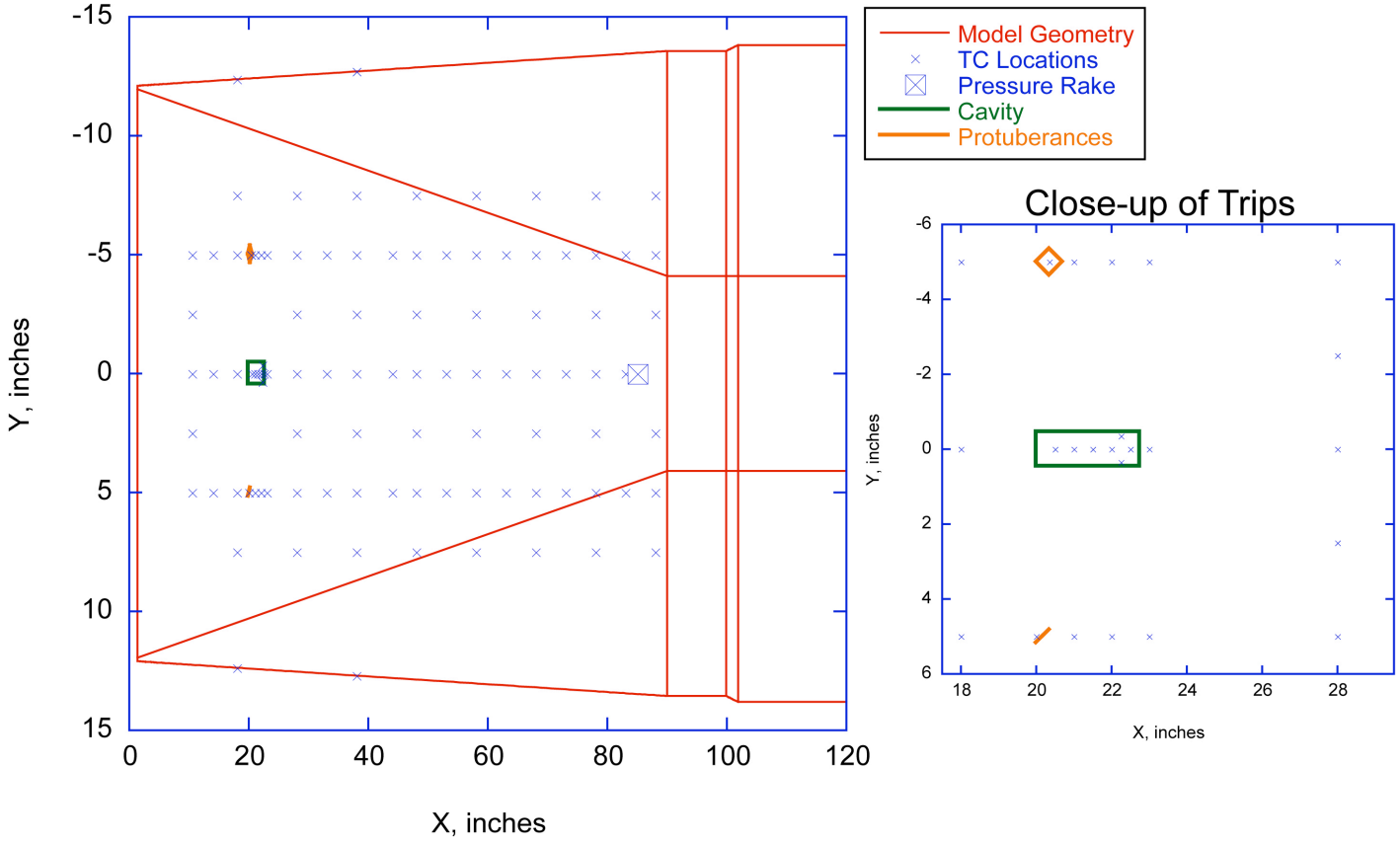

Figure 14. Side B instrumentation layout.

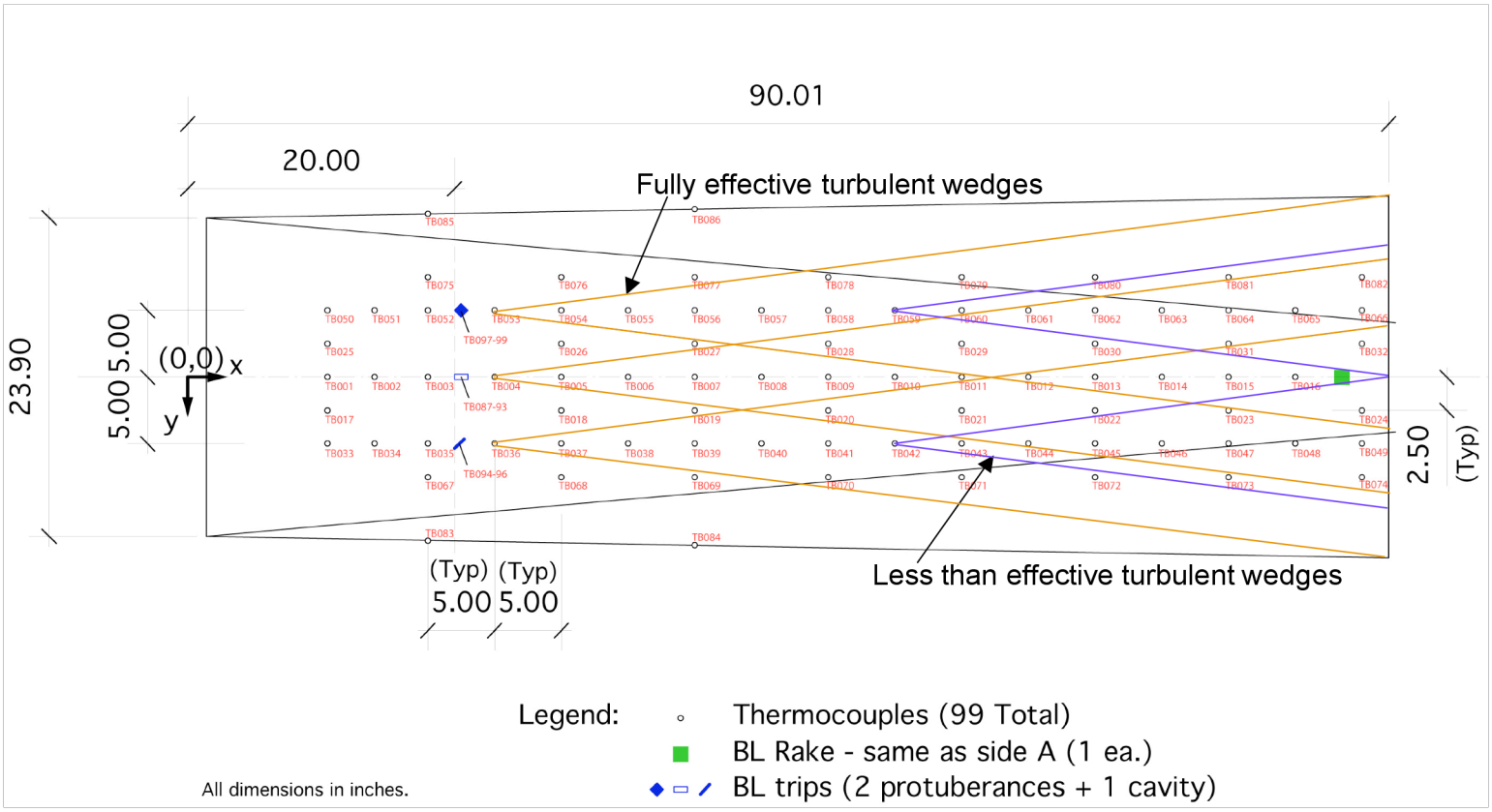

Figure 15. Side B instrumentation layout w.r.t. expected turbulent wedges downstream of boundary trips.

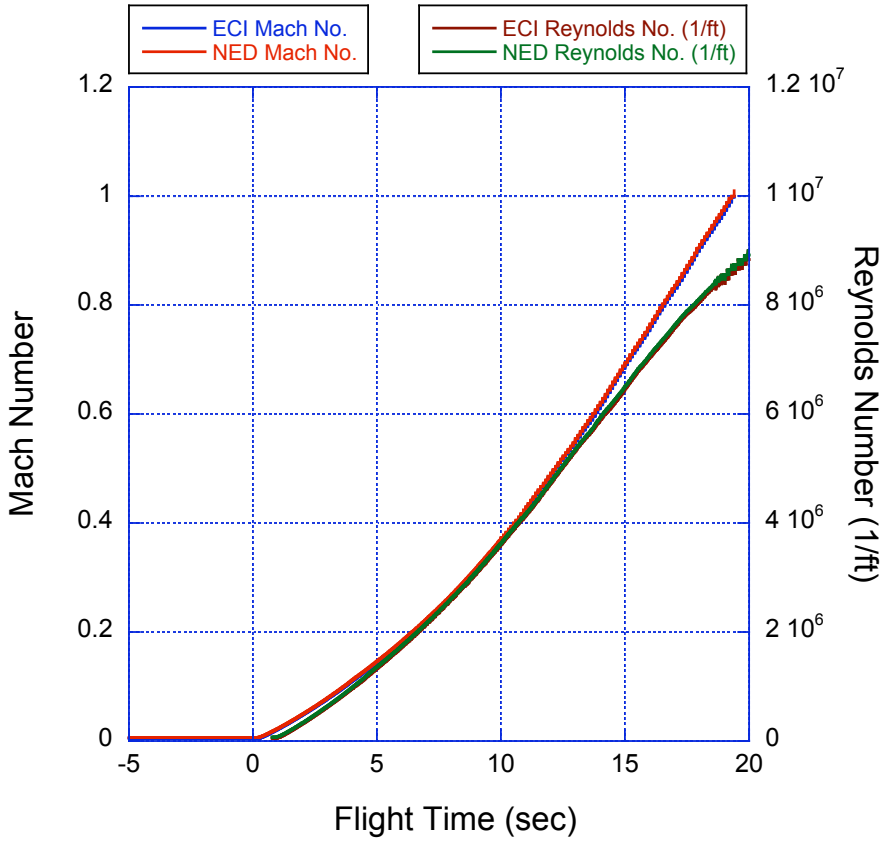

Note: ECI stands for Earth Centered Inertial and

NED stands for North East Down for reference systems

Figure 16. Flight Mach number and Reynolds number from ALV data.

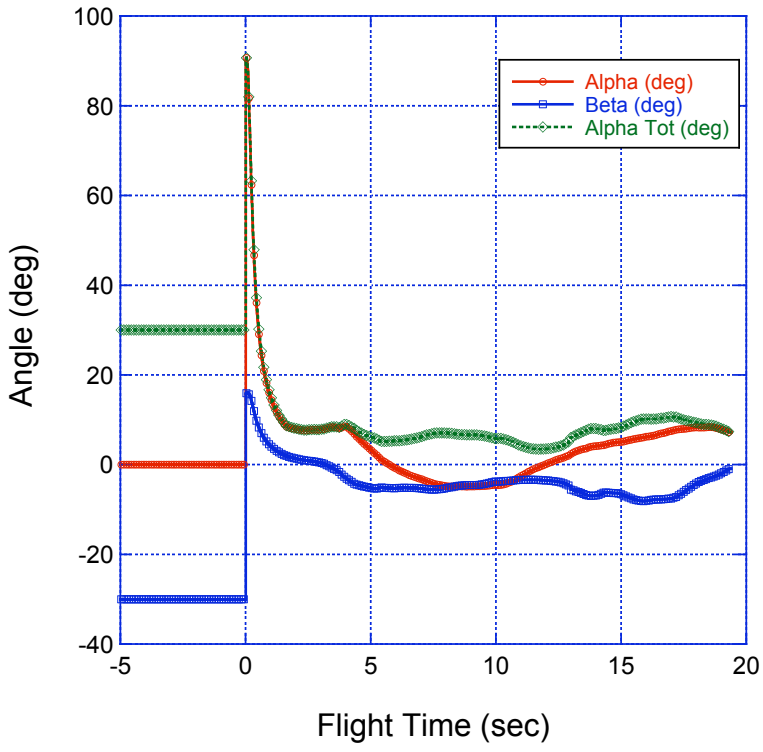

Figure 17. Flight alpha, beta and total alpha from ALV data.

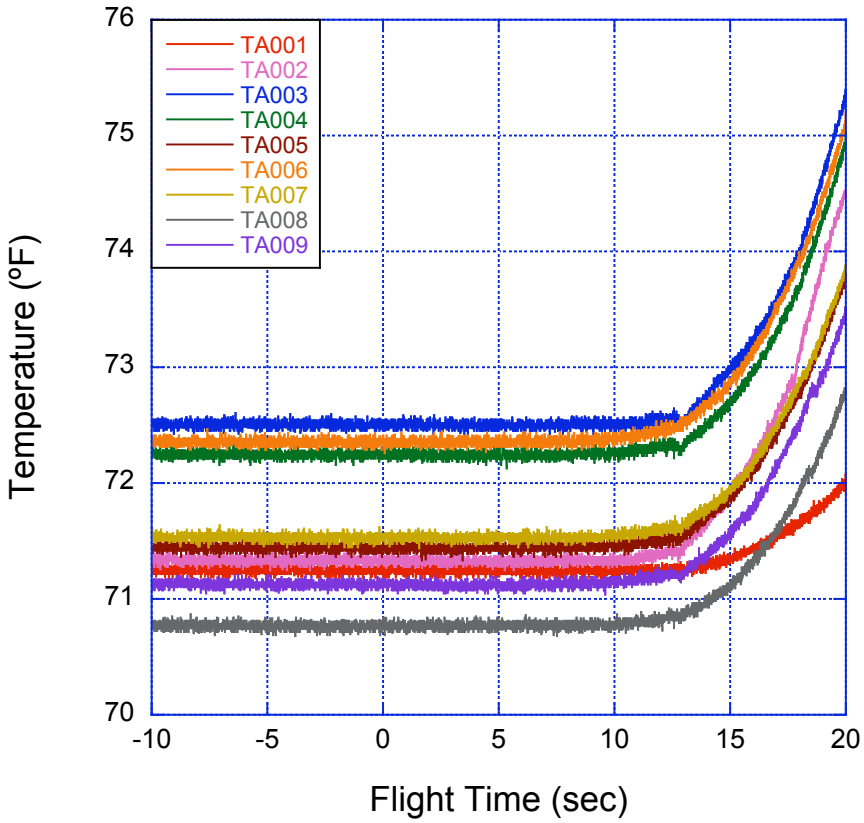

Figure 18a. Side A thermocouple data, TA001 – TA009.

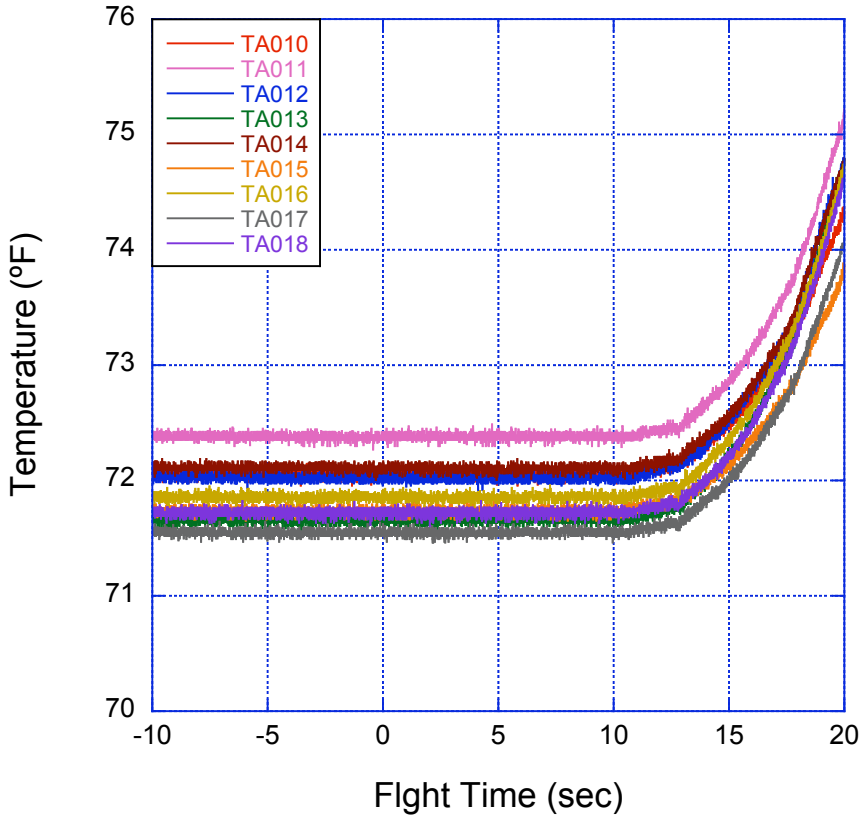

Figure 18b. Side A thermocouple data, TA010 – TA018.

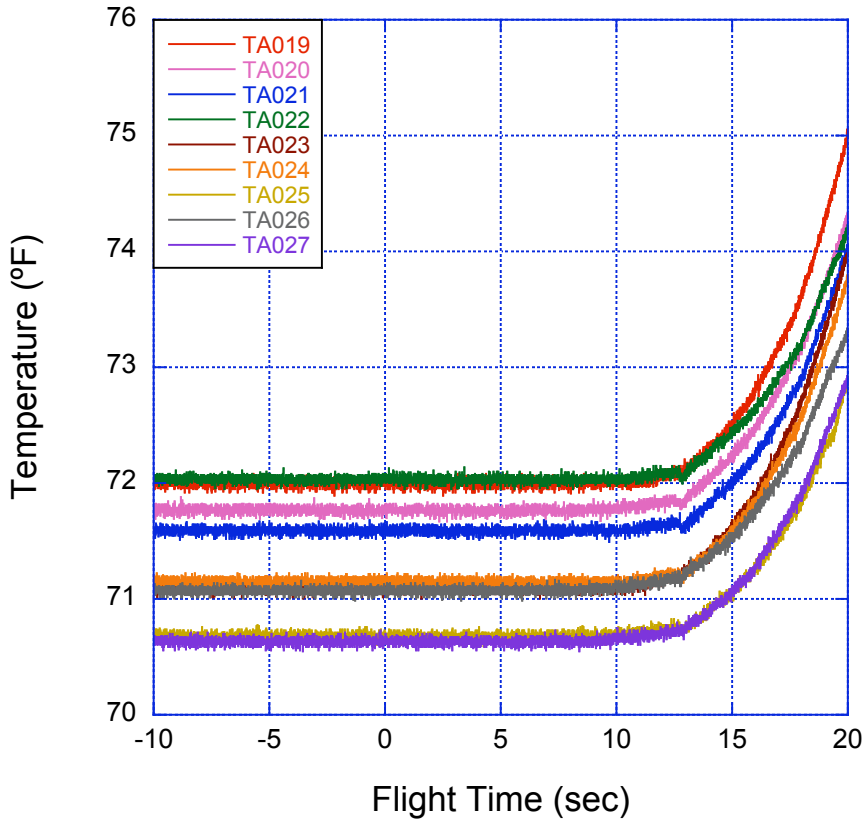

Figure 18c. Side A thermocouple data, TA019 – TA027.

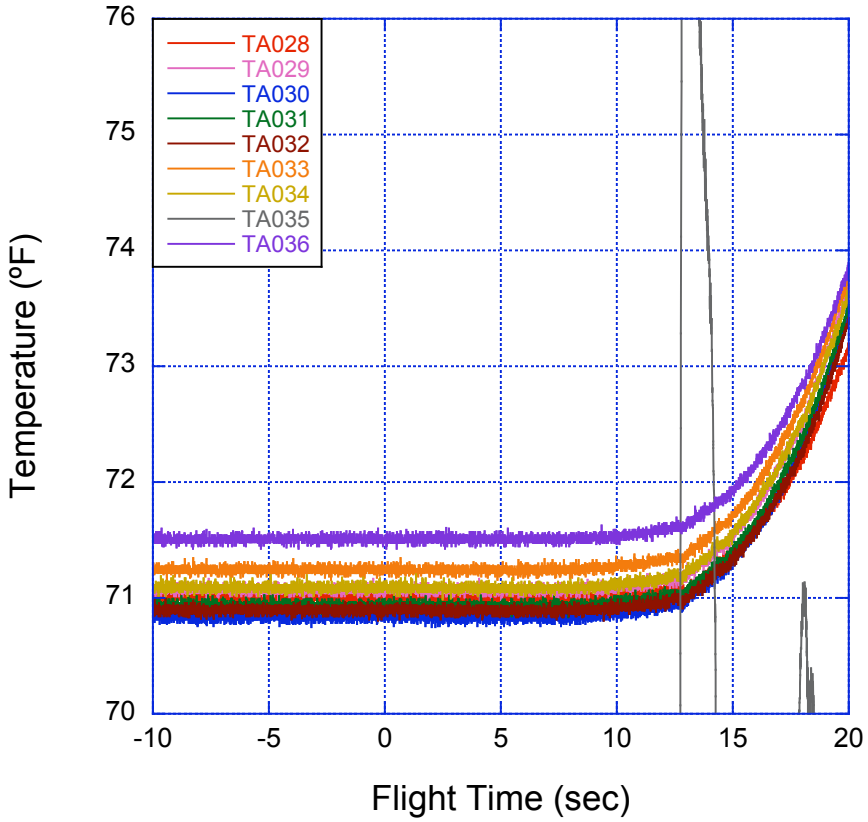

Figure 18d. Side A thermocouple data, TA028 – TA036.

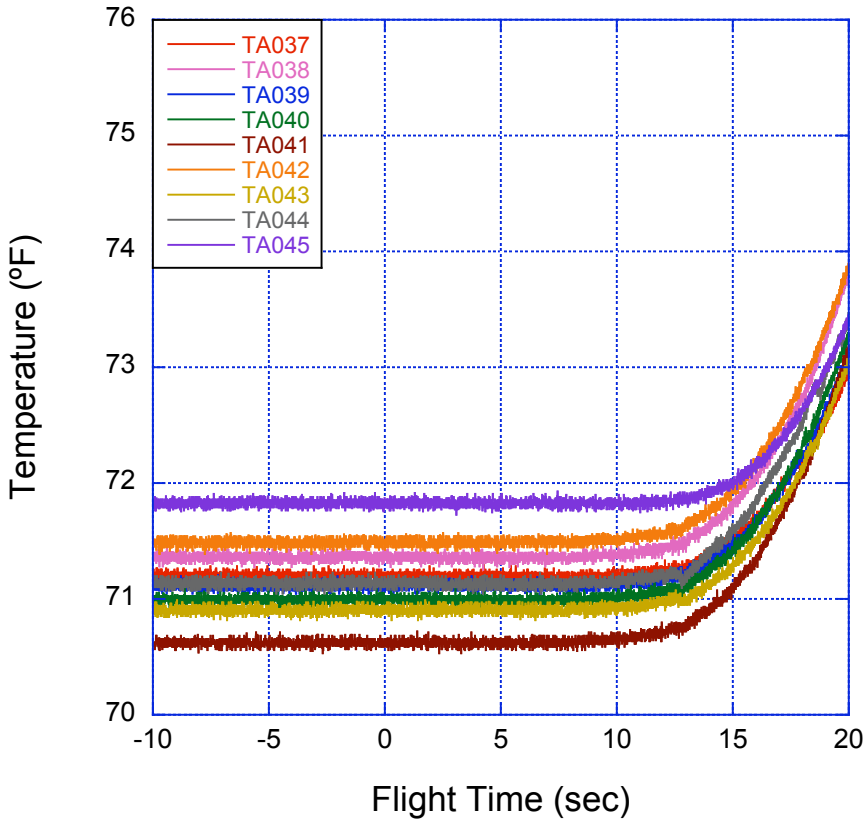

Figure 18e. Side A thermocouple data, TA037 – TA045.

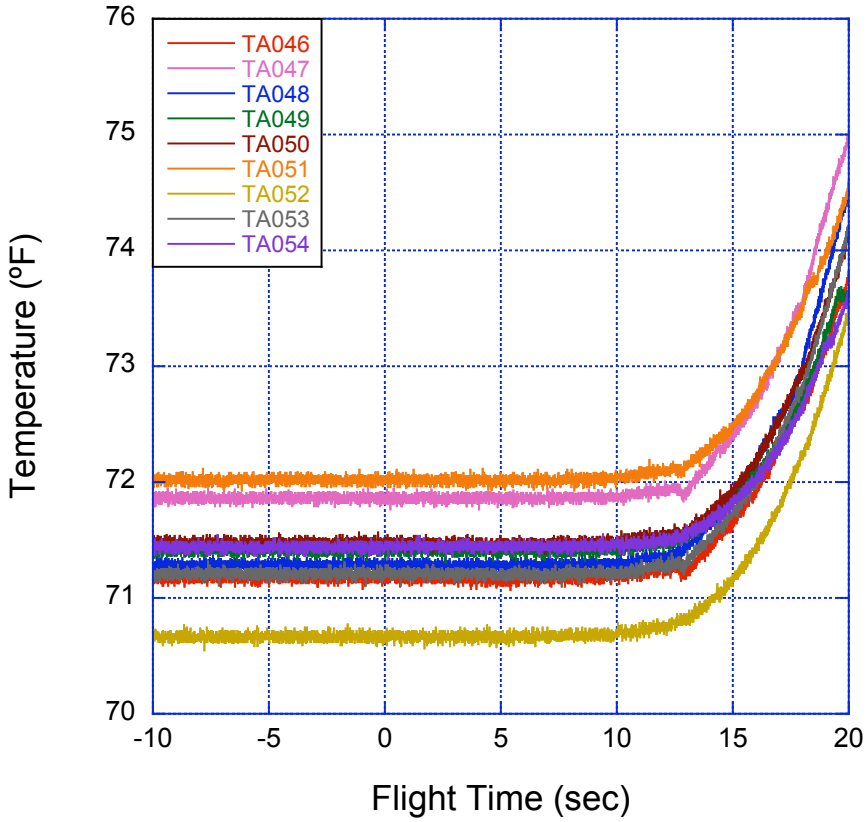

Figure 18f. Side A thermocouple data, TA046 – TA054.

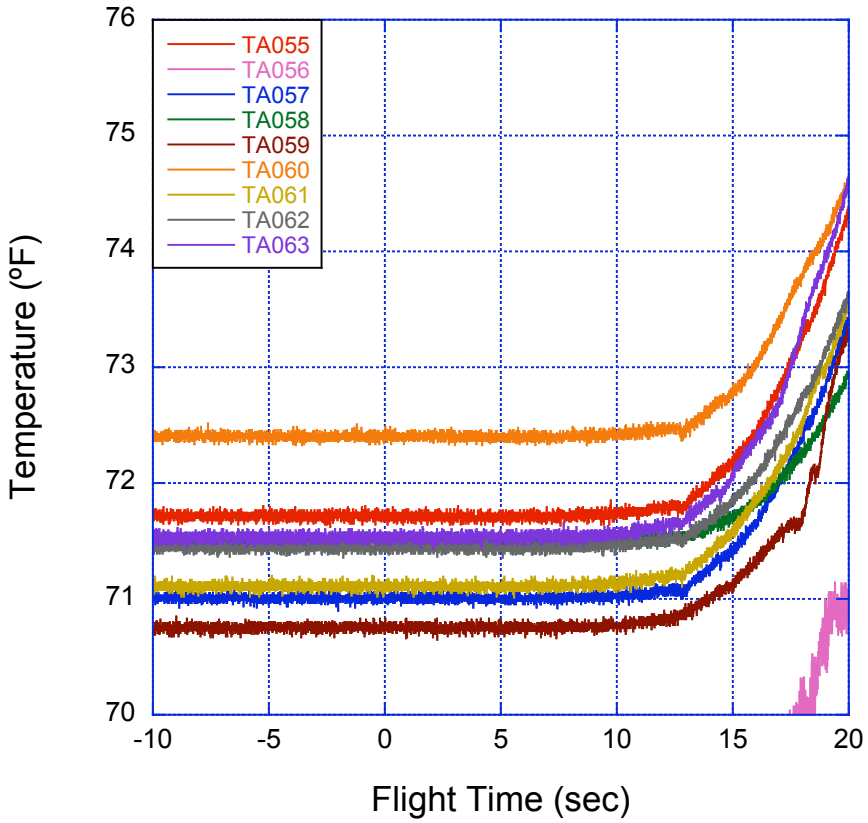

Figure 18g. Side A thermocouple data, TA055 – TA063.

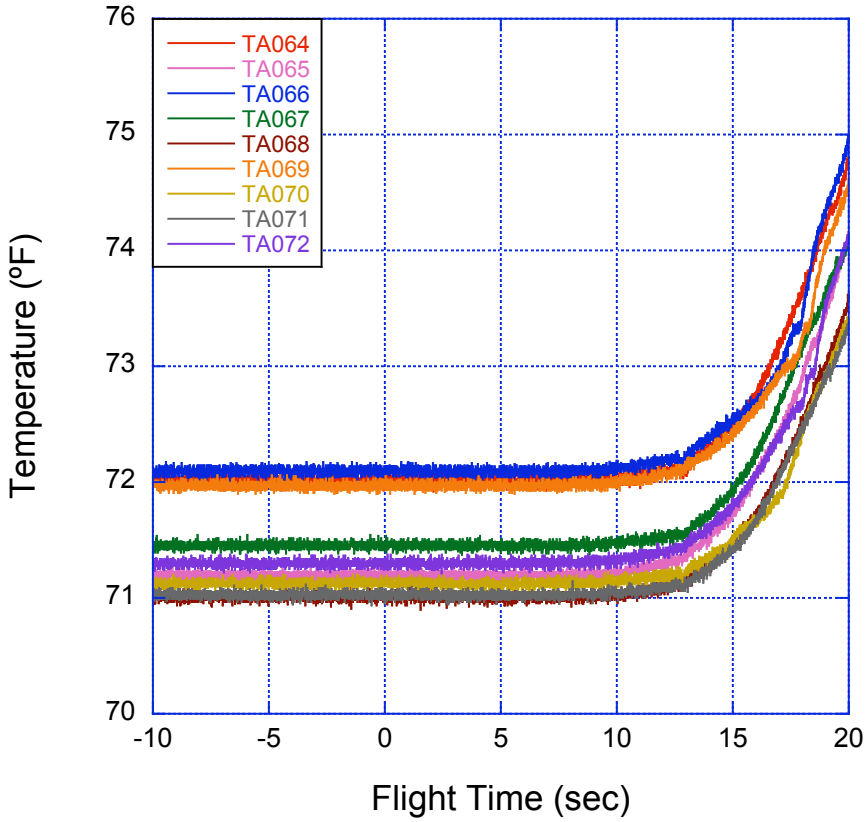

Figure 18h. Side A thermocouple data, TA064 – TA072.

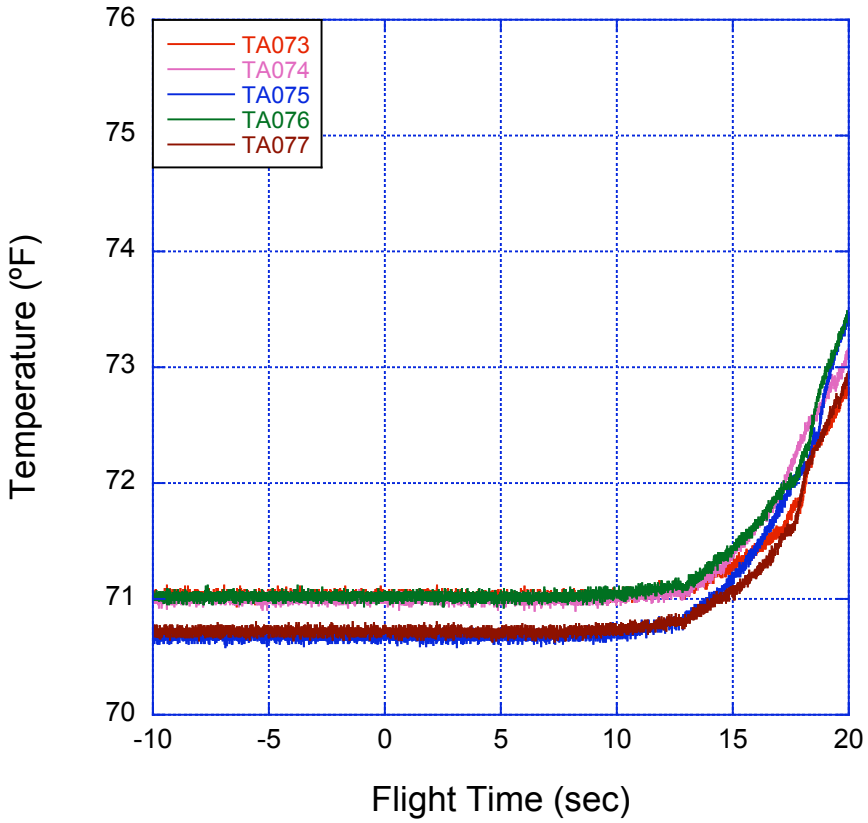

Figure 18i. Side A thermocouple data, TA073 – TA077.

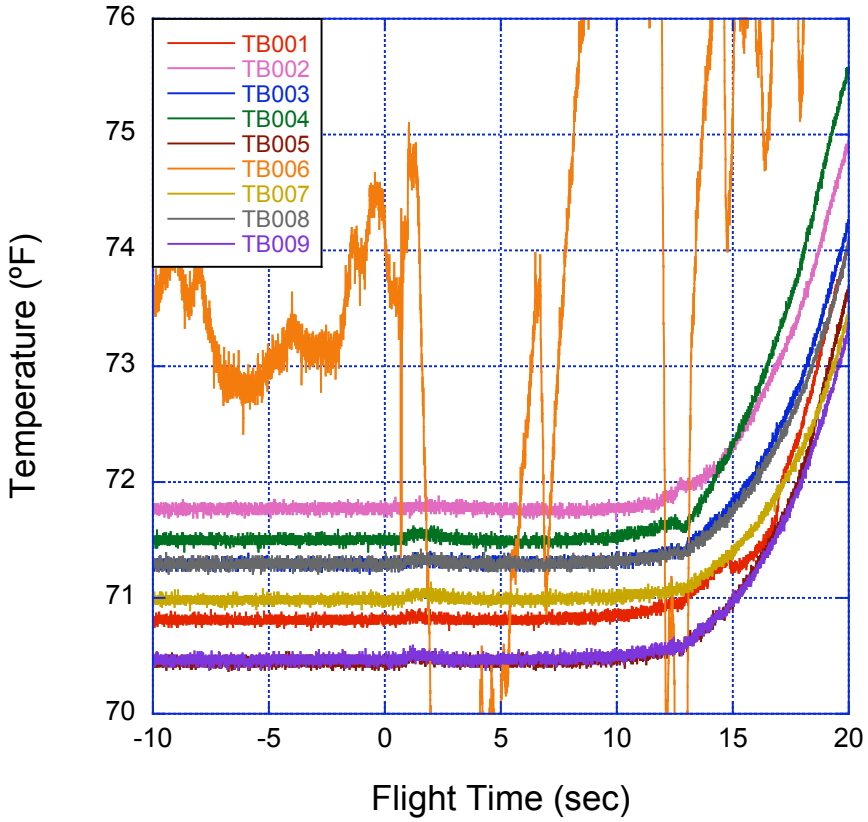

Figure 19a. Side B thermocouple data, TB001 – TB009.

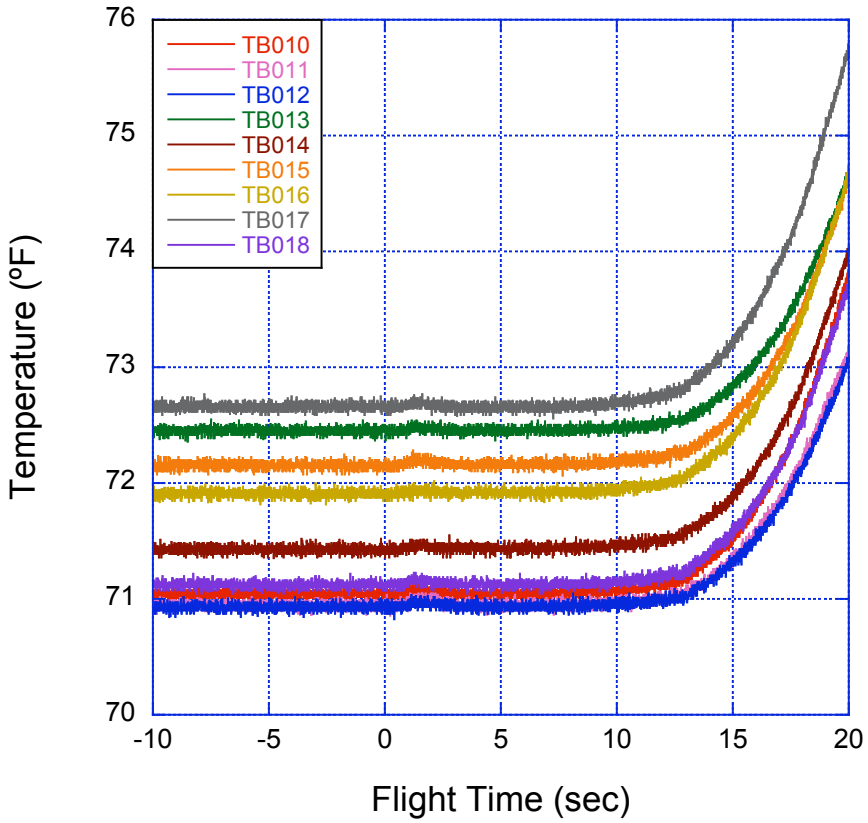

Figure 19b. Side B thermocouple data, TB010 – TB018.

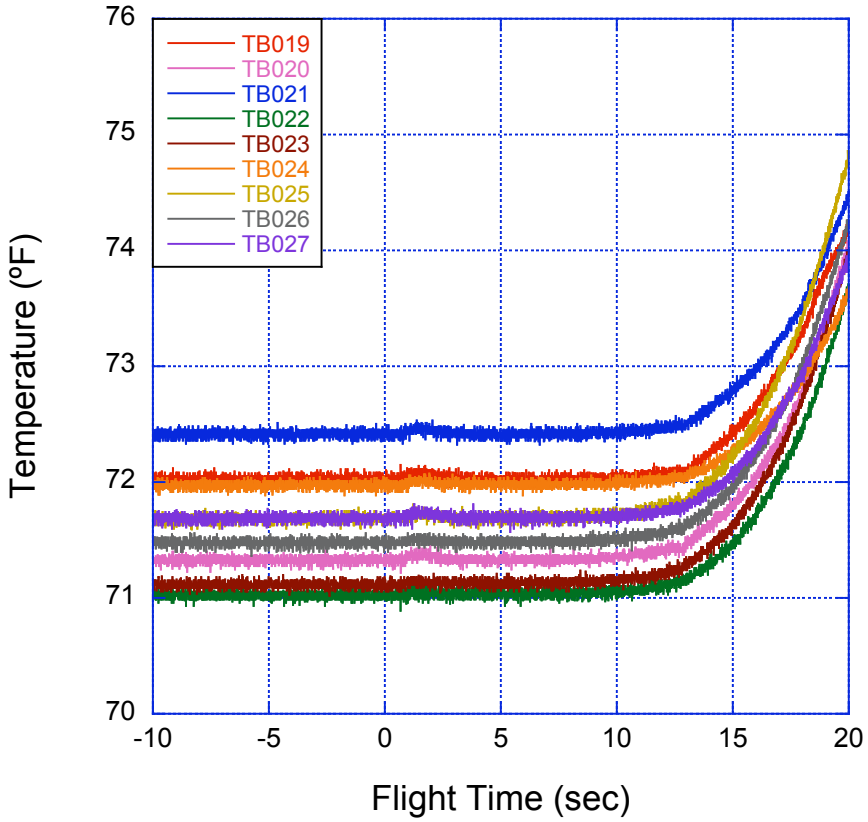

Figure 19c. Side B thermocouple data, TB019 – TB027.

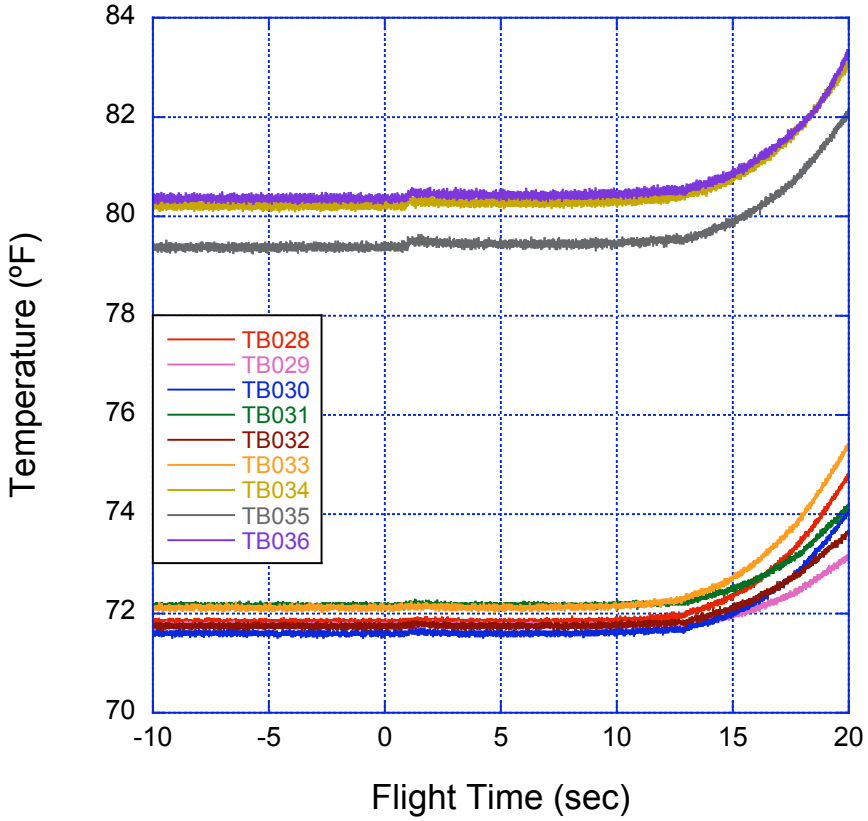

Figure 19d. Side B thermocouple data, TB028 – TB036.

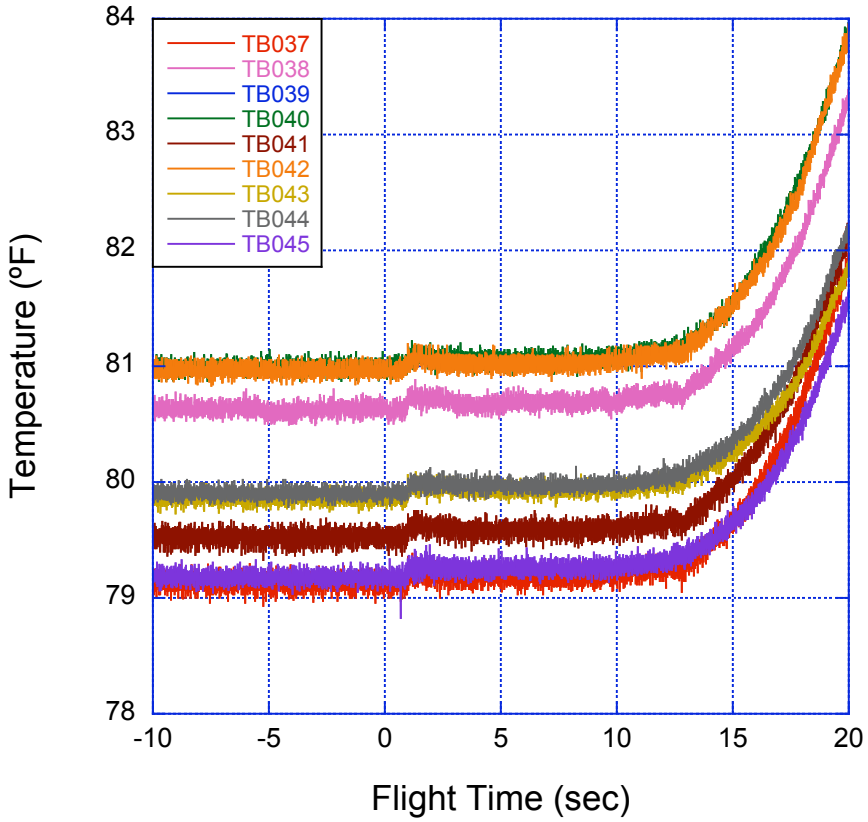

Figure 19e. Side B thermocouple data, TB037 – TB045.

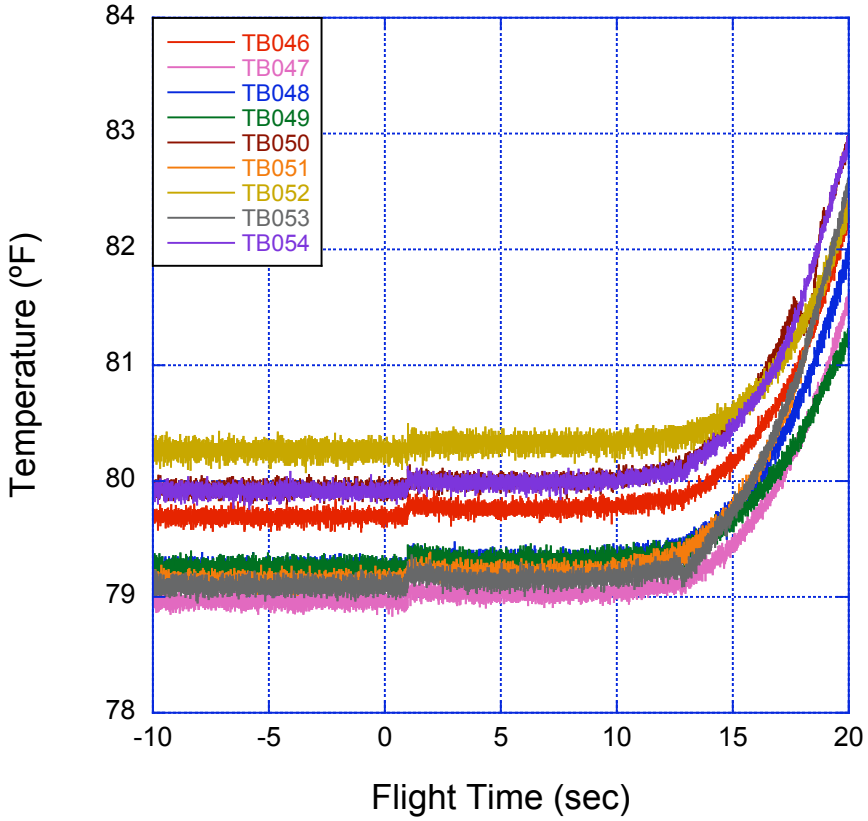

Figure 19f. Side B thermocouple data, TB046 – TB054.

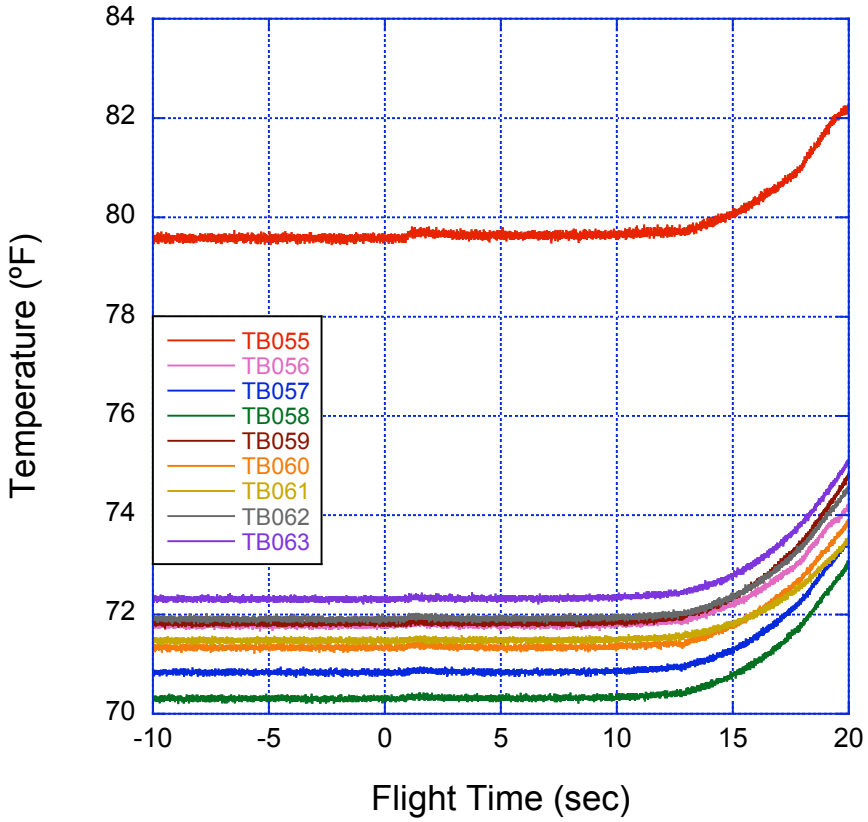

Figure 19g. Side B thermocouple data, TB055 – TB063.

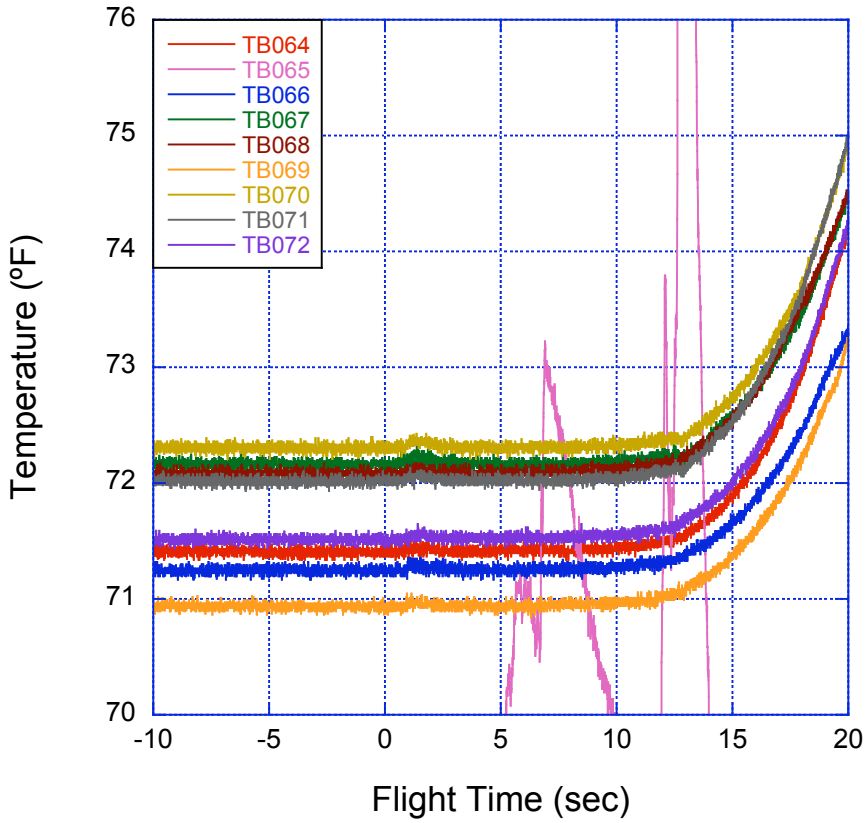

Figure 19h. Side B thermocouple data, TB064 – TB072.

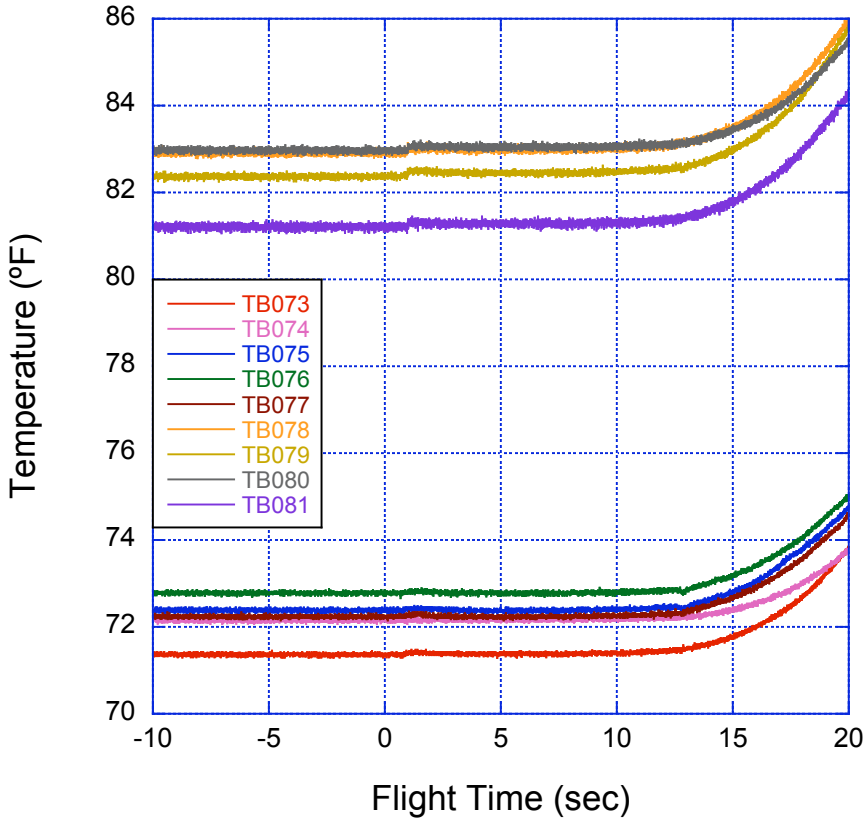

Figure 19i. Side B thermocouple data, TB073 – TB081.

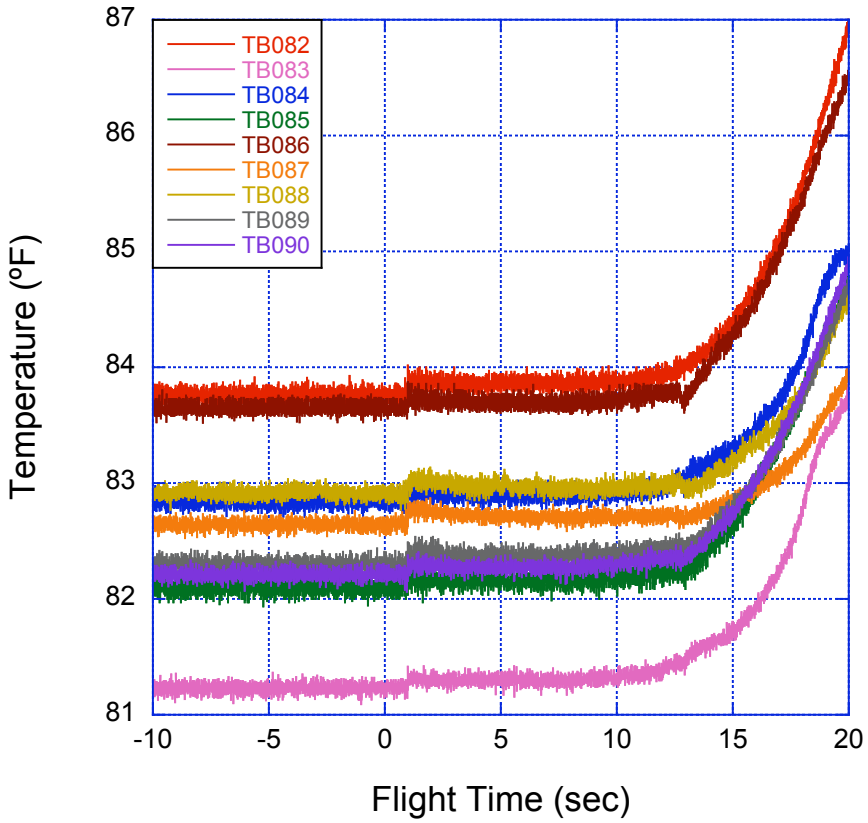

Figure 19j. Side B thermocouple data, TB082 – TB090.

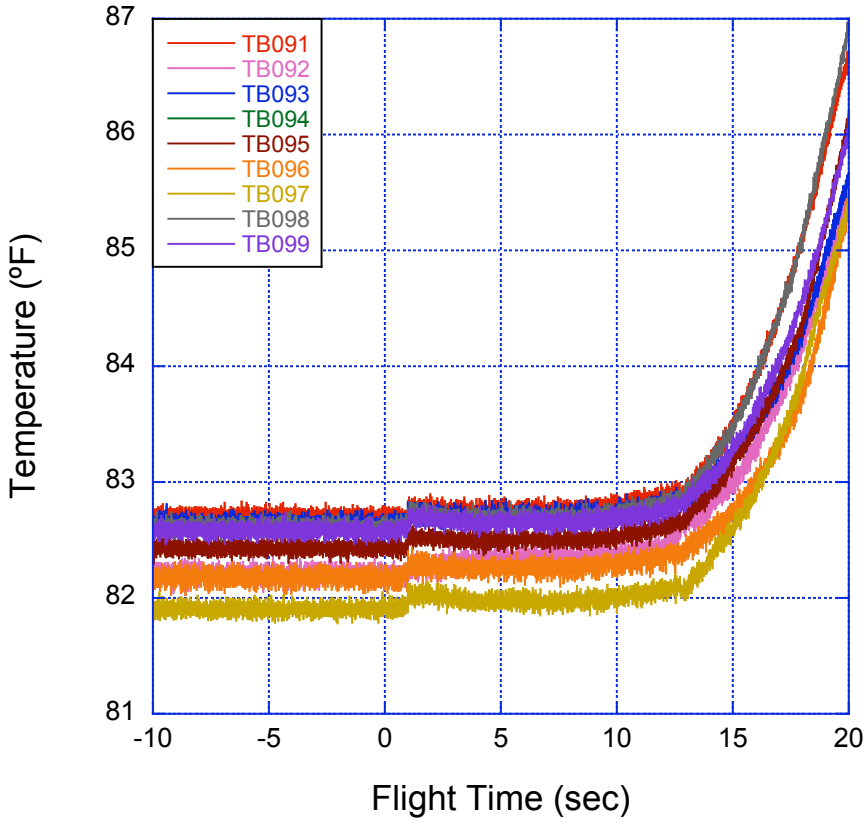

Figure 19k. Side B thermocouple data, TB091 – TB099.

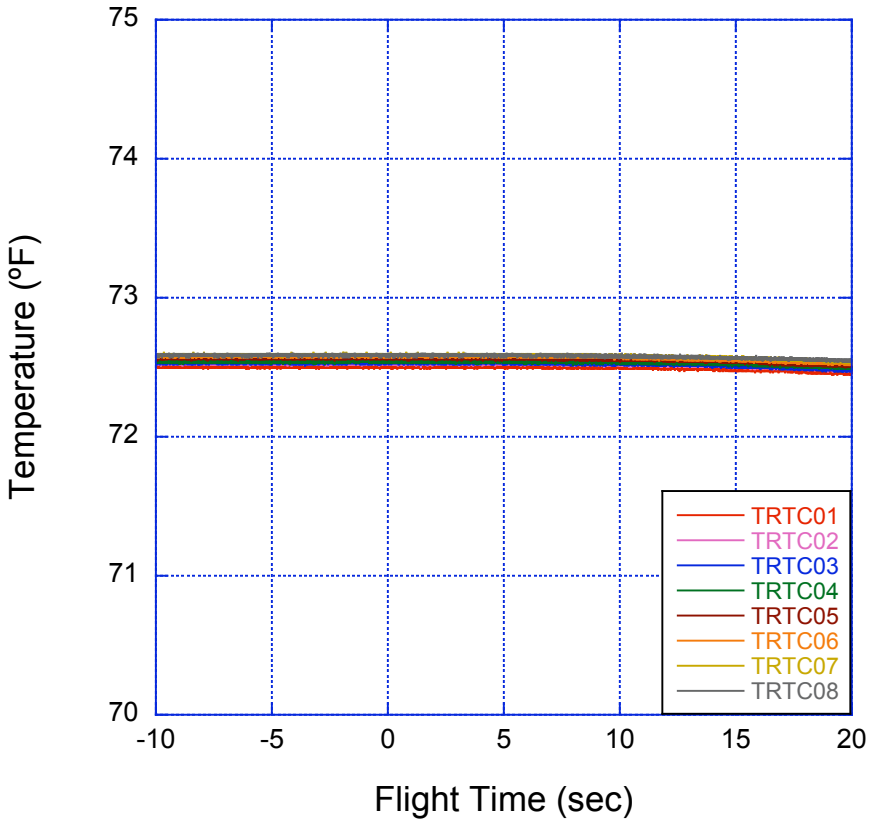

Figure 20a. Thermocouple reference temperature data, TRTC01 – TRTC08.

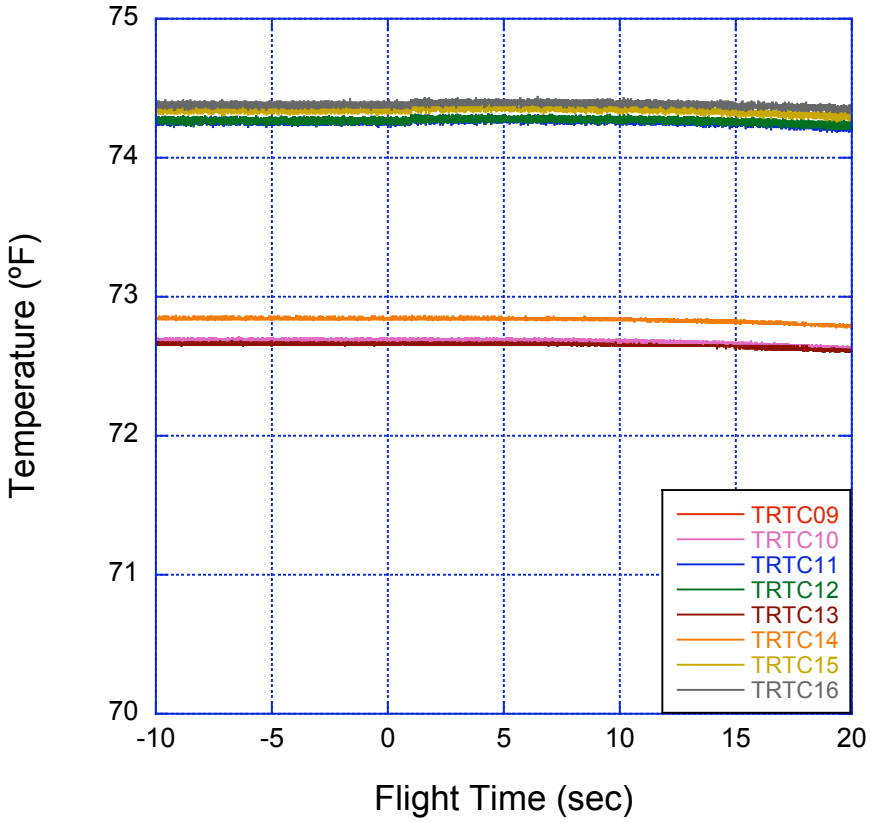

Figure 20b. Thermocouple reference temperature data, TRTC09 – TRTC16.

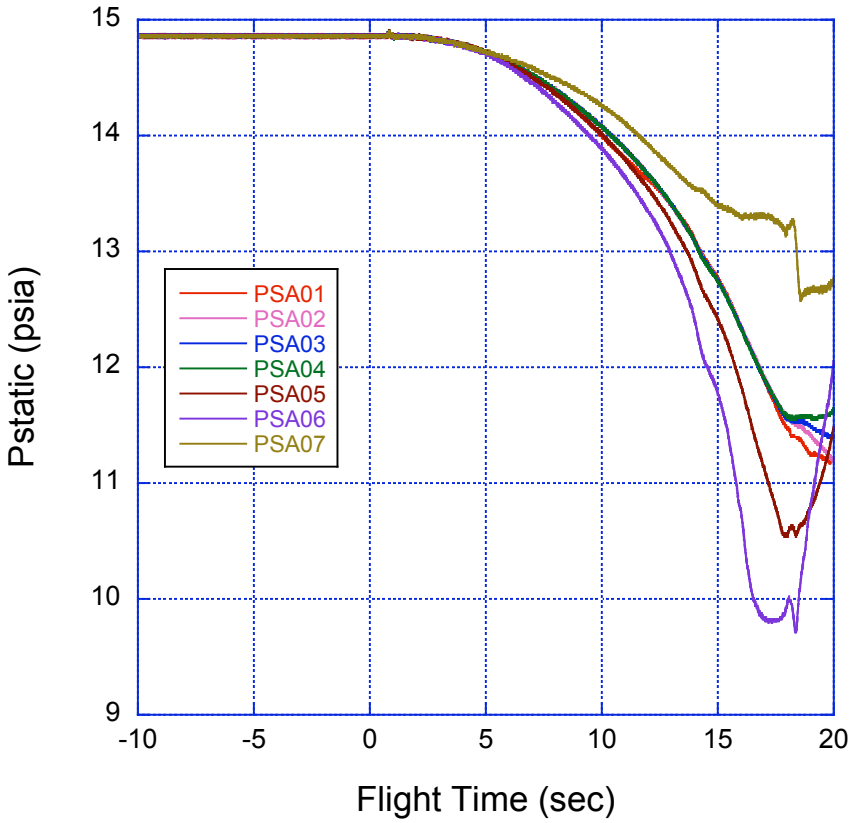

Figure 21a. Side A surface static pressure data, starboard side (+*Y*).

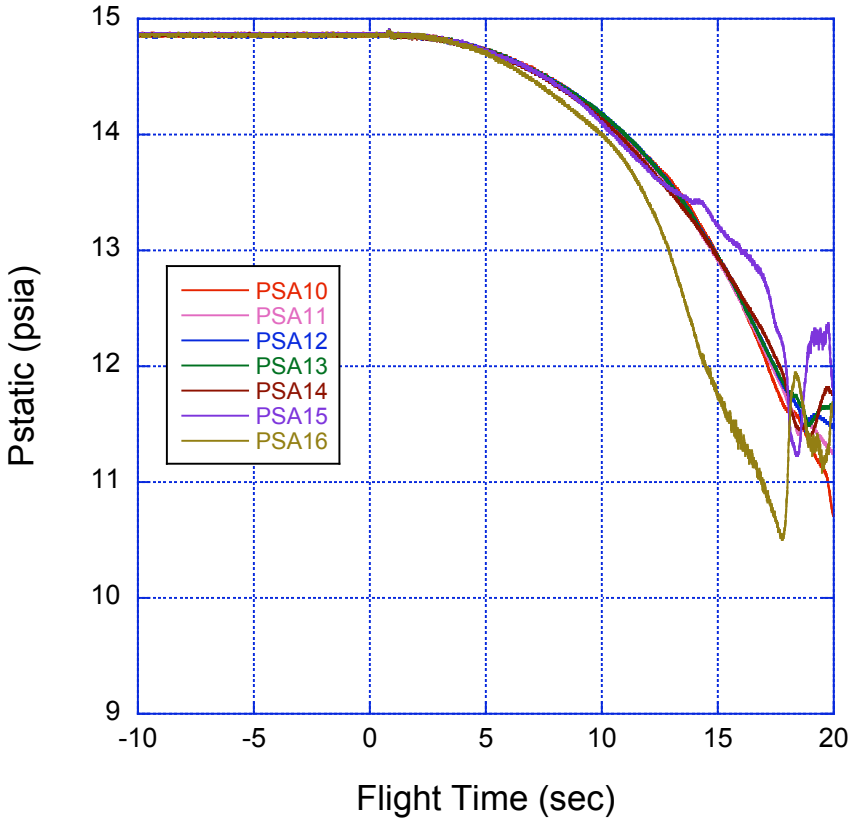

Figure 21b. Side A surface static pressure data, port side (-*Y*).

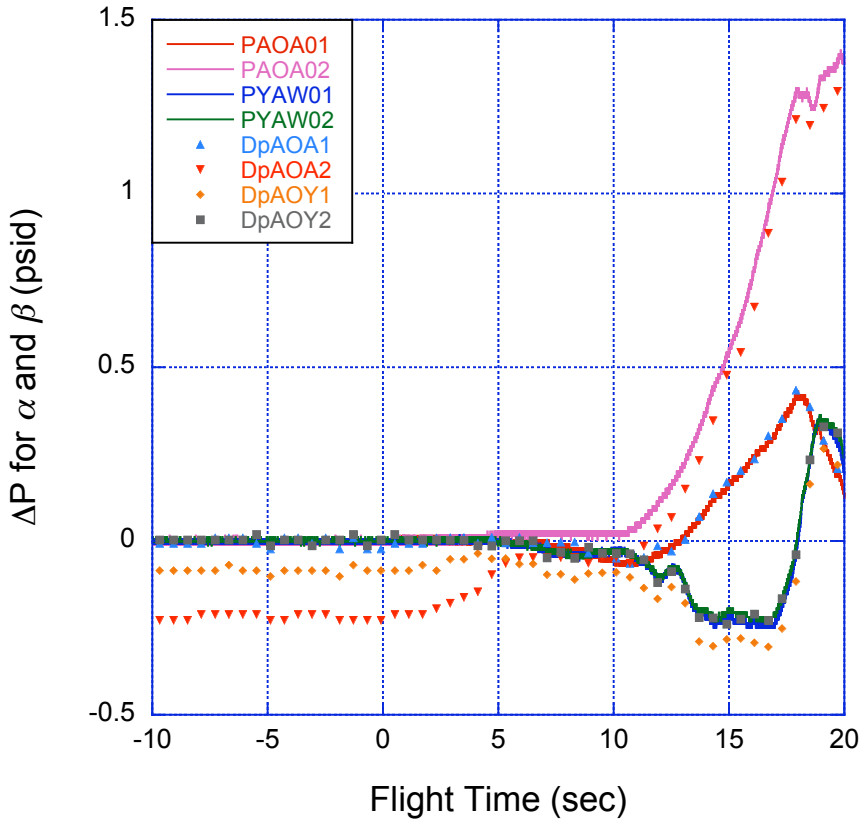

Figure 22a. Differential pressure data for angle of attack and angle of yaw.

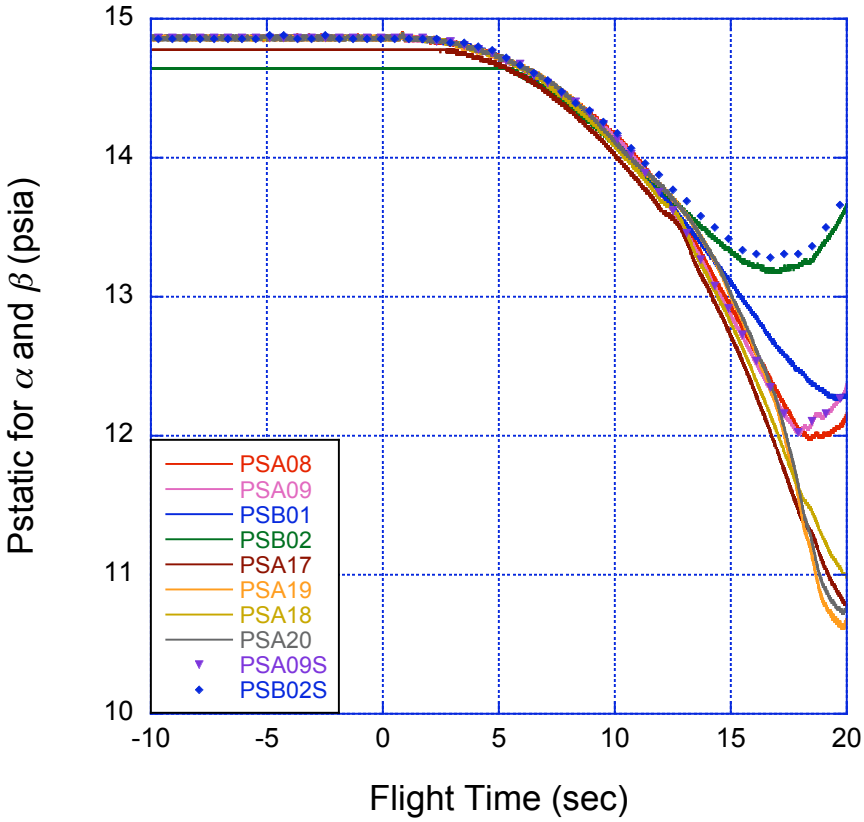

Figure 22b. Static pressure data for angle of attack and angle of yaw.

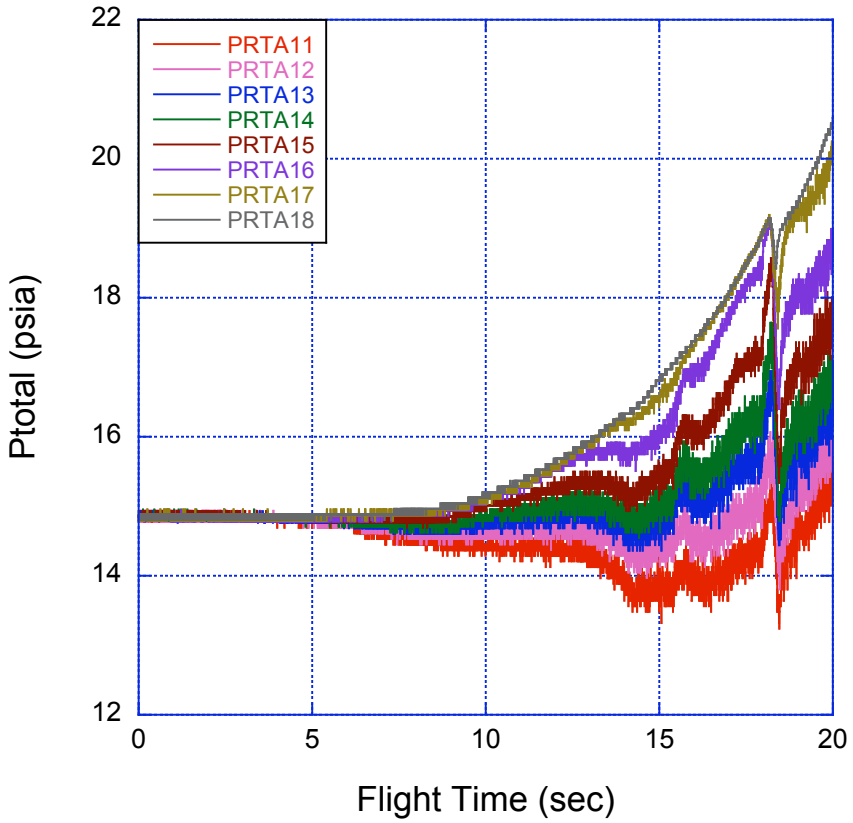

Figure 23a. Side A boundary-layer pressure rake data.

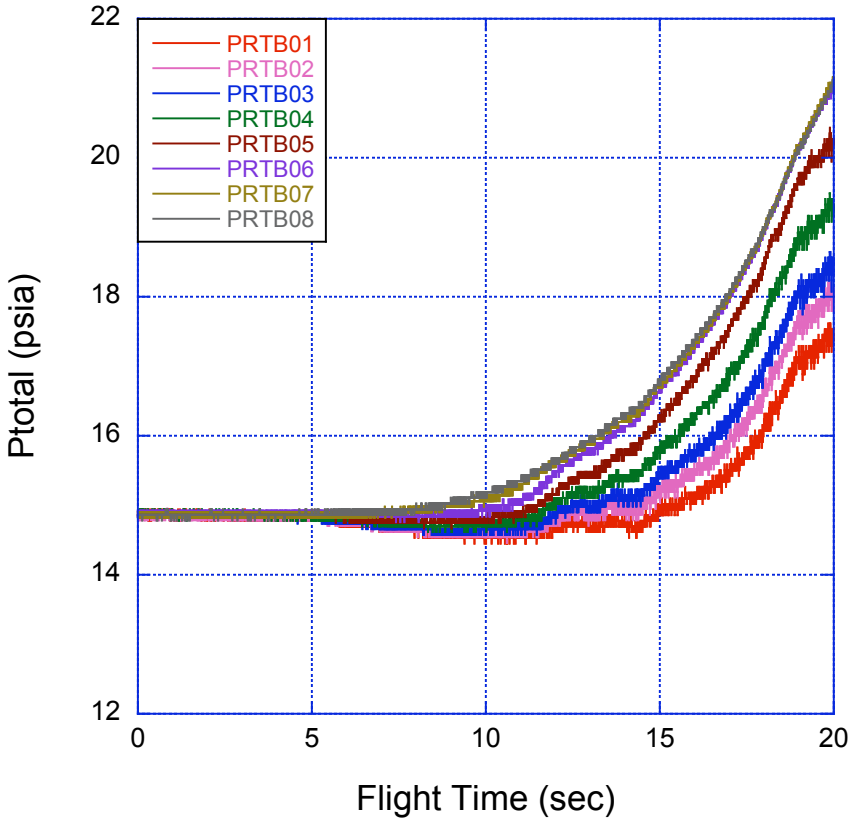

Figure 23b. Side B boundary-layer pressure rake data.

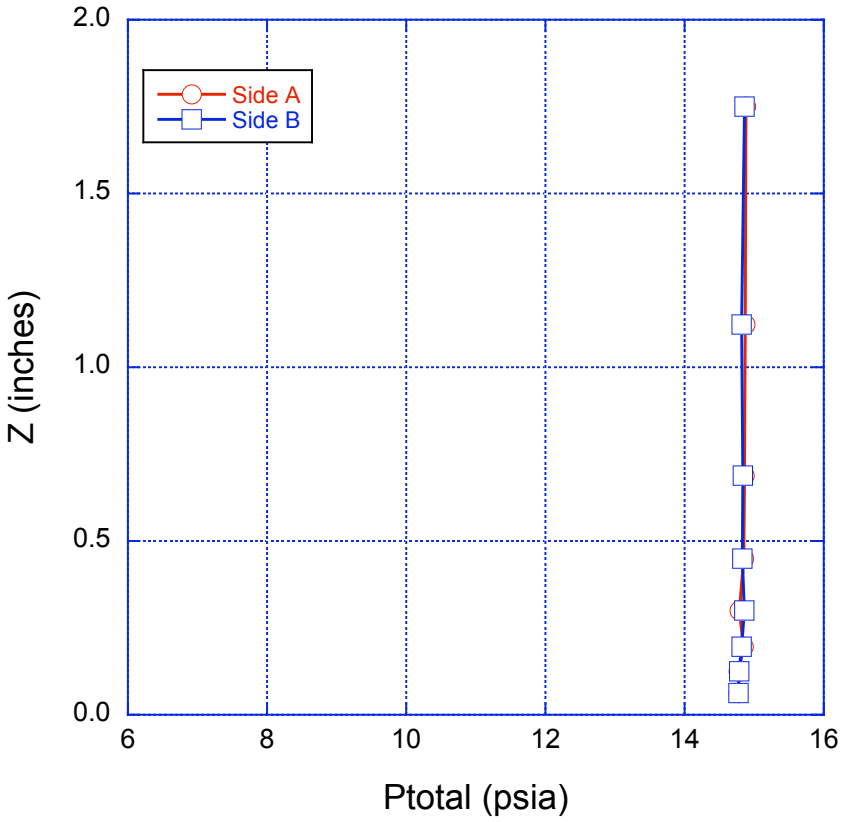

Figure 24a. Boundary-layer pressure profile data at *T0*+5.00s.

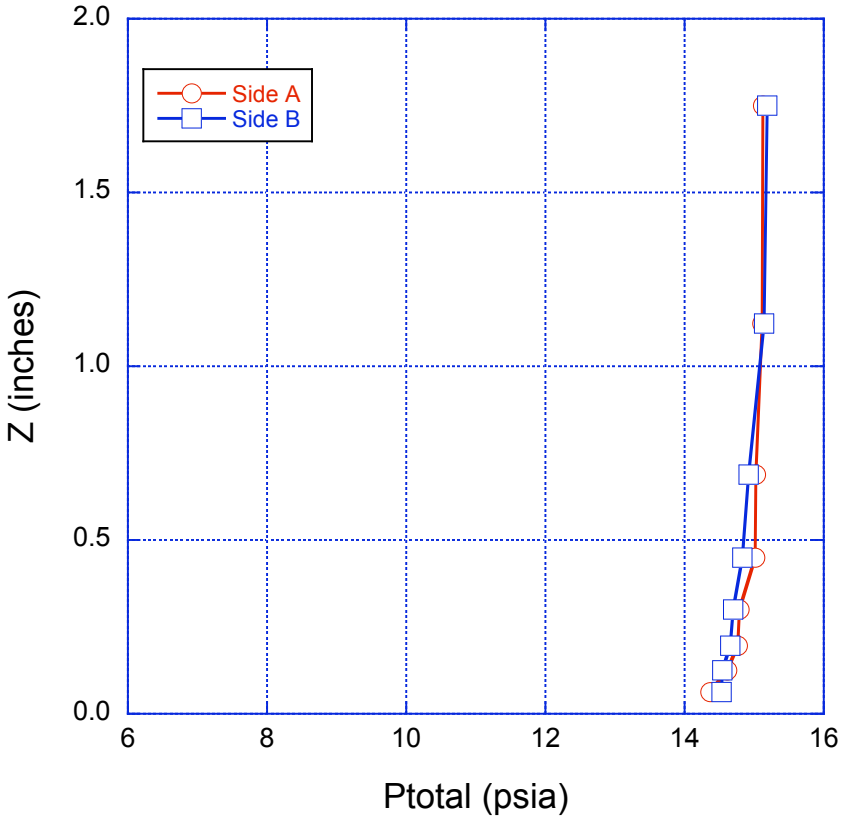

Figure 24b. Boundary-layer pressure profile data at *T0*+10.00s.

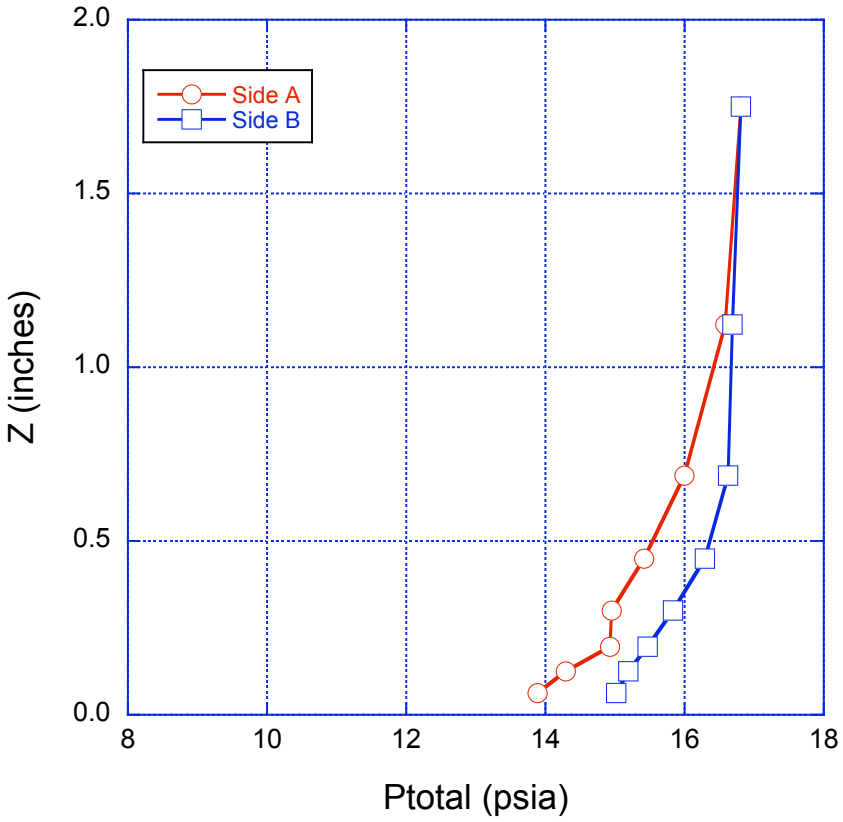

Figure 24c. Boundary-layer pressure profile data at *T0*+15.00s.

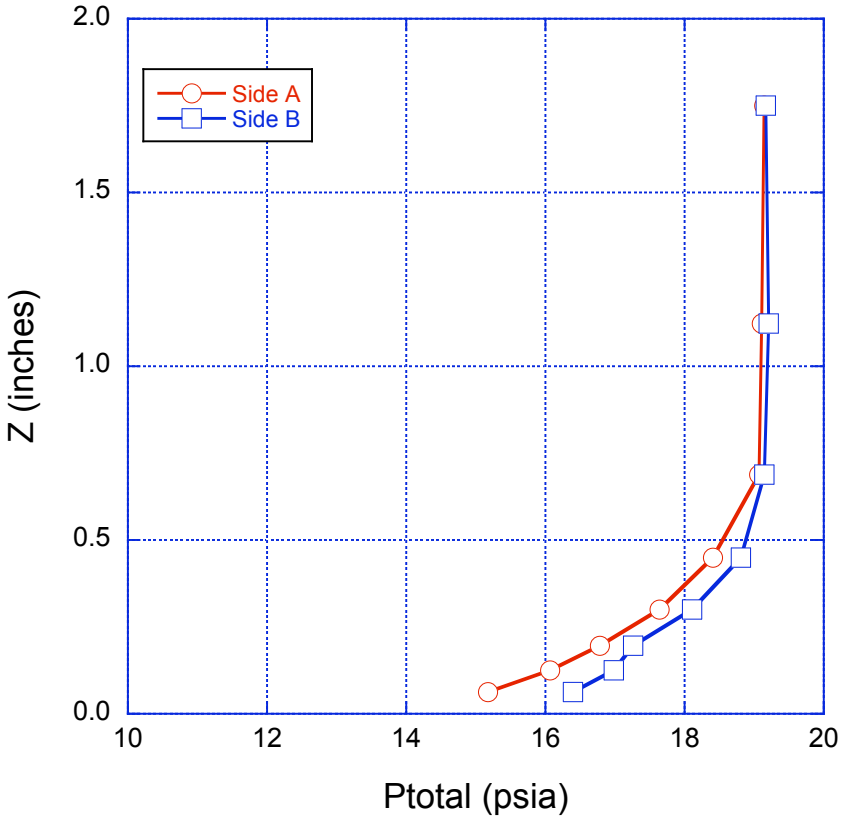

Figure 24d. Boundary-layer pressure profile data at *T0*+18.20s.

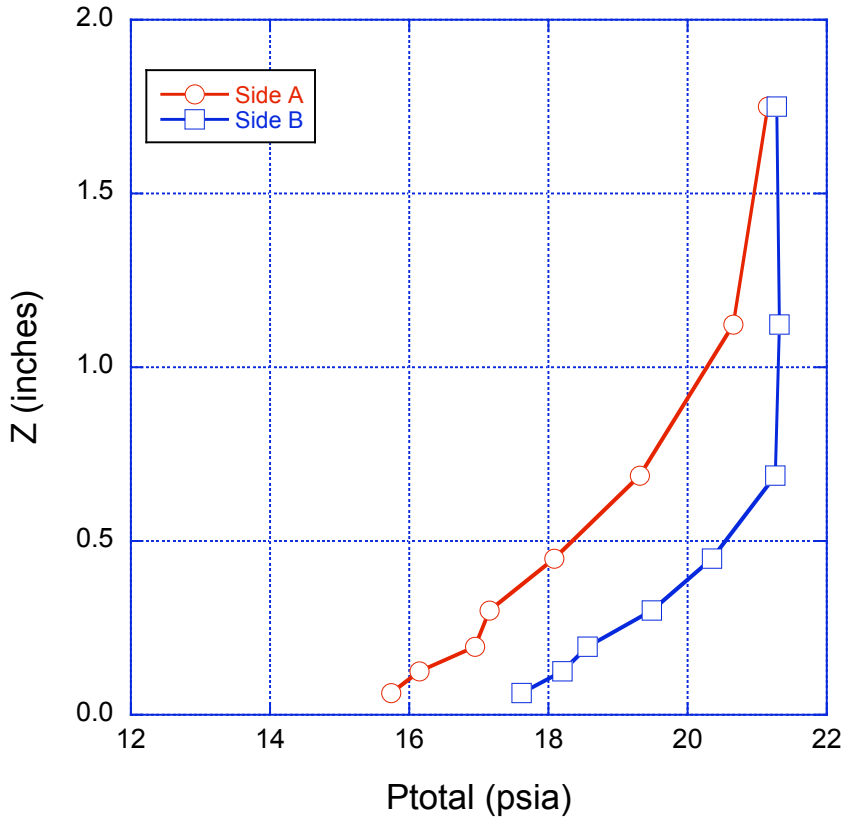

Figure 24e. Boundary-layer pressure profile data at *T0*+20.15s.

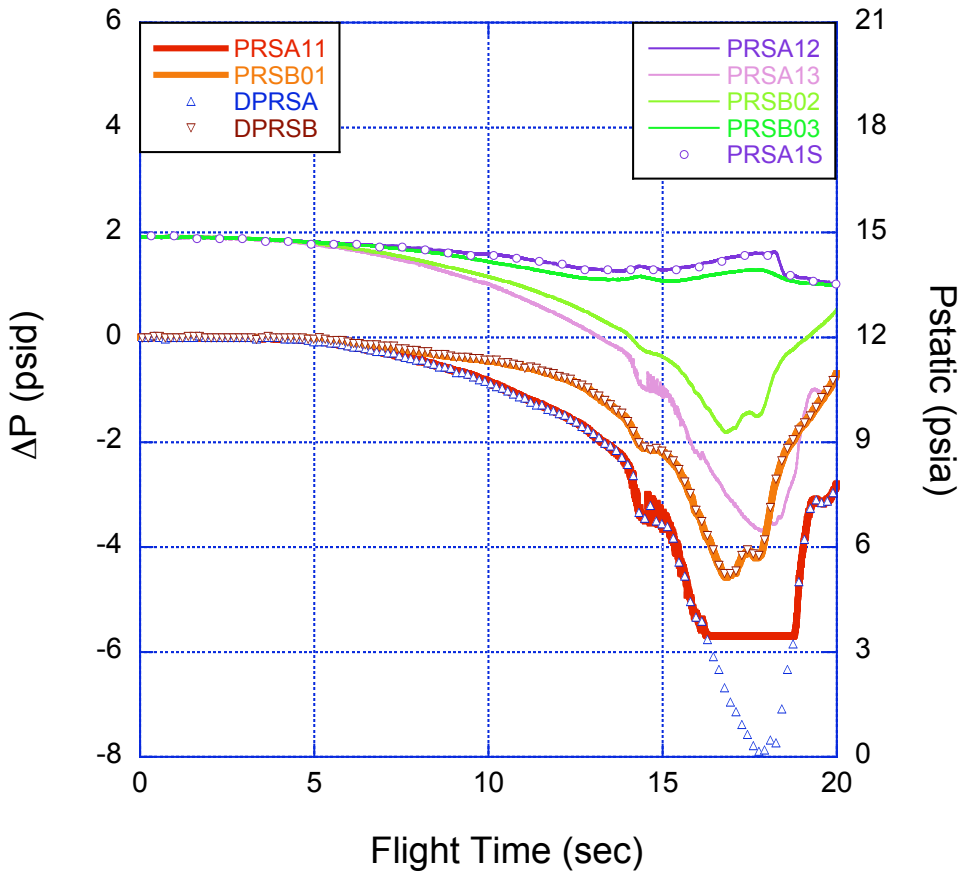

Figure 25. Pressure data of flow angles at boundary-layer pressure rakes.

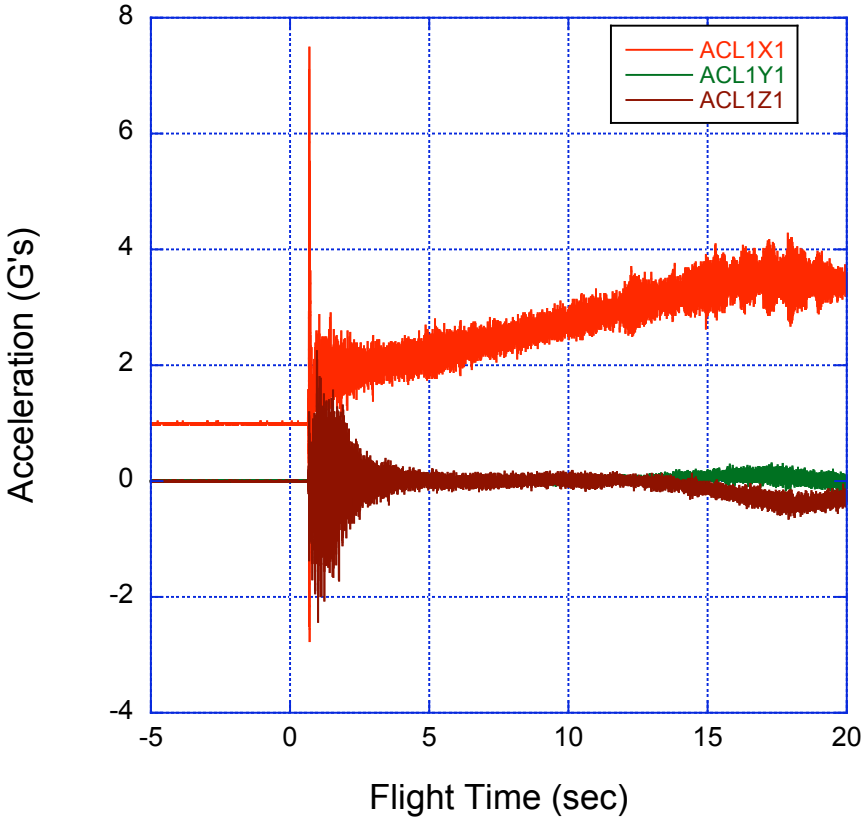

Figure 26. Acceleration data from 3-axis accelerometers.

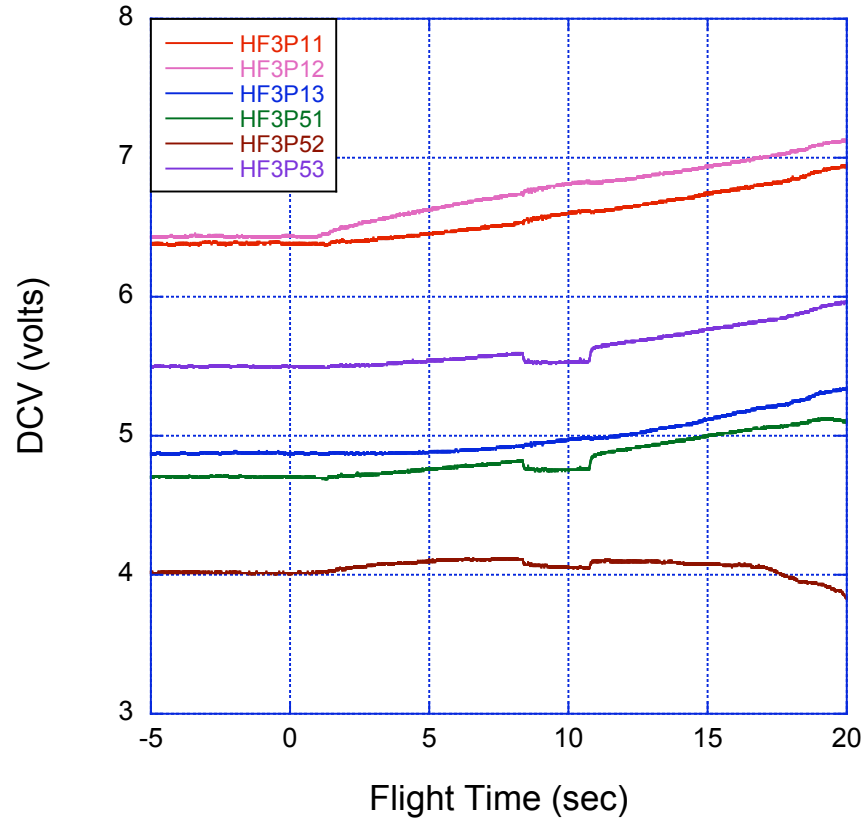

Figure 27. Surface hot-film DC voltage data.

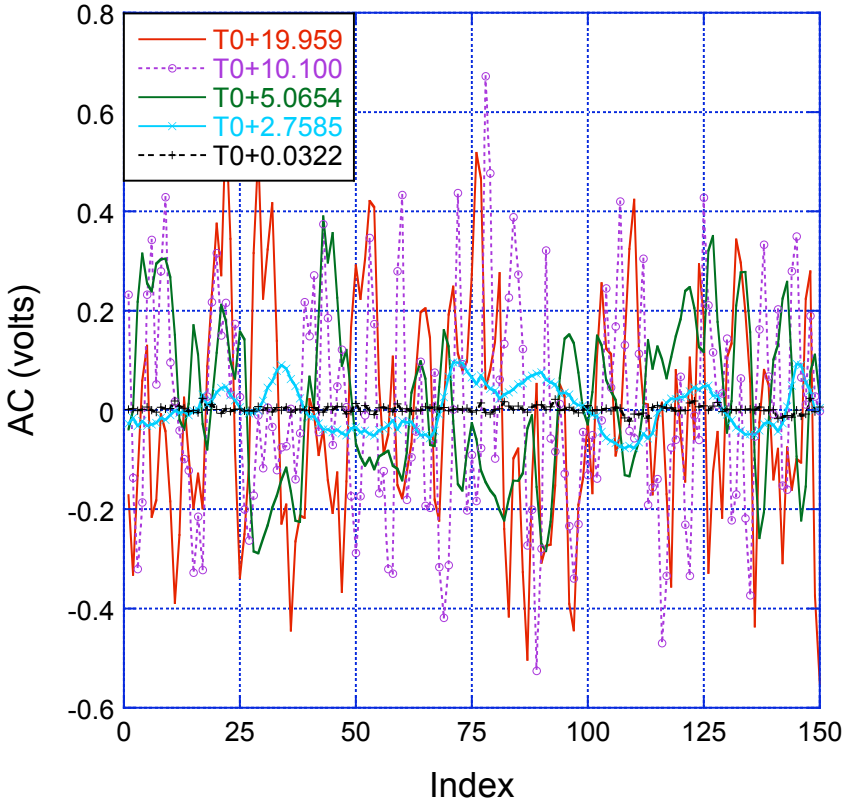

Figure 28a. Surface hot-film HF3A11 time series data.

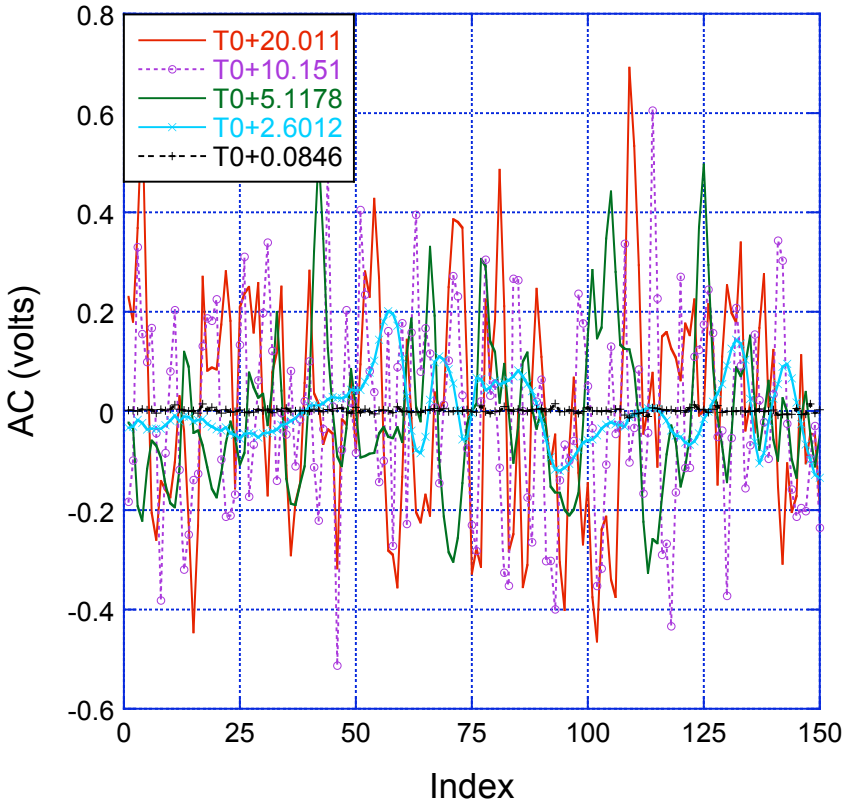

Figure 28b. Surface hot-film HF3A12 time series data.

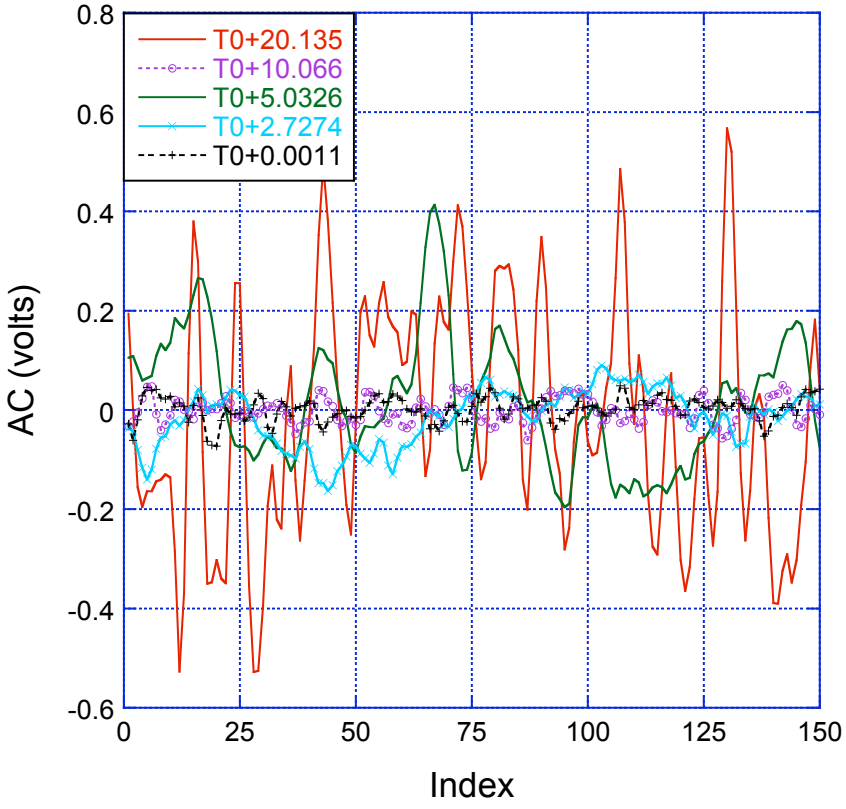

Figure 29a. Surface hot-film HF3A51 time series data.

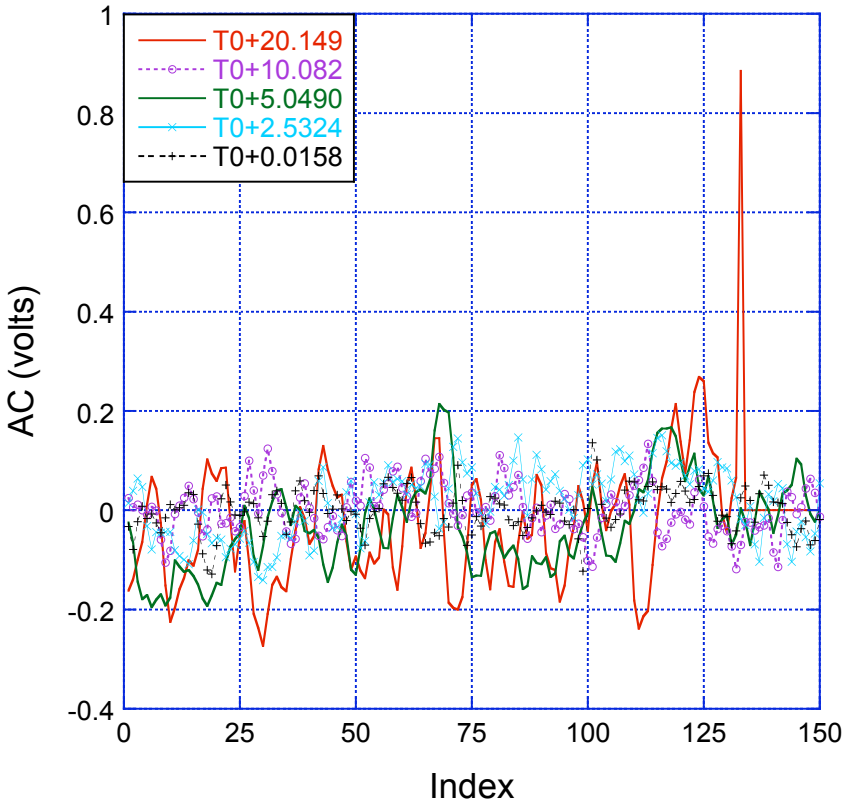

Figure 29b. Surface hot-film HF3A52 time series data.

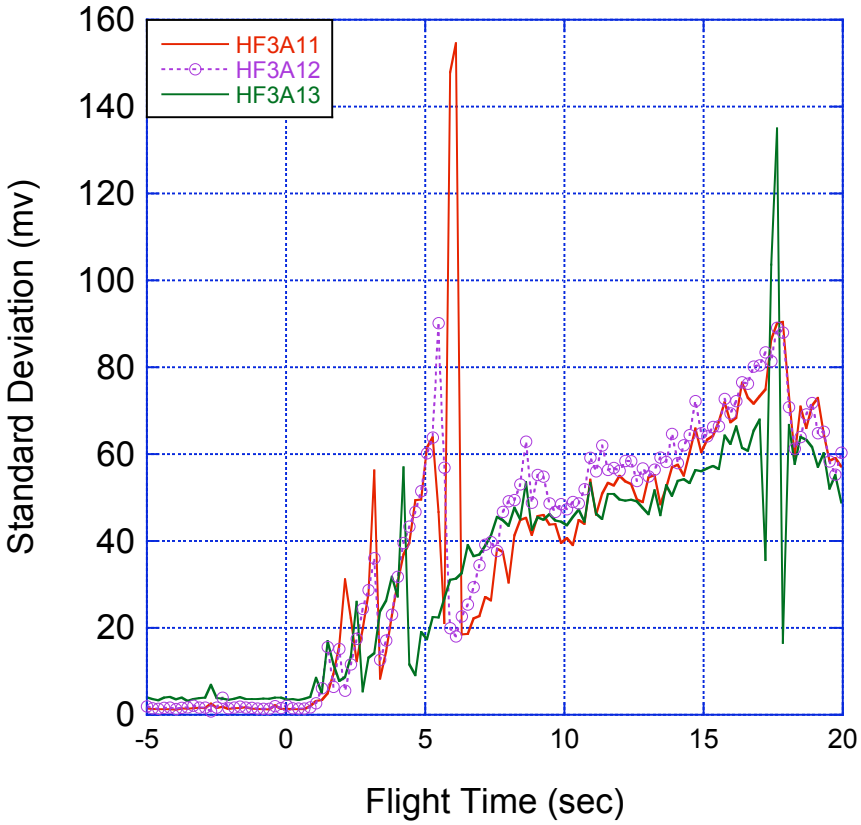

Figure 30a. Standard deviations of surface hot-film HF3A1# time series data.

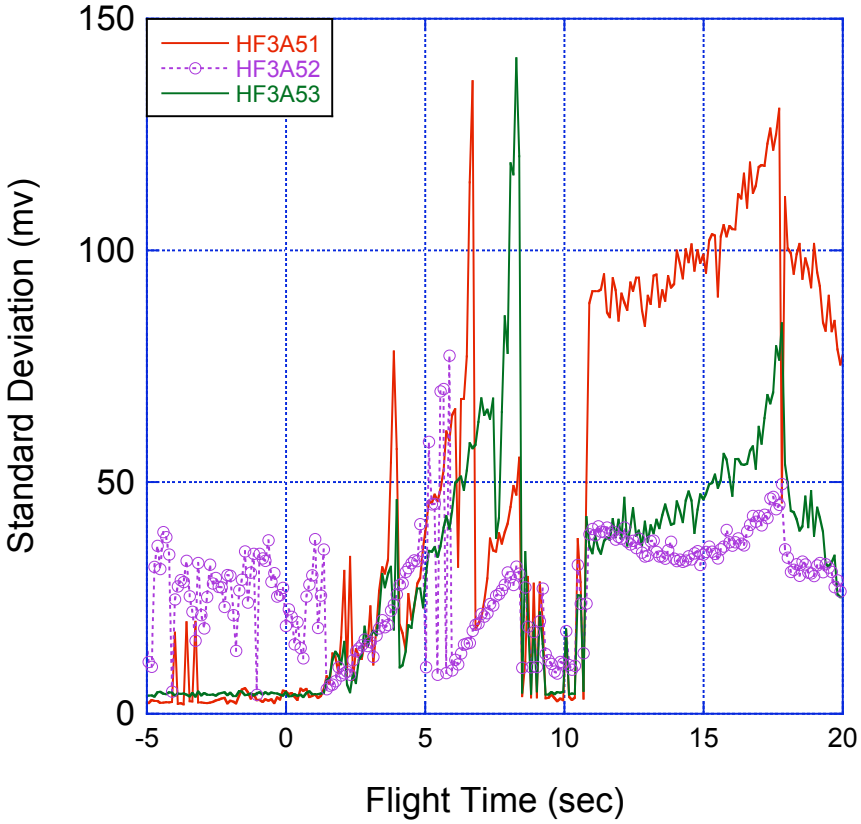

Figure 30b. Standard deviations of surface hot-film HF3A5# time series data.

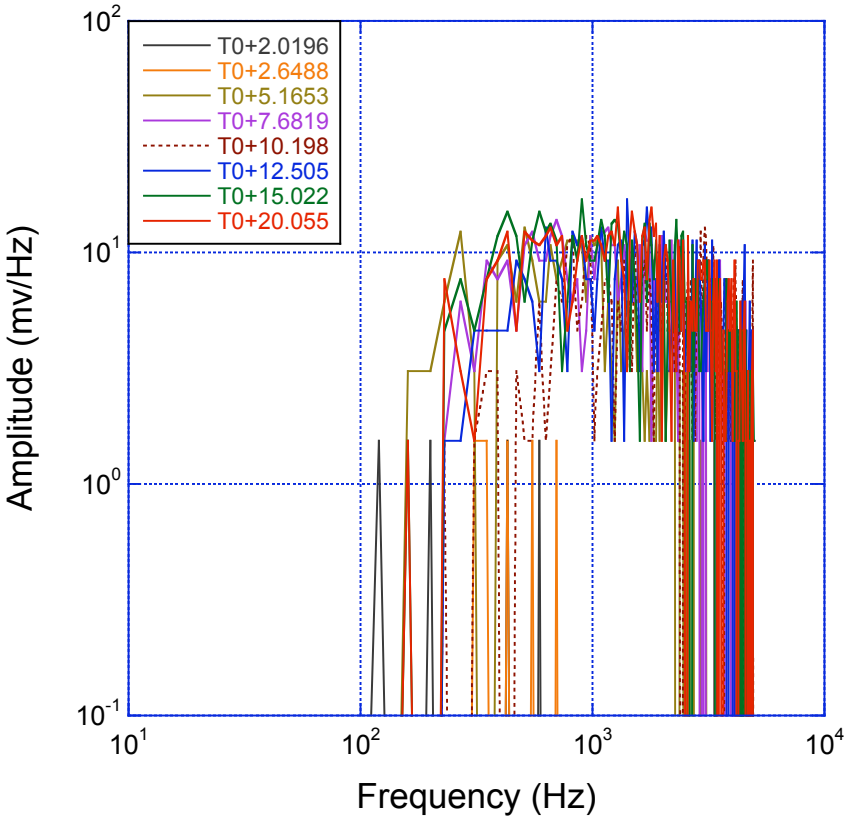

Figure 31a. Amplitude spectra of surface hot-film HF3A11 data.

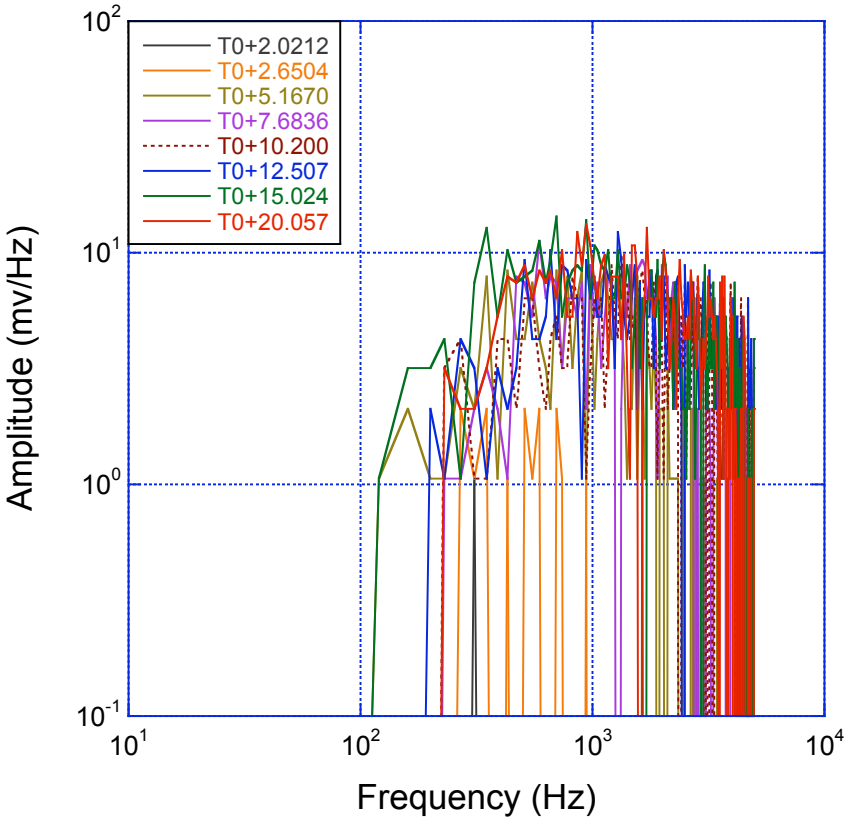

Figure 31b. Amplitude spectra of surface hot-film HF3A12 data.

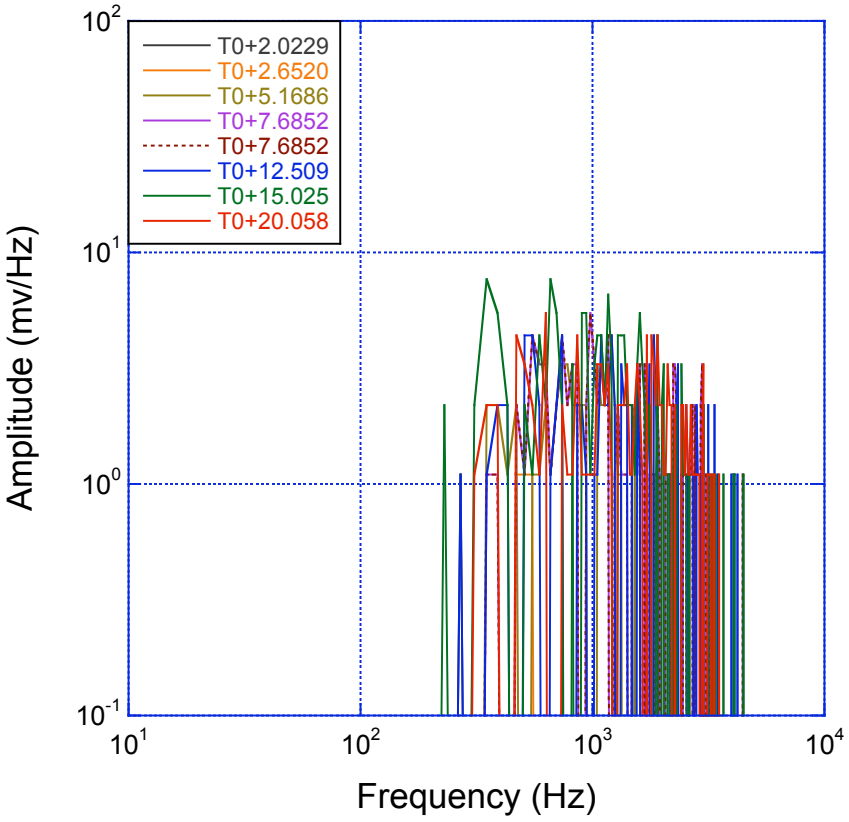

Figure 31c. Amplitude spectra of surface hot-film HF3A13 data.

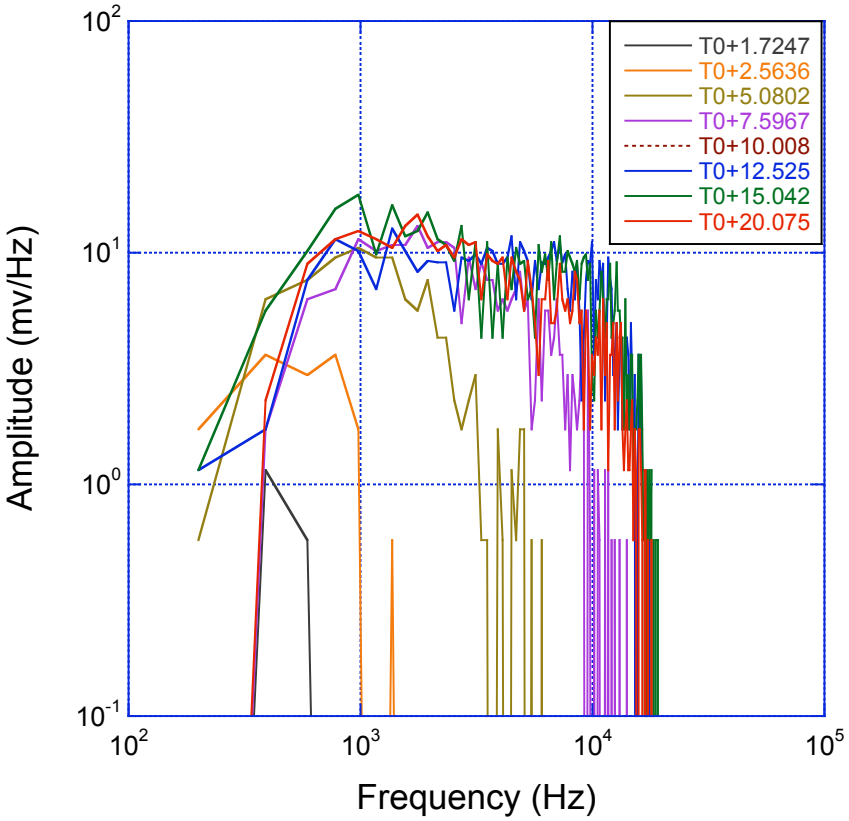

Figure 32a. Amplitude spectra of surface hot-film HF3A51 data.

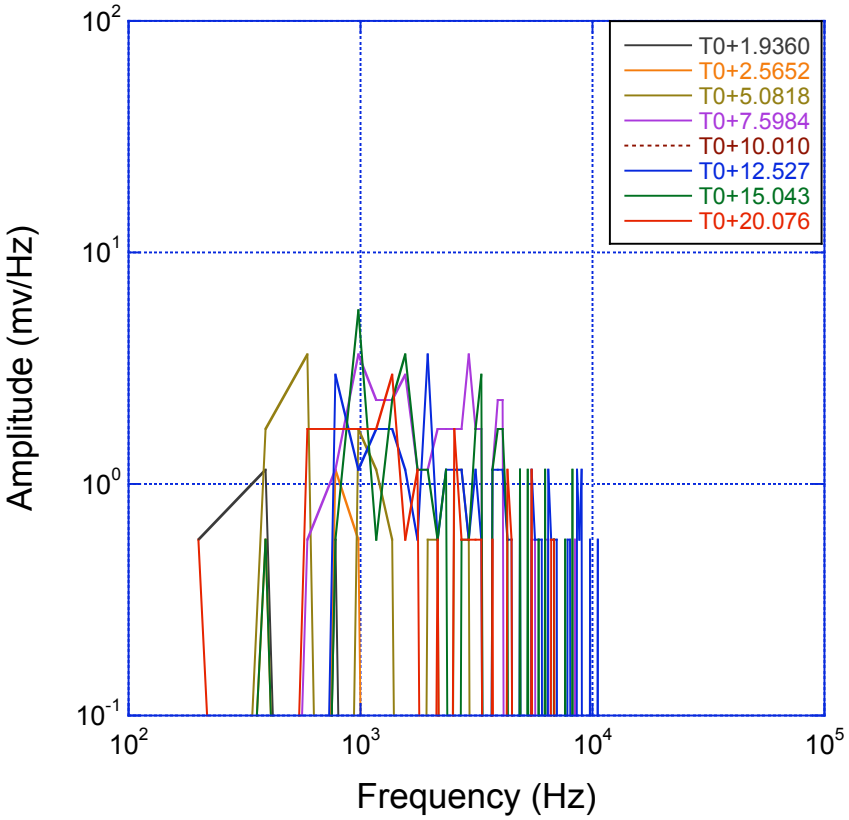

Figure 32b. Amplitude spectra of surface hot-film HF3A52 data.

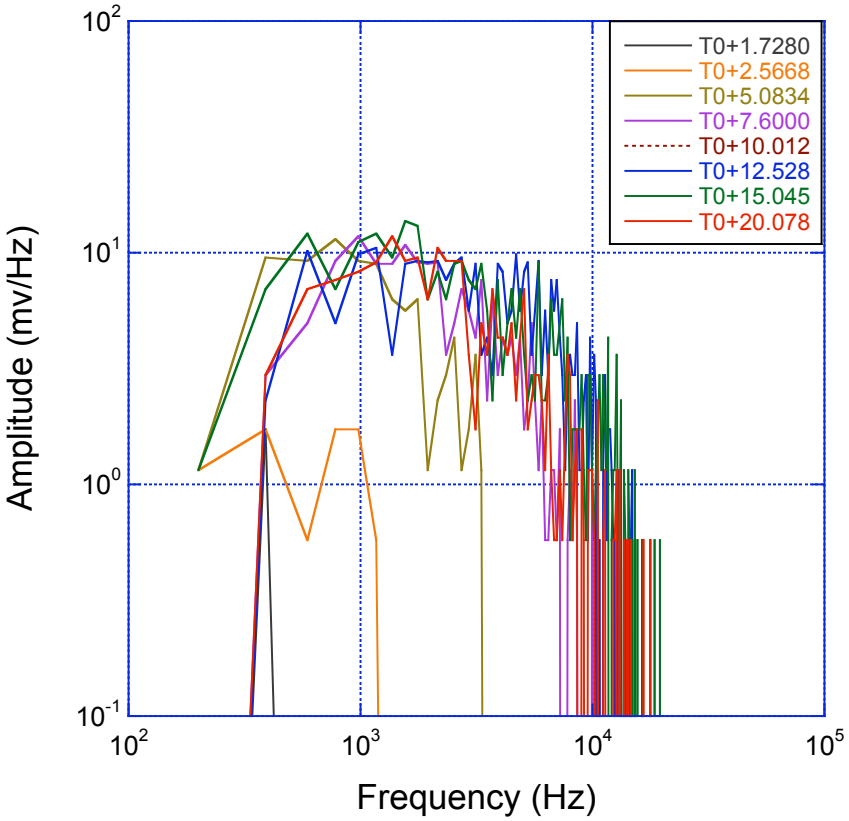

Figure 32c. Amplitude spectra of surface hot-film HF3A53 data.

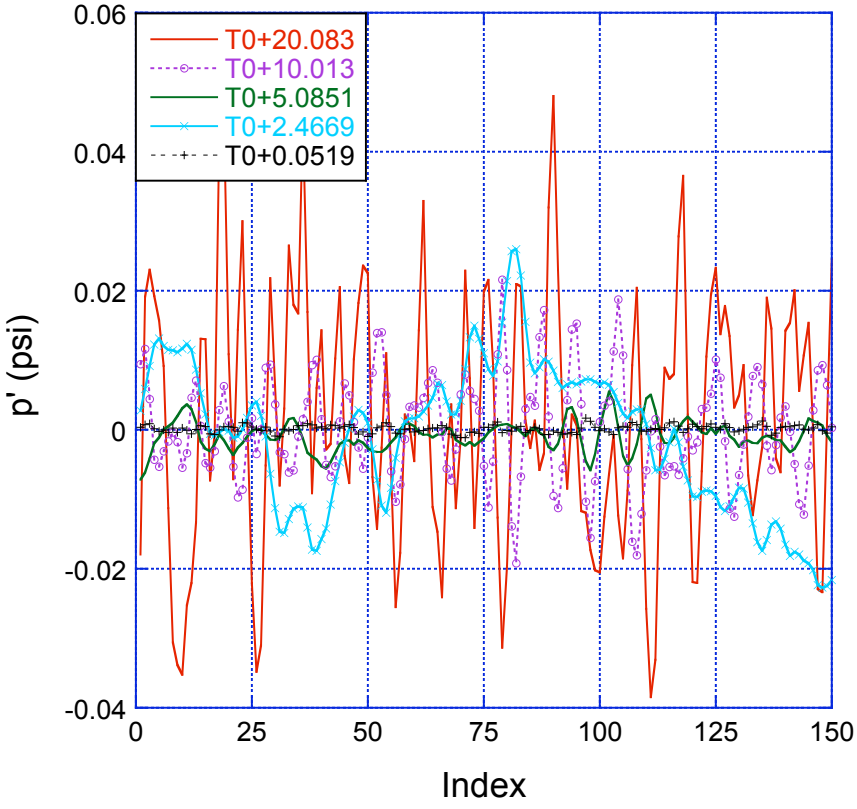

Figure 33a. Three-dynamic-pressure gage P3DA11 time series data.

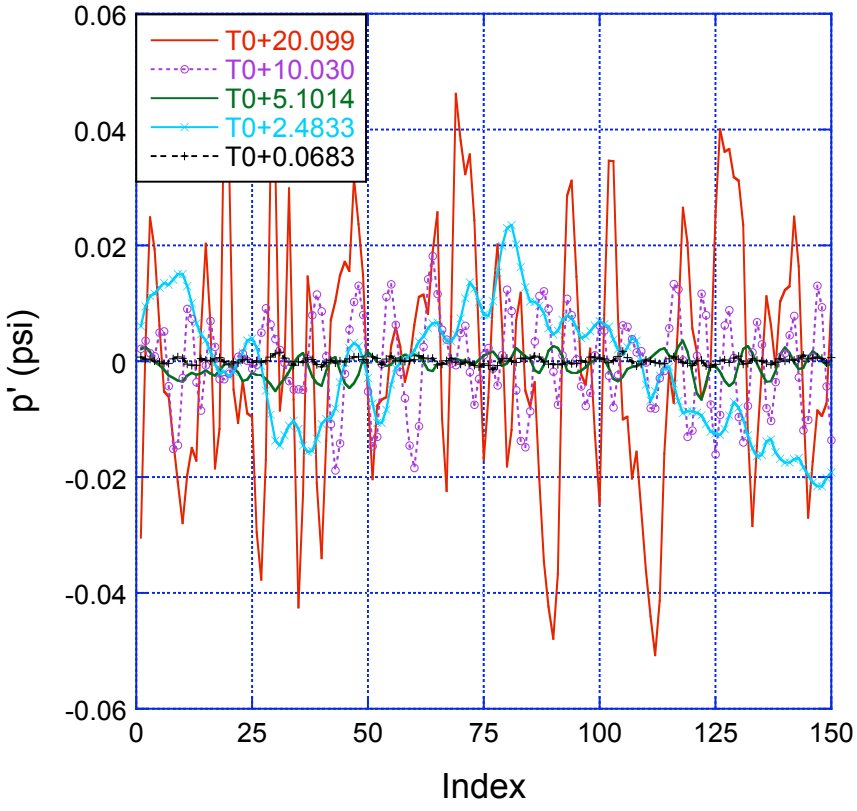

Figure 33b. Three-dynamic-pressure gage P3DA12 time series data.

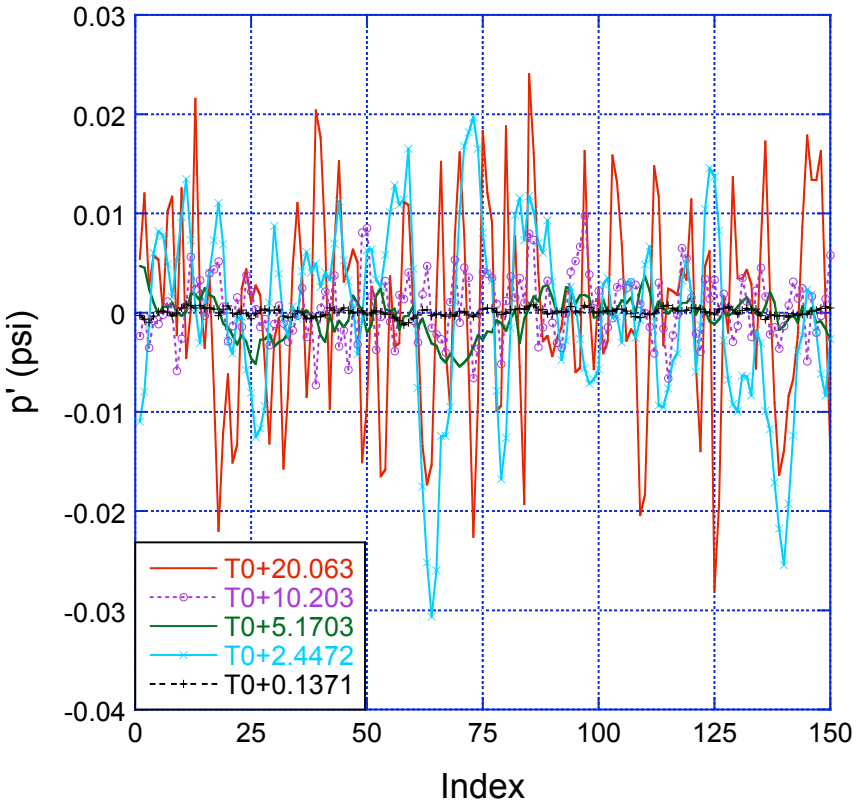

Figure 34a. Three-dynamic-pressure gage P3DA21 time series data.

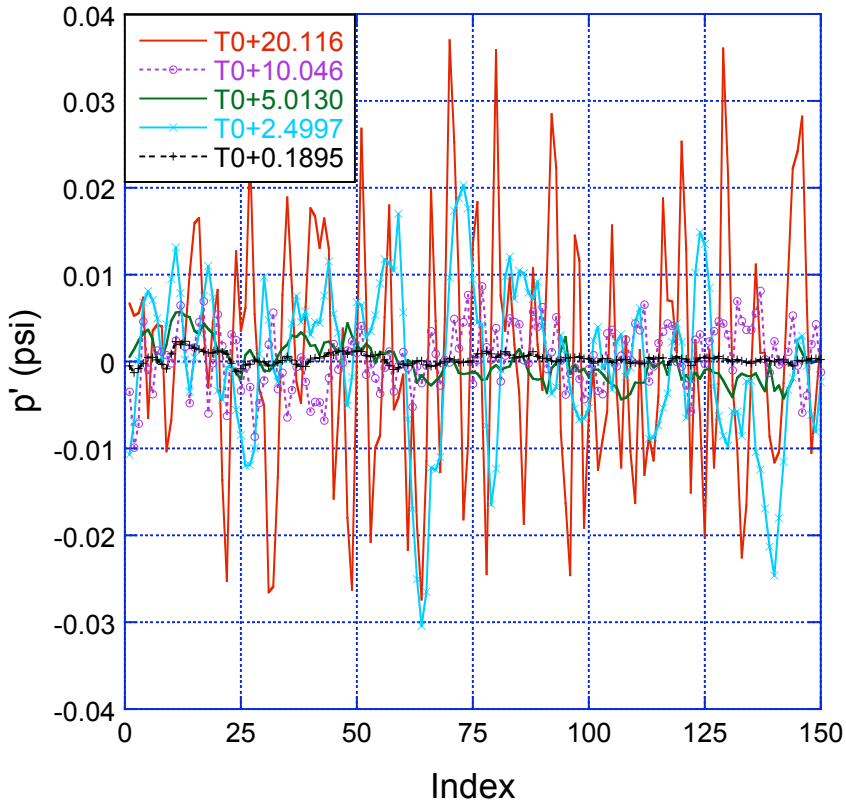

Figure 34b. Three-dynamic-pressure gage P3DA22 time series data.

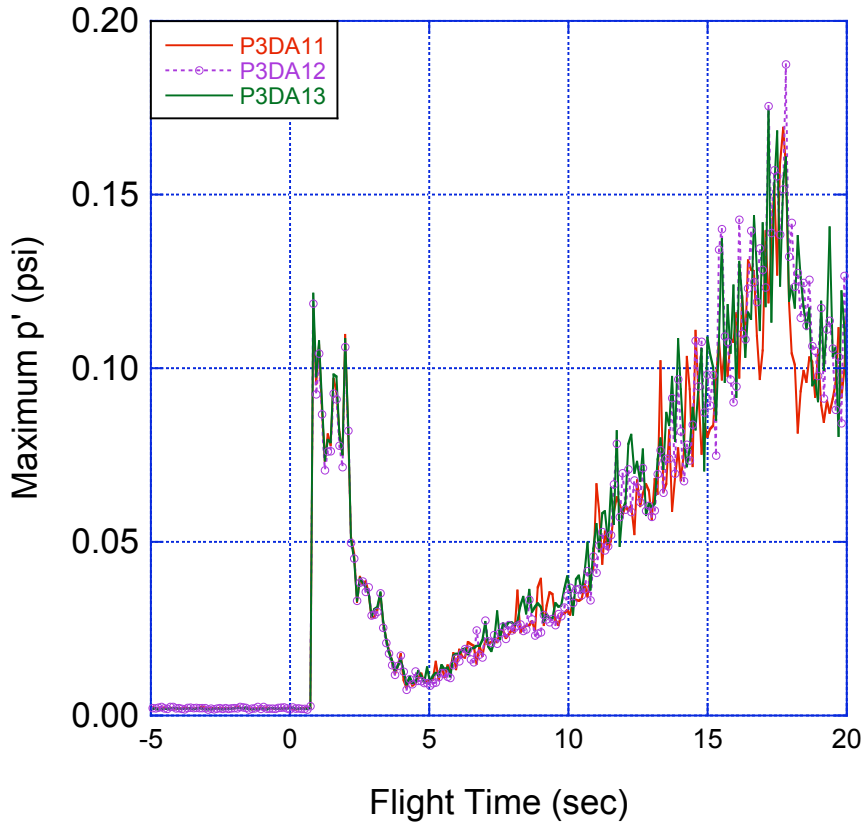

Figure 35a. Maximum pressure fluctuations of three-dynamic-pressure gage P3DA1# time series data.

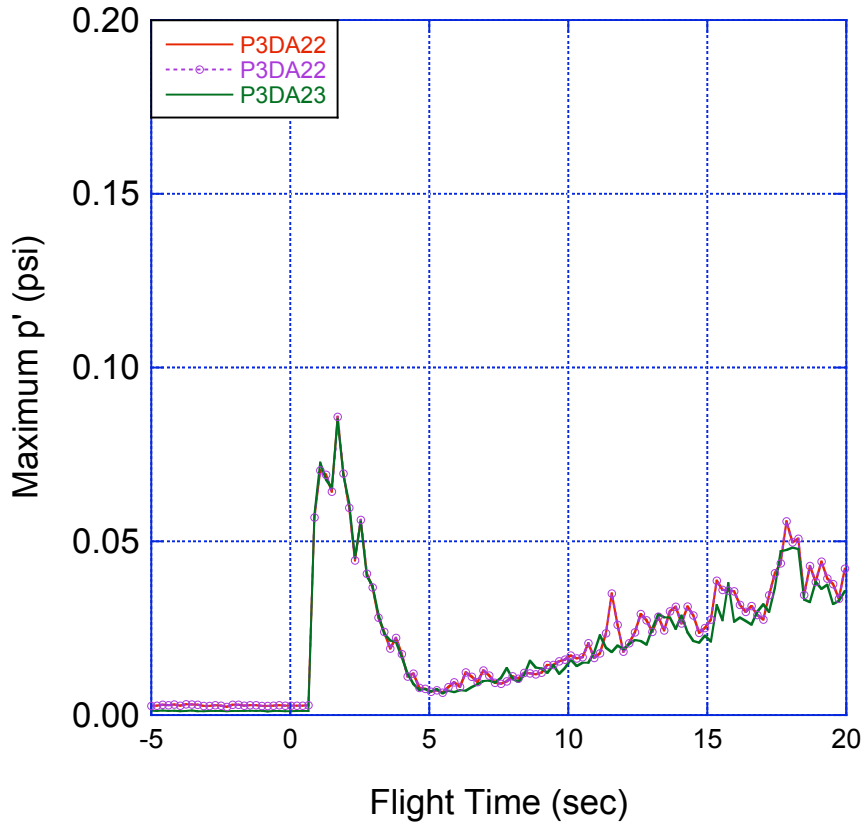

Figure 35b. Maximum pressure fluctuations of three-dynamic-pressure gage P3DA2# time series data.

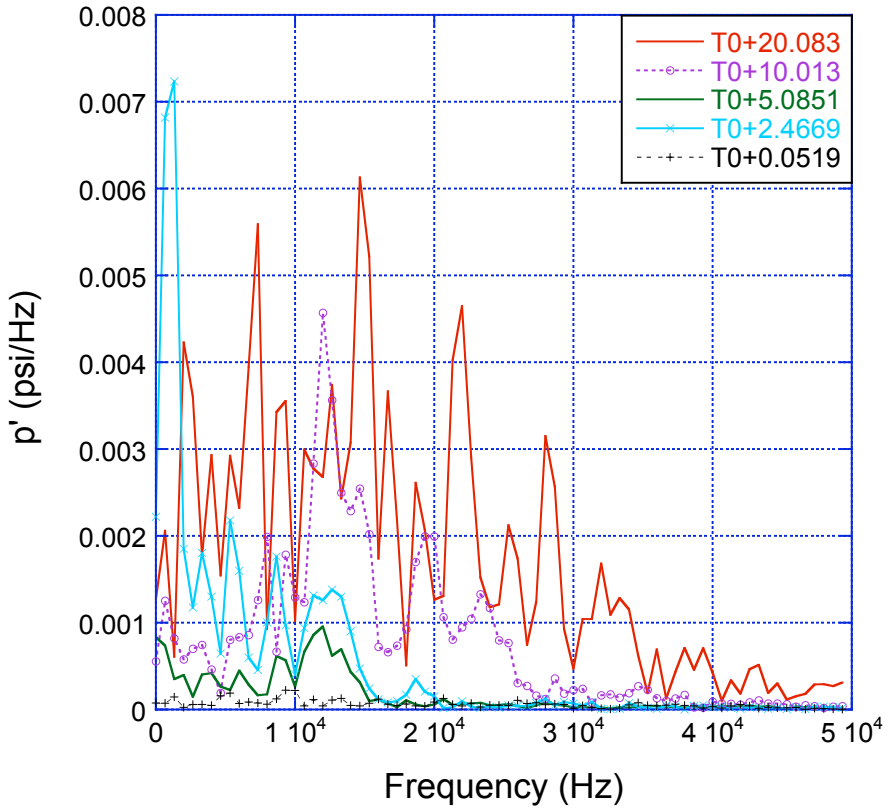

Figure 36a. Amplitude spectra of three-dynamic-pressure gage P3DA11 time series data of Figure 33a.

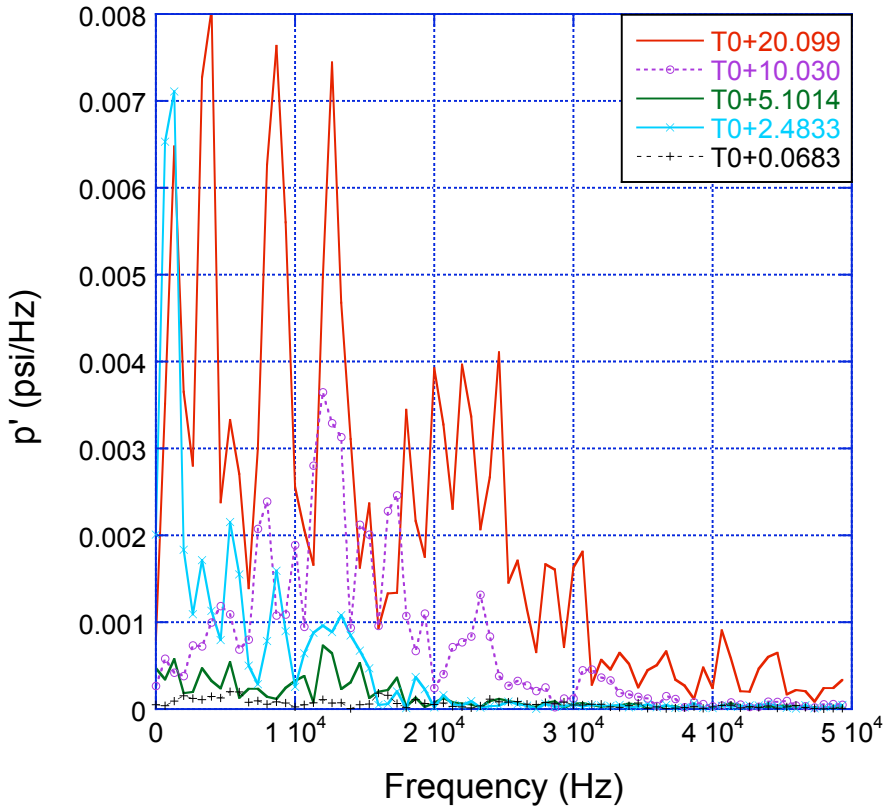

Figure 36b. Amplitude spectra of three-dynamic-pressure gage P3DA12 time series data of Figure 33b.

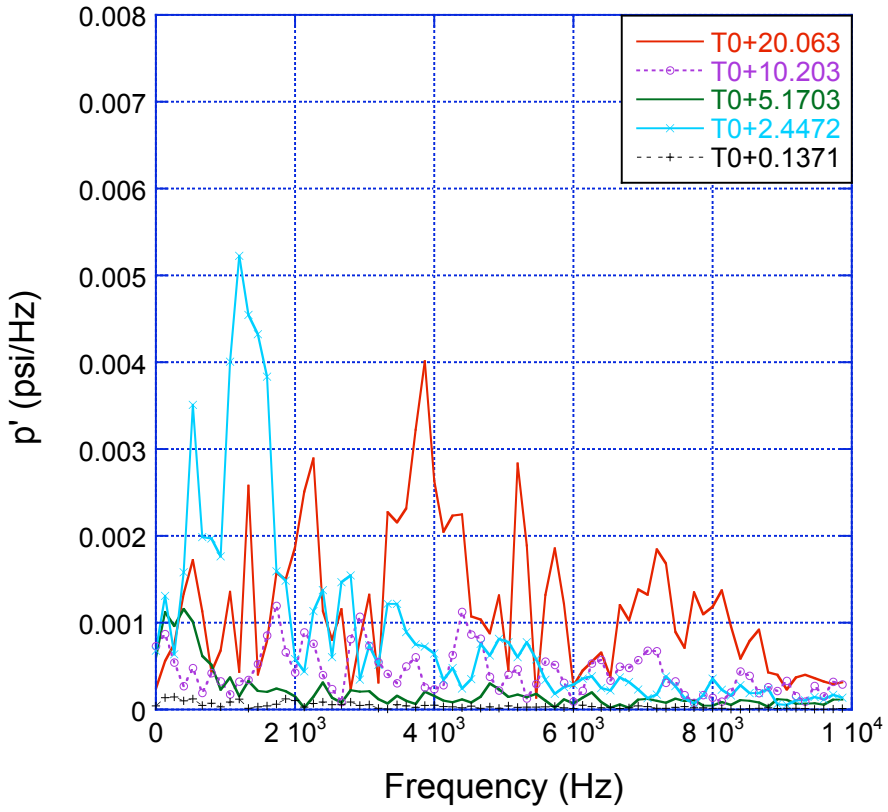

Figure 37a. Amplitude spectra of three-dynamic-pressure gage P3DA21 time series data of Figure 34a.

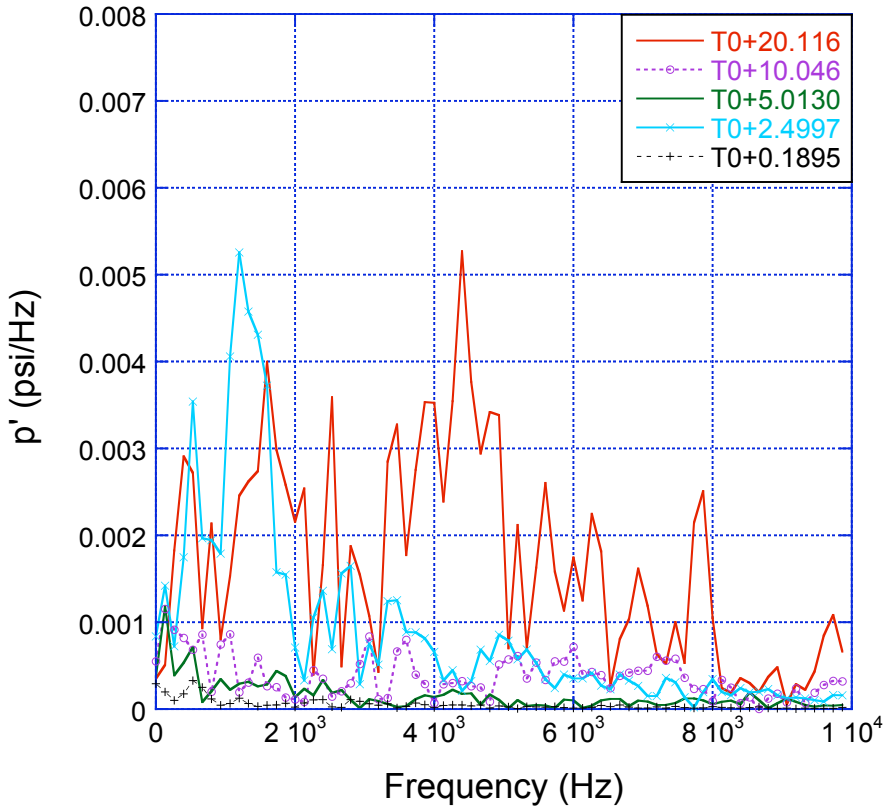

Figure 37b. Amplitude spectra of three-dynamic-pressure gage P3DA22 time series data of Figure 34b.

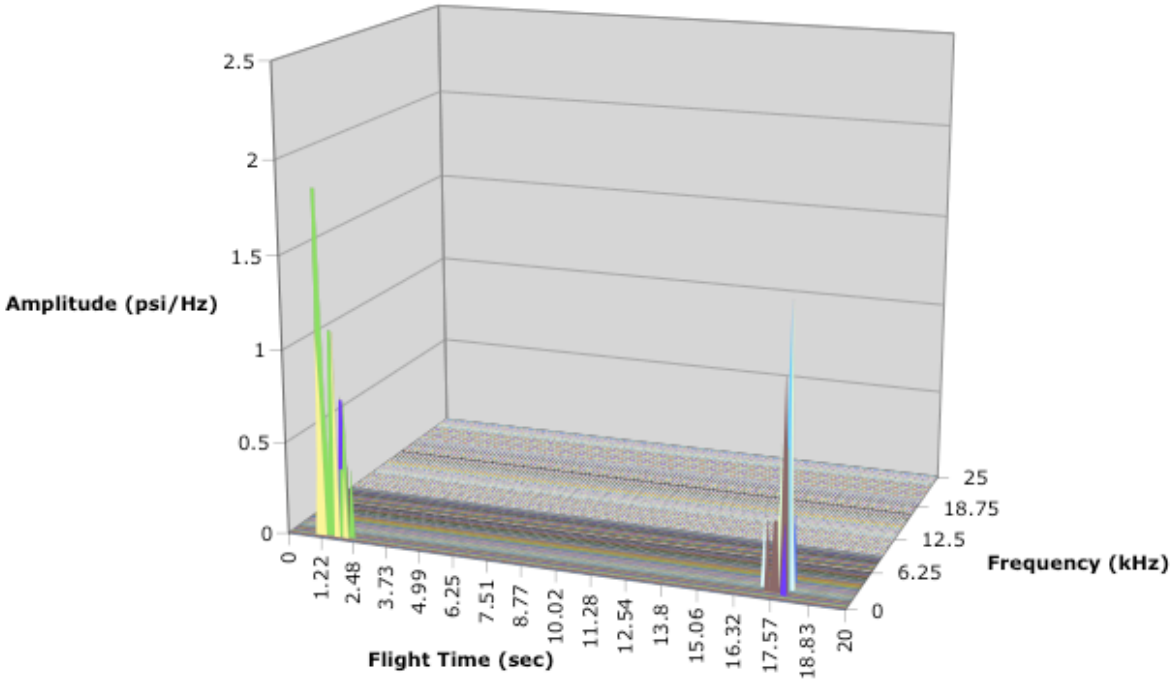

Figure 38a. Amplitude spectra of three-dynamic-pressure gage P3DA11 data.

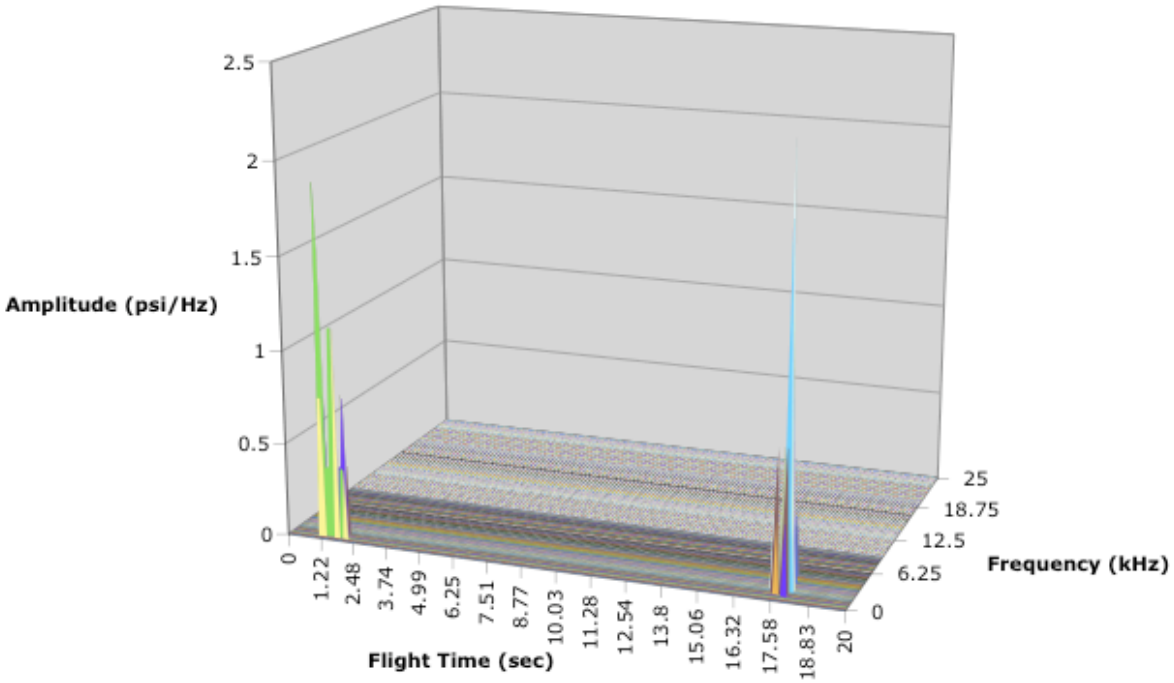

Figure 38b. Amplitude spectra of three-dynamic-pressure gage P3DA12 data.

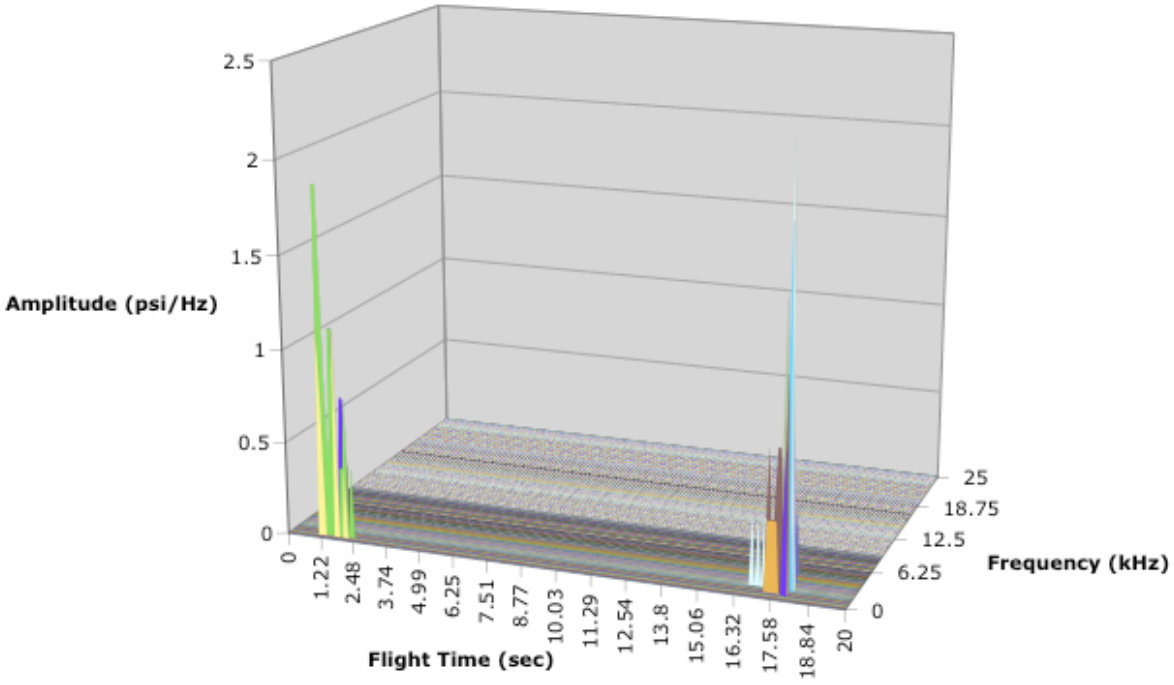

Figure 38c. Amplitude spectra of three-dynamic-pressure gage P3DA13 data.

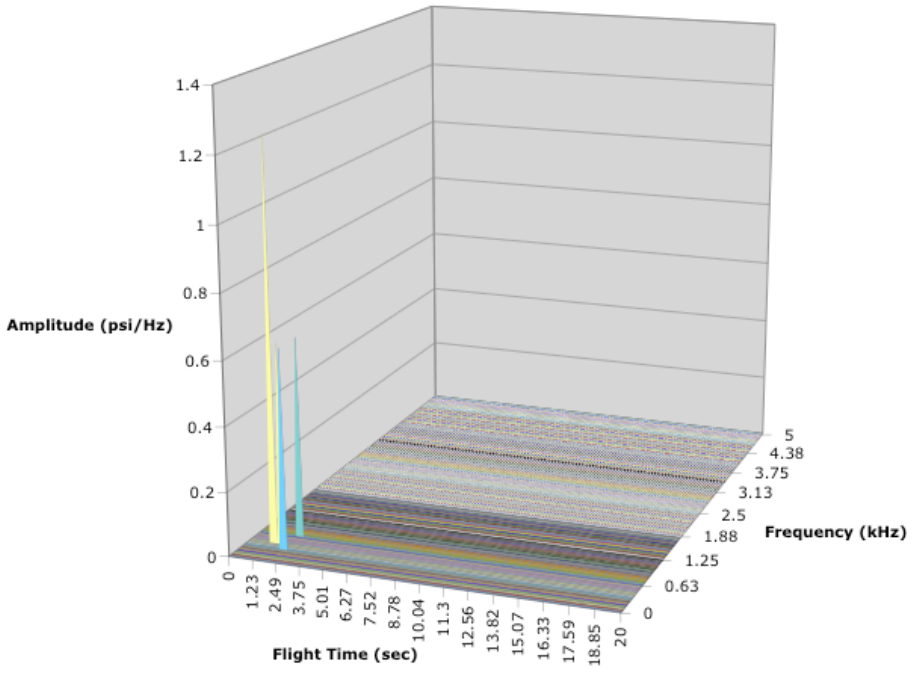

Figure 39a. Amplitude spectra of three-dynamic-pressure gage P3DA21 data.

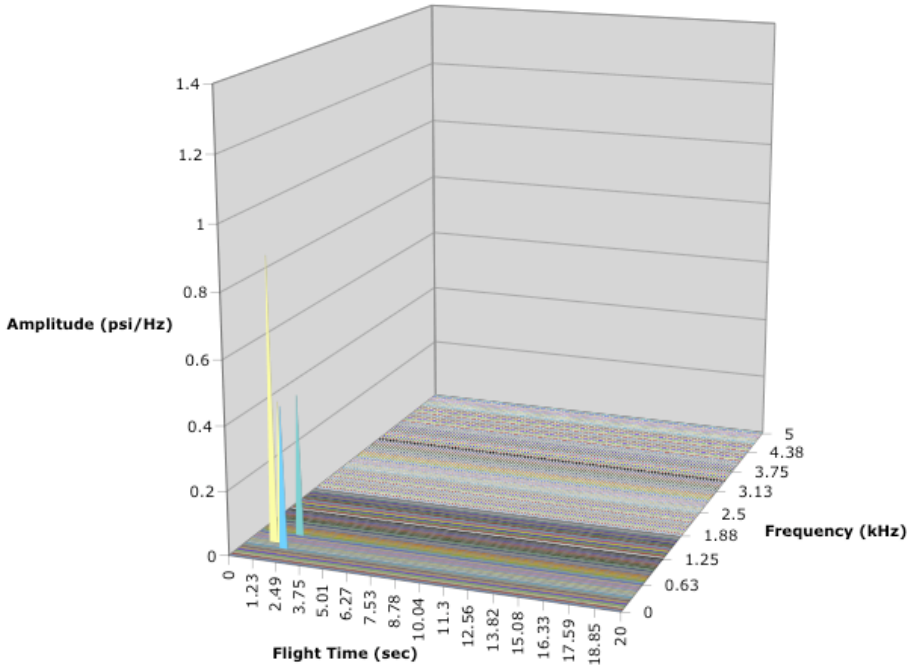

Figure 39b. Amplitude spectra of three-dynamic-pressure gage P3DA22 data.

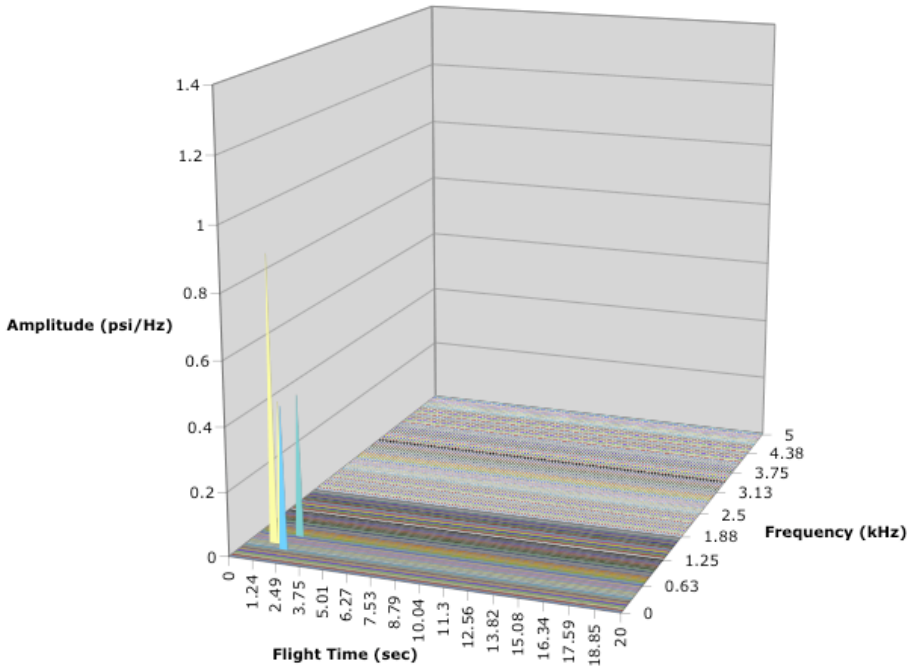

Figure 39c. Amplitude spectra of three-dynamic-pressure gage P3DA23 data.

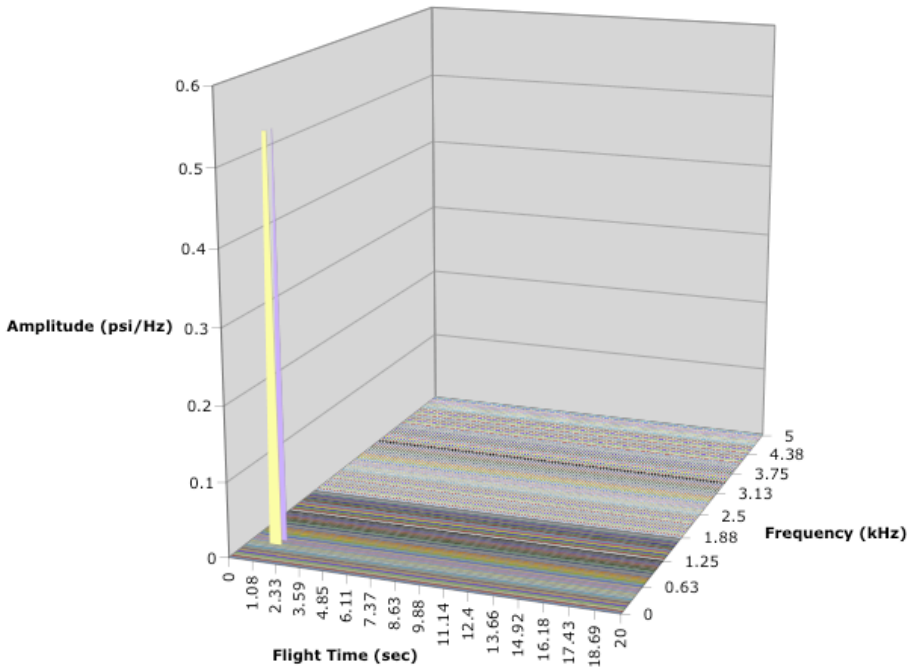

Figure 40a. Amplitude spectra of surface dynamic pressure gage PDA01 data.

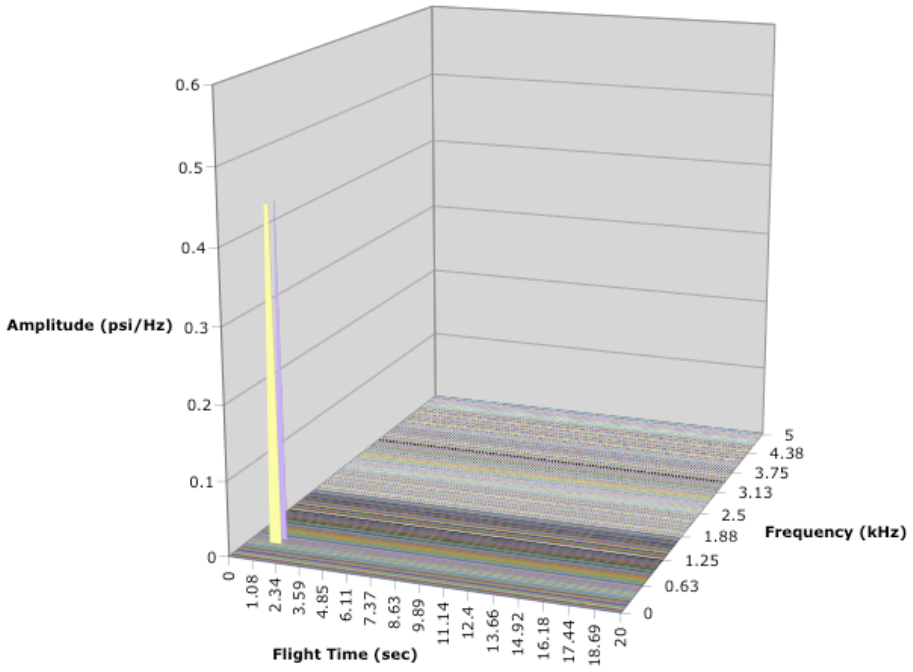

Figure 40b. Amplitude spectra of surface dynamic pressure gage PDA02 data.

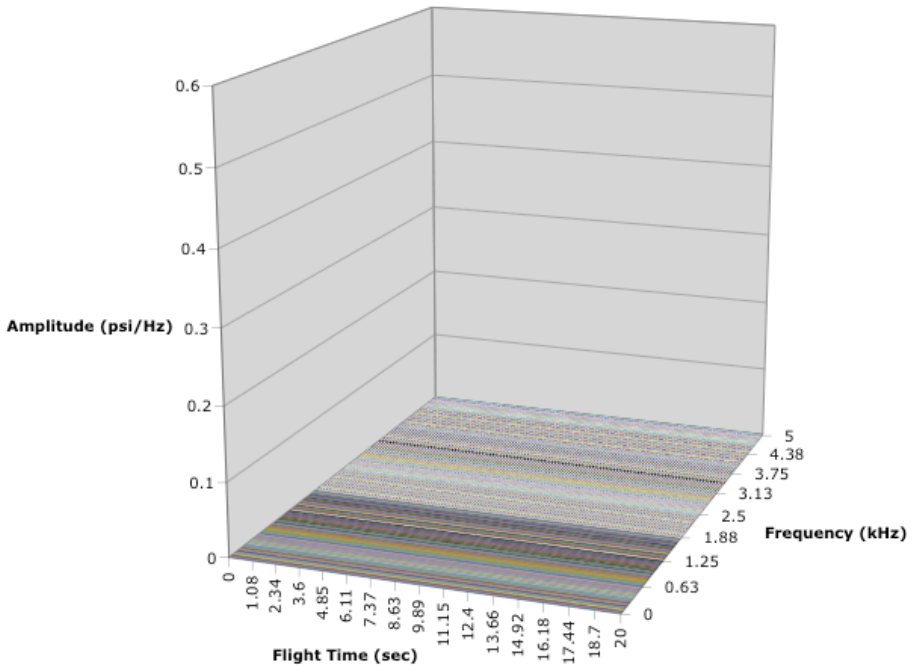

Figure 40c. Amplitude spectra of surface dynamic pressure gage PDA03 data.

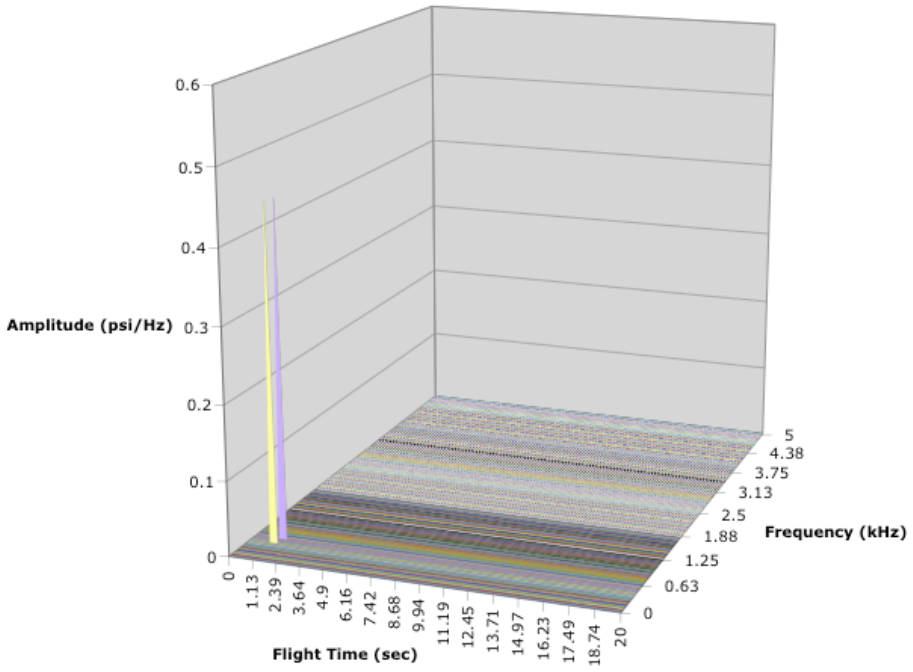

Figure 40d. Amplitude spectra of surface dynamic pressure gage PDA04 data.

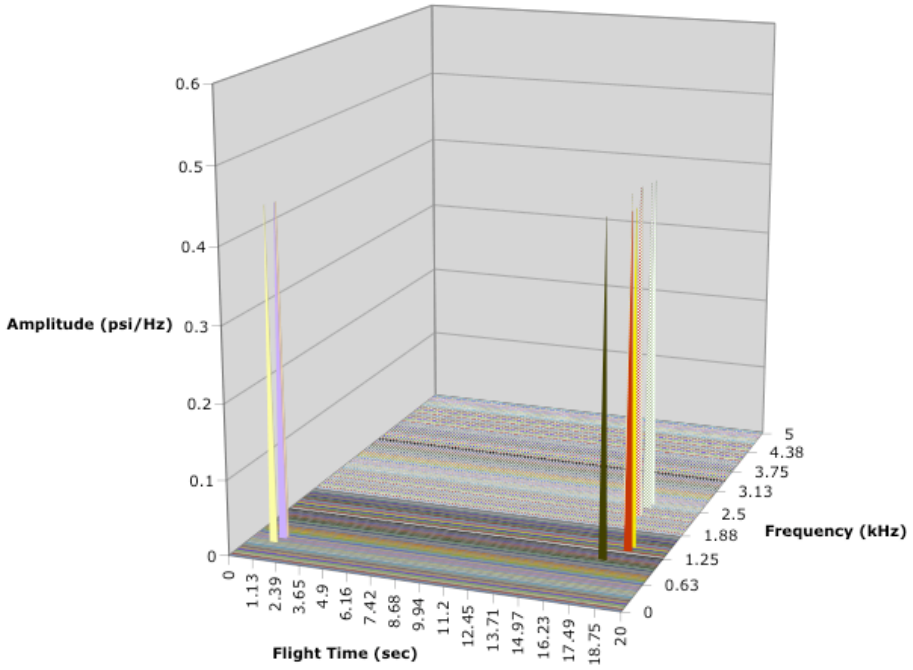

Figure 40e. Amplitude spectra of surface dynamic pressure gage PDA05 data.

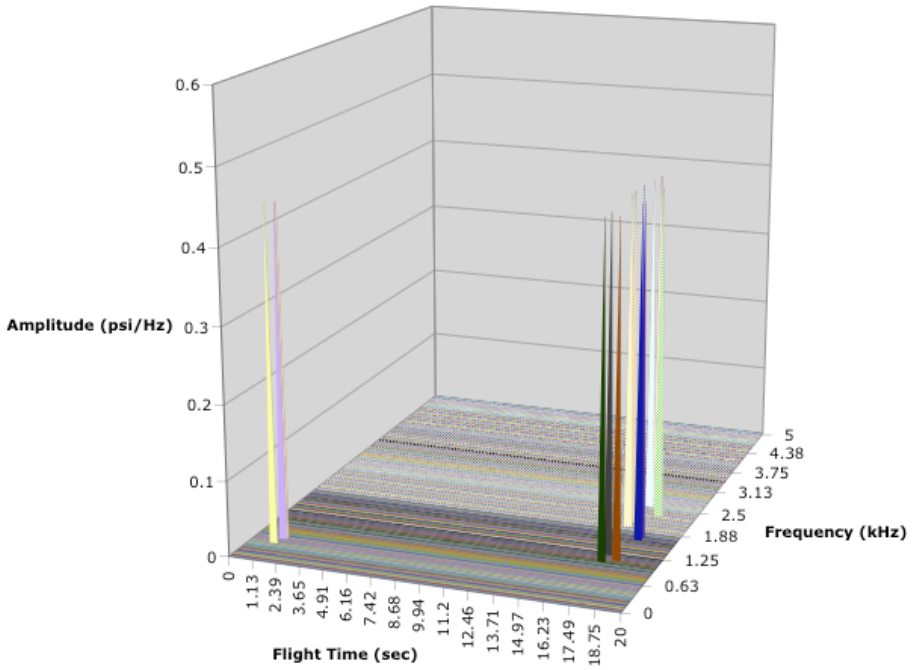

Figure 40f. Amplitude spectra of surface dynamic pressure gage PDA06 data.

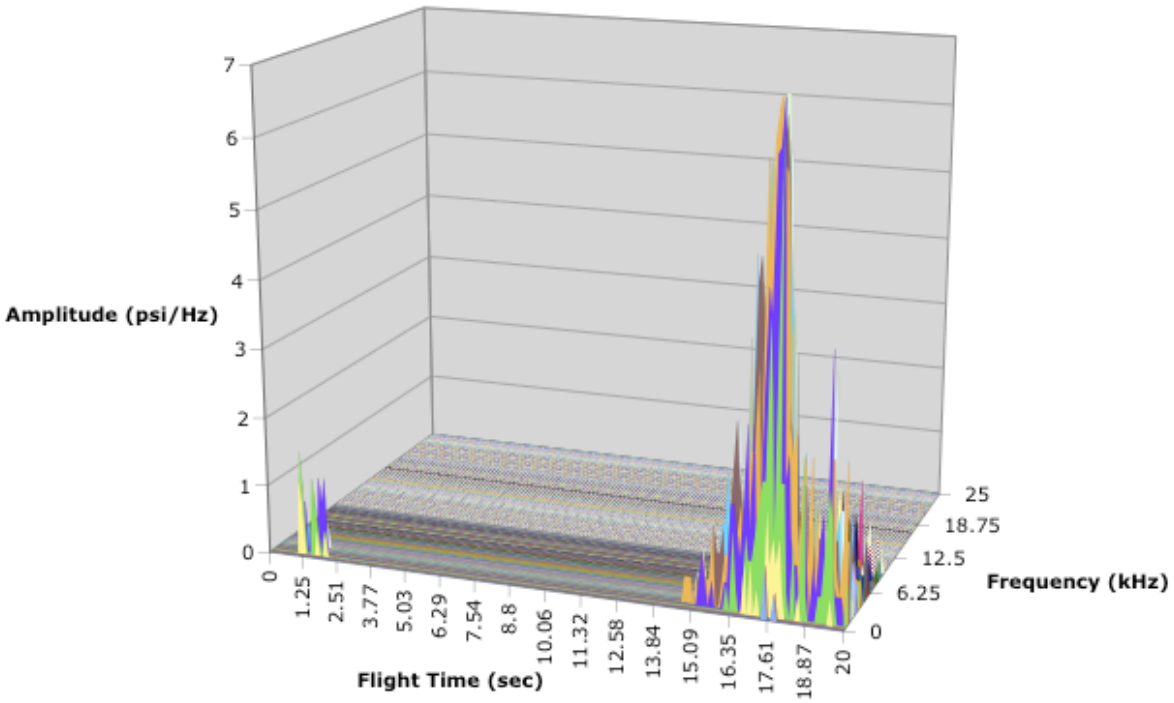

Figure 41a. Amplitude spectra of surface dynamic pressure gage PDA13 data.

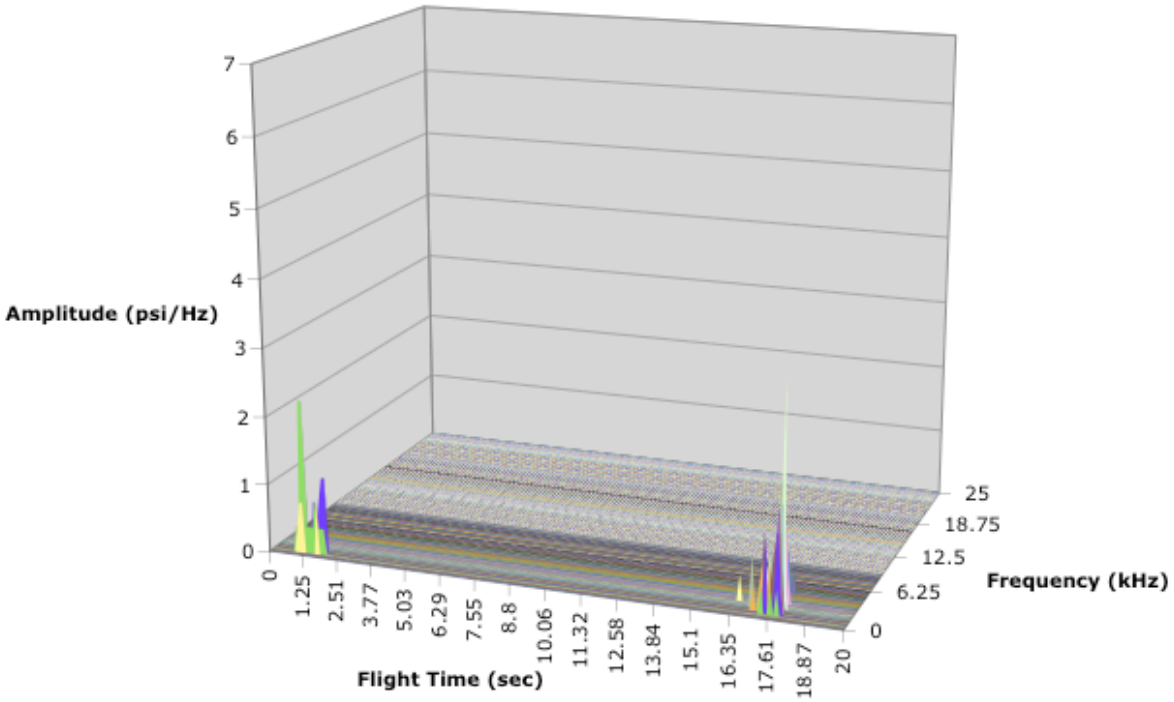

Figure 41b. Amplitude spectra of surface dynamic pressure gage PDA14 data.

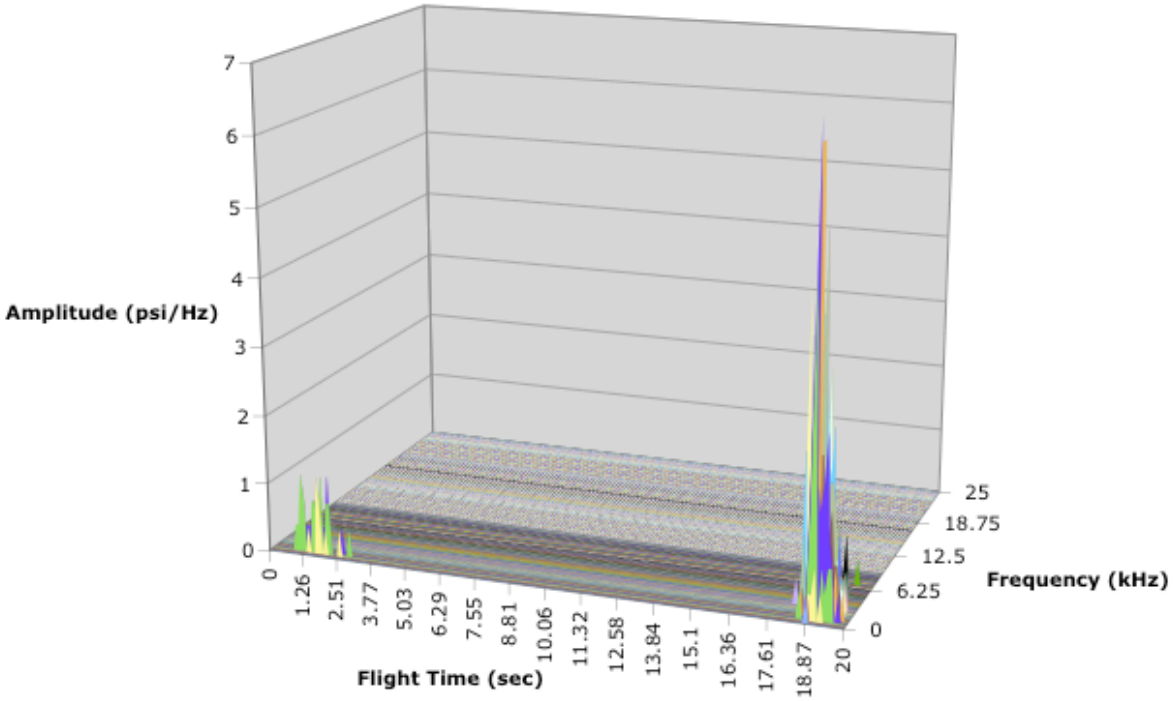

Figure 41c. Amplitude spectra of surface dynamic pressure gage PDA15 data.

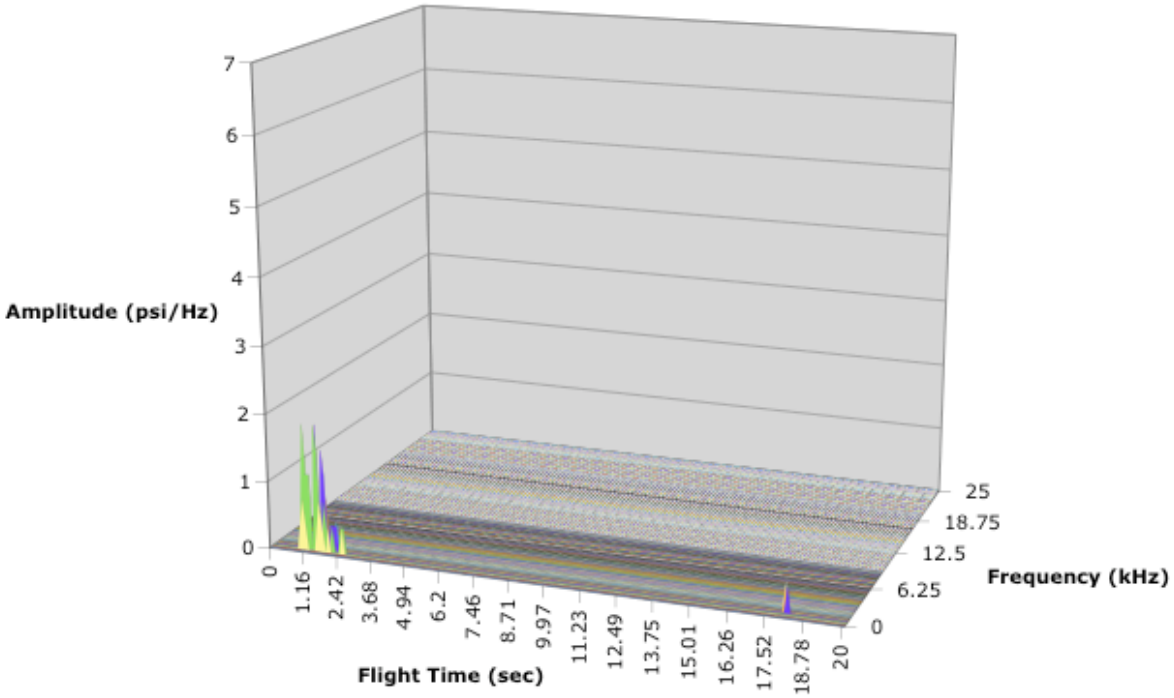

Figure 41d. Amplitude spectra of surface dynamic pressure gage PDA16 data.

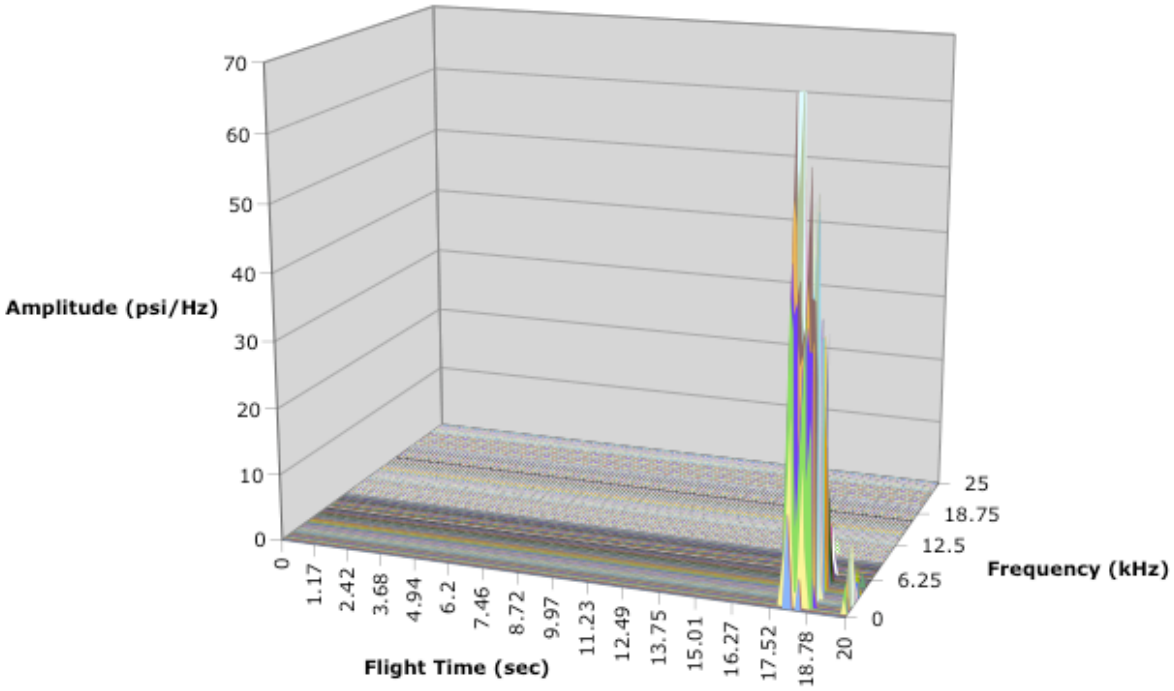

Figure 42. Amplitude spectra of freestream dynamic pressure probe PFSD01 data.

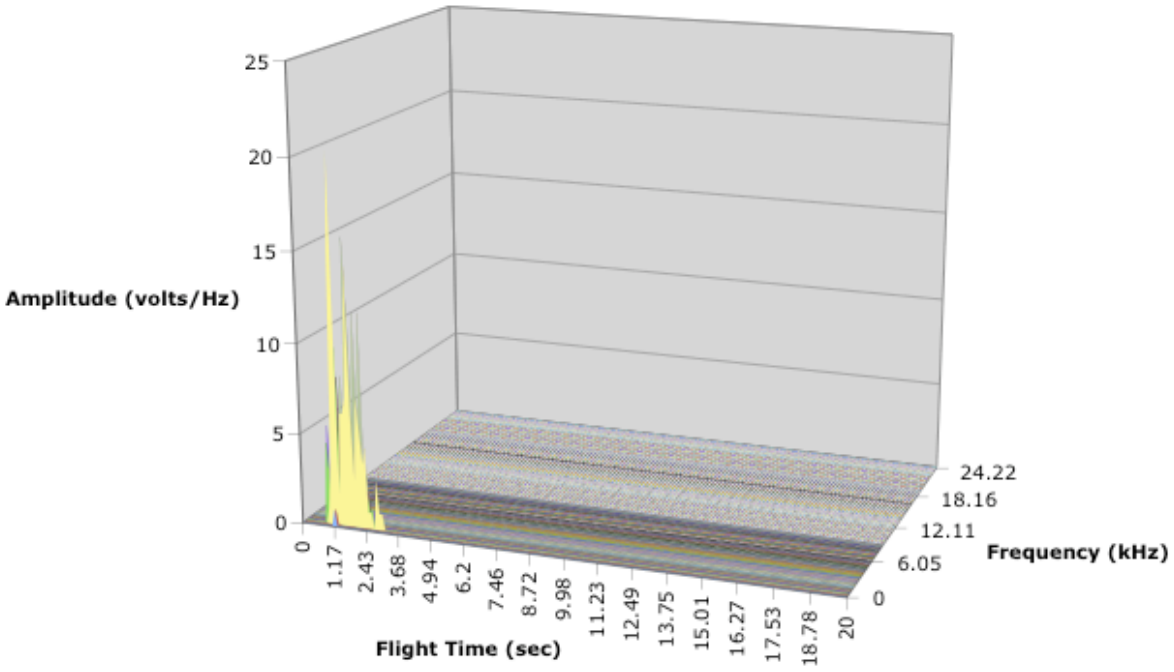

Figure 43. Amplitude spectra of embedded vibrometer VIB1Z data.

REPORT DOCUMENTATION PAGE

Form Approved
OMB No. 0704-0188

1. REPORT DATE *(DD-MM-YYYY)*	2. REPORT TYPE	3. DATES COVERED *(From - To)*
01- 07 - 2010	Technical Memorandum	

4. TITLE AND SUBTITLE

HyBoLT Flight Experiment

5a. CONTRACT NUMBER

5b. GRANT NUMBER

5c. PROGRAM ELEMENT NUMBER

6. AUTHOR(S)

Chen, Fang-Jenq (Frank); Berry, Scott A.

5d. PROJECT NUMBER

5e. TASK NUMBER

5f. WORK UNIT NUMBER

599489.02.07.07.04.11.01

7. PERFORMING ORGANIZATION NAME(S) AND ADDRESS(ES)

NASA Langley Research Center
Hampton, VA 23681-2199

8. PERFORMING ORGANIZATION REPORT NUMBER

L-19902

9. SPONSORING/MONITORING AGENCY NAME(S) AND ADDRESS(ES)

National Aeronautics and Space Administration
Washington, DC 20546-0001

10. SPONSOR/MONITOR'S ACRONYM(S)

NASA

11. SPONSOR/MONITOR'S REPORT NUMBER(S)

NASA/TM-2010-216725

12. DISTRIBUTION/AVAILABILITY STATEMENT

Unclassified - Unlimited
Subject Category 02
Availability: NASA CASI (443) 757-5802

13. SUPPLEMENTARY NOTES

14. ABSTRACT

HyBoLT was a Hypersonic Boundary Layer Transition flight experiment funded by the Hypersonics Project of the Fundamental Aeronautics Program in NASA's Aeronautics Research Mission Directorate. The HyBoLT test article mounted on the top of the ALV X-1 rocket was launched from Virginia's Wallops Island on August 22, 2008. Unfortunately a problem in the rocket's flight control system caused the vehicle to veer off the designed flight course. Launch officials activated a self-destruct mechanism in the rocket's nose cone after 20 seconds into flight. This report is a closeout document about the HyBoLT flight experiment. Details are provided of the objectives and approach associated with this experimental program as well as the 20 seconds flight data acquired before the vehicle was destroyed.

15. SUBJECT TERMS

HyBoLT; Hypersonic boundary layer transition; Natural transition; Roughness-induced transition; Flight experiment

16. SECURITY CLASSIFICATION OF:			17. LIMITATION OF ABSTRACT	18. NUMBER OF PAGES	19a. NAME OF RESPONSIBLE PERSON
a. REPORT	b. ABSTRACT	c. THIS PAGE			STI Help Desk (email: help@sti.nasa.gov)
					19b. TELEPHONE NUMBER *(Include area code)*
U	U	U	UU	77	(443) 757-5802